arXiv:hep-ph/9803244v1 4 Mar 1998

SISSA –154/97/EP
arch-iv/9803244

A Study of the Day - Night Effect for the Super - Kamiokande Detector: III. The Case of Transitions into Sterile Neutrino.

M. Maris [a,b)] and S. T. Petcov [1] [b,c)]

[a)] OAT: Osservatorio Astronomico di Trieste, Trieste, Italy.

[b)] Scuola Internazionale Superiore di Studi Avanzati, Trieste, Italy.

[c)] INFN - Sezione di Trieste, Trieste, Italy.

Abstract

Using the results of a high precision calculation of the solar neutrino survival probability for Earth crossing neutrinos in the case of MSW $\nu_e \rightarrow \nu_s$ transition solution of the solar neutrino problem, we derive predictions for the one-year averaged day-night (D-N) asymmetries in the deformed recoil-e$^-$ spectrum and in the energy-integrated event rate due to the solar neutrinos, to be measured with the Super - Kamiokande detector. The asymmetries are calculated for three event samples, produced by solar ν_e crossing the Earth mantle only, the core, and the mantle only + the core (the full night sample), for a large set of representative values of the MSW transition parameters Δm^2 and $\sin^2 2\theta_V$ from the "conservative" $\nu_e \rightarrow \nu_s$ solution regions, obtained by taking into account the possible uncertainties in the predictions for the ^{8}B and ^{7}Be neutrino fluxes. The effects of the uncertainties in the value of the bulk matter density and in the chemical composition of the Earth core on the predictions for the D-N asymmetries are investigated. The dependence of the D - N effect related observables on the threshold recoil - e$^-$ kinetic energy, $T_{e,th}$, is studied. It is shown, in particular, that for $\sin^2 2\theta_V \leq 0.030$ the one year average D-N - asymmetry in the sample of events due to the core-crossing neutrinos is larger than the asymmetry in the full night sample by a factor which, depending on the solution value of Δm^2, can be $\sim (3-4)$ ($\Delta m^2 < 5 \times 10^{-6}$ eV^2) or $\sim (1.5-2.5)$ (5×10^{-6} eV$^2 \lesssim \Delta m^2 \lesssim 8 \times 10^{-6}$ eV^2). We find, however, that at small mixing angles $\sin^2 2\theta_V \lesssim 0.014$, the D-N asymmetry in the case of solar $\nu_e \rightarrow \nu_s$ transitions is considerably smaller than if the transitions were into an active neutrino, $\nu_e \rightarrow \nu_{\mu(\tau)}$. In particular, a precision better than 1% in the measurement of any of the

---

[1] Also at: Institute of Nuclear Research and Nuclear Energy, Bulgarian Academy of Sciences, 1784 Sofia, Bulgaria.

three one year averaged D-N asymmetries considered by us would be required to test the small mixing angle nonadiabatic $\nu_e \rightarrow \nu_s$ solution at $\sin^2 2\theta_V \lesssim 0.01$. For $0.0075 \lesssim \sin^2 2\theta_V \leq 0.03$ the magnitude of the D-N asymmetry in the sample of events due to the core-crossing neutrinos is very sensitive to the value of the electron number fraction in the Earth core, $Y_e(core)$: a change of $Y_e(core)$ from the standard value of 0.467 to the conservative upper limit of 0.50 can lead to an increase of the indicated asymmetry by a factor of $\sim (3-4)$. Iso - (D-N) asymmetry contours in the $\Delta m^2 - \sin^2 2\theta_V$ plane for the Super-Kamiokande detector are derived in the region $\sin^2 2\theta_V \geq 10^{-4}$ for the three event samples studied for $T_{e,th} = 5$ MeV and 7.5 MeV, and in the case of the samples due to the core crossing and (only mantle crossing + core crossing) neutrinos - for $Y_e(core) = 0.467$ and 0.50. The possibility to discriminate between the $\nu_e \rightarrow \nu_s$ and $\nu_e \rightarrow \nu_{\mu(\tau)}$ solutions of the solar neutrino problem by performing high precision D-N asymmetry measurements is also discussed.

1 Introduction

In the present article we continue the systematic study of the D-N effect for the Super - Kamiokande detector began in refs. [1] and [2]. Assuming that the solar neutrinos undergo two - neutrino MSW $\nu_e \rightarrow \nu_{\mu(\tau)}$ transitions in the Sun, and that these transitions are at the origin of the solar neutrino deficit, we have performed in [2] a high - precision calculation of the one - year averaged solar ν_e survival probability for Earth crossing neutrinos, $P_{\oplus}(\nu_e \rightarrow \nu_e)$, reaching the Super - Kamiokande detector. The probability $P_{\oplus}(\nu_e \rightarrow \nu_e)$ was calculated by using, in particular, the elliptical orbit approximation (EOA) to describe the movement of the Earth around the Sun. Results for $P_{\oplus}(\nu_e \rightarrow \nu_e)$ as a function of $E_\nu/\Delta m^2$, E_ν and Δm^2 being the neutrino energy and the neutrino mass squared difference, have been obtained for neutrinos crossing the Earth mantle only, the core, the inner 2/3 of the core and the mantle + core (full night) for a large representative set of values of $\sin^2 2\theta_V$, where θ_V is the neutrino mixing angle in vacuum, from the "conservative" MSW solution region in the Δm^2 - $\sin^2 2\theta_V$ plane, derived by taking into account the possible uncertainties in the fluxes of ^{8}B and ^{7}Be neutrinos (see, e.g., ref. [3, 4]; for earlier studies see ref. [5]).

We have found in [2], in particular, that for $\sin^2 2\theta_V \leq 0.013$ the one - year averaged D-N asymmetry [2] in the probability $P_{\oplus}(\nu_e \rightarrow \nu_e)$ for neutrinos crossing the Earth core can be larger than the asymmetry in the probability for (only mantle crossing + core crossing) neutrinos by a factor of up to six. The enhancement is even larger for neutrinos crossing the inner 2/3 of the core. We have also pointed out to certain subtleties in the calculation of the time averaged ν_e survival probability $P_{\oplus}(\nu_e \rightarrow \nu_e)$ for neutrinos crossing the Earth, which become especially important when $P_{\oplus}(\nu_e \rightarrow \nu_e)$ is computed, for instance, for the core crossing neutrinos only [3].

The results obtained in [2] were used in [1] to investigate the D-N asymmetries in the spectrum of the recoil electrons from the reaction $\nu + e^- \rightarrow \nu + e^-$ caused by the ^{8}B neutrinos and in the energy-integrated event rate, to be measured by the Super - Kamiokande experiment. We have computed in [13] the D-N asymmetry in the recoil-e^- spectrum for the same large set of representative values of Δm^2 and $\sin^2 2\theta_V$ from the "conservative" MSW solution region for which results in [2] have been presented. The D-N asymmetry in the e^--spectrum was found for neutrinos crossing the Earth mantle only, the core and the mantle + core. In [1] we have included only 12 representative plots showing the magnitude of the D-N asymmetry in the recoil-e$^-$ spectrum to be expected in the case of the two - neutrino MSW $\nu_e \rightarrow \nu_{\mu(\tau)}$ transition solution of the solar neutrino problem. The spectrum asymmetry for the sample of events due to core crossing neutrinos only was found to be strongly enhanced for $\sin^2 2\theta_V \lesssim 0.013$ with respect to the analogous asymmetries for the mantle and for the (only mantle crossing + core crossing) neutrinos. We presented in [1] also detailed results for the one-year averaged D-N asymmetry in the Super - Kamiokande signal for the indicated three samples of events. We have found that indeed for $\sin^2 2\theta_V \leq 0.013$ the asymmetry in the sample corresponding to core crossing neutrinos can be larger than the asymmetry in the sample produced by only mantle crossing or by (only mantle crossing + core crossing) neutrinos by a factor of up to six. We have investigate in [1] the dependence of the D-N asymmetries in the three event samples defined above on the threshold e$^-$ kinetic energy being used for the event selection. The effect of the uncertainties in the Earth matter density and electron number density distributions on the predicted values of the D-N asymmetries were studied as well. We derived also iso - (D-N) asymmetry contours in the region of $\sin^2 2\theta_V \gtrsim 10^{-4}$ in the Δm^2- $\sin^2 2\theta_V$ plane for the signals in the Super - Kamiokande detector, produced by neutrinos crossing the mantle only, the core and the mantle + core (full night sample). The iso-asymmetry contours for the sample of events due to core-crossing neutrinos were obtained for two values of the fraction of electrons, Y_e, in the core: for $Y_e(core) = 0.467$ and 0.500 [4]. The results derived in [1] confirmed the conclusion drawn in [2] that the Super - Kamiokande detector will be able to probe not only the large mixing angle adiabatic solution region, but also an important and substantial part of the $\sin^2 2\theta_V \lesssim 0.014$ nonadiabatic region of the MSW $\nu_e \rightarrow \nu_{\mu(\tau)}$ transition solution of the solar neutrino problem. We have found, in particular, that in a large sub-region of the "conservative" nonadiabatic solution region located at $\sin^2 2\theta_V \lesssim 0.0045$, the D-N asymmetry in the sample of events due to the core-crossing neutrinos only is negative and has a value in the interval (-1%) - (-3%).

---

[2] A rather complete list of references on the D-N effect is given in ref. [1]; for relatively recent discussions of the effect see, e.g., [7, 6, 8, 9, 10, 11]

[3] For further details concerning the technical aspects of the calculations see ref. [2] as well as ref. [12].

In the present article we realize the same program of studies for the Super-Kamiokande detector for the alternative possibility of solar neutrinos undergoing two-neutrino matter-enhanced transitions in the Sun and in the Earth into a sterile neutrino, ν_s. As is well-known, the solar ν_e matter-enhanced transitions into a sterile neutrino, $\nu_e \rightarrow \nu_s$, provide one of the possible neutrino physics solutions of the solar neutrino problem (see, e.g., [15, 7, 16, 3]). The reference solution region in the $\Delta m^2 - \sin^2 2\theta$ plane, i.e., the region obtained (at 95% C.L.) by using the predictions of the reference solar model of Bahcall and Pinsonneault from 1995 with heavy element diffusion [14] (BP95) for the different components of the solar neutrino flux (pp, pep, ^{7}Be, ^{8}B and CNO), lies within the bounds:

---

[4] Results for other D-N effect related observables, as the D-N asymmetry in the zenith angle distribution of the events and in the mean recoil-e$^-$ energy, have been obtained in refs. [9, 10], where iso - (D-N) asymmetry contour plots for the full night (i.e., mantle + core) signal for the Super - Kamiokande detector for one value of $Y_e(core) = 0.0467$ have been presented as well.

$$2.8 \times 10^{-6}\ \mathrm{eV}^2 \lesssim \Delta m^2 \lesssim 7.0 \times 10^{-6}\ \mathrm{eV}^2, \tag{1}$$

$$4.8 \times 10^{-3} \lesssim \sin^2 2\theta \lesssim 1.4 \times 10^{-2}\ . \tag{2}$$

The reference solution is of the small mixing angle nonadiabatic type. A reference large mixing angle (adiabatic) solution (present in the case of $\nu_e \rightarrow \nu_{\mu(\tau)}$ transitions) is practically ruled out by the solar neutrino data [15, 16, 3]. If we allow for possible uncertainties in the predictions for the fluxes of the ^{8}B and ^{7}Be neutrinos [16], the solar neutrino data is described in terms of the hypothesis of $\nu_e \rightarrow \nu_s$ transitions for larger ranges of values of the parameters Δm^2 and $\sin^2 2\theta$, belonging to the intervals:

$$2.8 \times 10^{-6}\ \mathrm{eV}^2 \lesssim \Delta m^2 \lesssim 8.0 \times 10^{-6}\ \mathrm{eV}^2, \tag{3}$$

$$8.0 \times 10^{-4} \lesssim \sin^2 2\theta \lesssim 3.0 \times 10^{-2}\ . \tag{4}$$

and

$$5.3 \times 10^{-6}\ \mathrm{eV}^2 \lesssim \Delta m^2 \lesssim 1.2 \times 10^{-5}\ \mathrm{eV}^2, \tag{5}$$

$$0.13 \lesssim \sin^2 2\theta \lesssim 0.55\ . \tag{6}$$

The "conservative" solution regions lying within the bounds determined by eqs. (3) - (4), and eqs. (5) - (6) have been obtained by treating the ^{8}B neutrino flux as a free parameter in the relevant analysis of the solar neutrino data, while the the ^{7}Be neutrino flux was assumed to have a value in the interval $\Phi_{Be} = (0.7 - 1.3)\ \Phi_{Be}^{BP}$, where Φ_{Be}^{BP} is the flux in the reference solar model [14]. For values of Δm^2 and $\sin^2 2\theta$ from the solution regions (5) and (6) the $\nu_e \rightarrow \nu_s$ transitions of ^{8}B neutrinos having energy $E_\nu \geq 5$ MeV are adiabatic. However, this adiabatic solution is possible only for large values of the ^{8}B neutrino flux [16], $\Phi_B \cong (2.5 - 5.0)\ \Phi_B^{BP}$, Φ_B^{BP} being the reference model flux [14]. Such values of Φ_B seem totally unrealistic from the point of view of the contemporary solar models and we consider the indicated adiabatic solution here for completeness. It should be added that in deriving the conservative solution regions represented by eqs. (3) - (4) and eqs. (5) - (6) the limit on the D-N effect derived in [7] on the basis of the data obtained in the Kamiokande II and III experiments [17] was utilized.

Let us note that the preliminary result on the D-N effect from the Super-Kamiokande experiment after approximately one year (374.2 days) of data taking reads [18]:

$$\bar{A}^{SK}_{D-N} \equiv \frac{\bar{R}^D - \bar{R}^N}{\bar{R}^D + \bar{R}^N} = -0.031 \pm 0.024 \pm 0.014, \tag{7}$$

where $\bar{A}^{SK}_{D-N}$ is the average energy integrated D-N asymmetry and $\bar{R}^D$ and $\bar{R}^N$ are the observed average event rates caused by the solar neutrinos during the day and during the night in the Super-Kamiokande detector in the period of data taking. The first error in eq. (7) is statistical and the second error is systematic. The data were obtained with a recoil$-e^-$ threshold energy $E_{e,th} =$ 6.5 MeV.

In addition of performing i) detailed high precision calculations of the D-N asymmetries in the recoil-e$^-$ spectrum and ii) of the energy-integrated D-N asymmetries for the three samples of events (due to core crossing, only mantle crossing and only mantle + core crossing neutrinos), and of studying iii) the effects of the recoil-e$^-$ energy threshold variation and iv) of the uncertainties in the chemical composition and matter density of the Earth's core on the calculated D-N effect related observables, we also analyze qualitatively the possibility to distinguish between the two solutions of the solar neutrino problem involving matter-enhance transitions of the solar ν_e respectively into active neutrinos and into sterile neutrinos, $\nu_e \rightarrow \nu_{\mu(\tau)}$ and $\nu_e \rightarrow \nu_s$, by performing high-precision D-N asymmetry measurements.

2 Specific Features of the Earth Matter Effect for Solar Neutrino Transitions Into Sterile Neutrino

In the present study we utilize the same high precision methods of calculation of i) the position of the Sun (at a given time of the year t) with respect to the Super-Kamiokande detector (elliptical orbit approximation which accounts for the change with t of the Earth orbital velocity as well), ii) the solar ν_e survival probability in the Sun, $\bar{P}_{\odot}(\nu_e \rightarrow \nu_e)$, and iii) the $\nu_2 \rightarrow \nu_e$ transition probability in the Earth (see, e.g., [2]), P_{e2}, ν_2 being the heavier of the two vacuum mass-eigenstate neutrinos, which were used in our studies of the D-N effect for the Super-Kamiokande detector in the case of solar ν_e transitions into active neutrinos, $\nu_{\mu(\tau)}$. They are described in detail in refs. [1, 2]. In the present Section we discuss the differences between the $\nu_2 \to \nu_e$ transitions in the Earth in the cases of the $\nu_e \to \nu_s$ and $\nu_e \to \nu_{\mu(\tau)}$ transition solutions of the solar neutrino problem, which are relevant for our further analysis and also allow to understand qualitatively the differences between the results on the D-N effect in the two cases.

As we have indicated above, the calculation of the Earth effect related observables in the case of interest requires the knowledge of the probabilities $\bar{P}_{\odot}(\nu_e \to \nu_e)$ and P_{e2} which account for the matter-enhanced transitions of the solar neutrinos in the Sun and in the Earth, respectively. The neutrino effective potential in matter which enters in the system of evolution equations describing the $\nu_e \to \nu_s$ transitions is [19]:

$$V_s(x) = \sqrt{2} G_F (n_e(x) - \frac{1}{2} n_n(x)), \tag{8}$$

where G_F is the Fermi constant and $n_e(x)$ and $n_n(x)$ are the electron and neutron number densities at a given point x of the neutrino trajectory.

For the Sun we use the electron and neutron number density distributions given by the standard solar model [14] with heavy element diffusion [5]. The ratio 0.5 n_n/n_e changes from approximately 0.22 in the central part to 0.08 in most of the Sun outside the neutrino (energy) production region (see, e.g., [14]), so the presence of the neutron number density term in $V_s(x)$ does not play important role in the solar neutrino transitions in the Sun, although it has to be taken into account in the calculation of $\bar{P}_{\odot}(\nu_e \to \nu_e)$.

The electron and neutron number densities in the Earth are directly related to the local matter density, $\rho(r)$, where r is the distance from the Earth center, and the local chemical composition which is accounted for by the electron fraction number, $Y_e(r)$: $Y_e(r) = n_e(r)/(n_n(r) + n_p(r))$, $n_p(r)$ being the proton number density, $n_p(r) = n_e(r)$. As in [1, 2], the Stacey model from 1977 [20] is utilized as a reference Earth model in the calculations performed for the present study. The Earth radius in the Stacey model is $R_{\oplus} = 6371$ km. As in all Earth models known to us, the density distribution is spherically symmetric and there are two major density structures - the core and the mantle, and a large number of substructures (shells or layers). The core has a radius $R_c = 3485.7$ km, so the Earth mantle depth is approximately $R_{man} = 2885.3$ km. The mean matter densities in the core and in the mantle read, respectively: $\bar{\rho}_c \cong 11.5$ g/cm^3 and $\bar{\rho}_{man} \cong 4.5$ g/cm^3. Let us note that the density distribution in the 1977 Stacey model practically coincides with the density distribution in the more recent PREM model [21].

---

[5] All solar models compatible with the currently existing observational constraints (helioseismological and other) give practically the same electron and neutron number density distributions in the Sun.

The onion like (shell) structure of the Earth is reproduced in the Stacey model by a set of polynomial functions describing the radial change of the matter density $\rho(r)$. Assuming the chemical composition in each geological structure (core, mantle, etc.) to be to a good approximation constant, the effective number density of scattering centers in eq. (1), $(n_e - 1/2n_n)$, is obtained for each shell by simply rescaling the matter density of the $i-th$ shell, $\rho_i(r)/m_N$, m_N being the nucleon mass, by the factor:

$$\frac{1}{2}(3Y_{e,i} - 1), \;\; i = \text{geological shell index} \tag{9}$$

where $Y_{e,i}$ is the electron fraction in the i-th shell. Let us note that due to the factor 3/2 in front of Y_e in eq. (2), the $\nu_e \to \nu_s$ transitions are more sensitive to the uncertainty in the value of Y_e in a given Earth shell than the $\nu_e \to \nu_{\mu(\tau)}$ transitions.

If we denote by $V_a(x)$ the neutrino effective potential in matter relevant for the solar ν_e transitions into an active neutrino, $V_a(x) = \sqrt{2}G_F n_e(x)$, we always have $V_s(x) < V_a(x)$ in the case of interest. Actually, in the Earth

$$V_s(r) \cong \frac{1}{2}\; V_a(r) \tag{10}$$

due to the approximate isotopic symmetry $(n_p(r) \cong n_n(r))$ and neutrality $(n_p(r) = n_e(r))$ of the Earth matter. This has several important implications. For a fixed neutrino energy E_ν and given Δm^2 and $\cos 2\theta$, the resonance density for the $\nu_e \to \nu_s$ transitions,

$$\rho_s^{res} = \frac{\Delta m^2 \cos 2\theta}{2E\sqrt{2}G_F \frac{1}{2}(3Y_e - 1)}, \tag{11}$$

is approximately by a factor of two larger than the resonance density for the $\nu_e \to \nu_{\mu(\tau)}$ transitions, $\rho_a^{res} = \Delta m^2 \cos 2\theta/(2E\sqrt{2}G_F Y_e)$:

$$\rho_s^{res} \cong 2\; \rho_a^{res}. \tag{12}$$

Correspondingly, for a given $\rho(r)$ and $\cos 2\theta$, the resonance condition in the $\nu_e \to \nu_s$ case will be fulfilled for a value of $E_\nu/\Delta m^2$, which is two times bigger than the analogous resonance $E_\nu/\Delta m^2$ value for the $\nu_e \rightarrow \nu_{\mu(\tau)}$ transitions, $(E_\nu/\Delta m^2)^{res}_s \cong 2\ (E_\nu/\Delta m^2)^{res}_a$. Thus, the oscillation length in matter at resonance in the Earth, $L^{res}_m = 4\pi (E_\nu/\Delta m^2)^{res}/\sin 2\theta$, for solar neutrino transitions into sterile neutrino will exceed the resonance oscillation length in matter for transitions into an active neutrino by a factor of two: $L^{res}_{m,s} \cong 2\ L^{res}_{m,a}$. At small mixing angles the probability P_{e2} typically should have a maximum at $\rho^{res} \cong \bar{\rho}$ ($\sin^2 2\theta_m \cong 1$, θ_m being the mixing angle in matter) independently of the type of the transition, $\nu_e \rightarrow \nu_s$ or $\nu_e \rightarrow \nu_{\mu(\tau)}$, where $\bar{\rho}$ is the effective mean density along the neutrino trajectory in a given Earth density structure. For the neutrino trajectories for which the matter effect is significant one has $\bar{\rho}_c \cong (10 - 12)$ g/cm^3 for the core and $\bar{\rho}_{man} \cong (3.5 - 5.0)$ g/cm^3 for the mantle.

The small mixing angle (SMA) $\nu_e \rightarrow \nu_s$ and $\nu_e \rightarrow \nu_{\mu(\tau)}$ transition solutions of the solar neutrino problem take place roughly for the same values of Δm^2 and $\sin^2 2\theta$ [6]. It is easy to convince oneself that for the energies of ^{8}B neutrinos of interest, $E_\nu \cong (5 - 14)$ MeV, and values of Δm^2 from the region of the SMA solutions, $\Delta m^2 \cong (3 - 10) \times 10^{-6}$ eV^2, we have for a resonance taking place in the mantle ($\rho^{res} \cong \bar{\rho}_{man}$): $(2\pi R/L^{res}_m)^2 \ll 1$. As a consequence at resonance (where $\rho^{res} = \bar{\rho}$ and $\sin^2 2\theta_m = 1$), as can be shown, one approximately has: $(P_{e2} - \sin^2\theta) \sim 0.5 (2\pi R/L^{res}_m)^2$. Thus, for the only mantle crossing neutrinos, at small mixing angles ($\sin^2 2\theta \lesssim 0.03$) and for a given Δm^2, the Earth matter effect term $(P_{e2} - \sin^2\theta)$ in the solar ν_e survival probability $P_\oplus(\nu_e \rightarrow \nu_e)$ is approximately by a factor of (3.5 - 4.0) smaller in the case of $\nu_e \rightarrow \nu_s$ transitions than if the solar ν_e underwent $\nu_e \rightarrow \nu_{\mu(\tau)}$ transitions. This conclusion agrees very well with our numerical results for the probability P_{e2} for solar neutrinos crossing only the mantle when they traverse the Earth. For the core crossing neutrinos the analysis is more complicated and the above simple estimate for the ratio of the maximal values of $(P_{e2} - \sin^2\theta)$ corresponding to the $\nu_e \rightarrow \nu_s$ and $\nu_e \rightarrow \nu_{\mu(\tau)}$ transitions has to be modified: actually, the corresponding factor is smaller than the one for the only mantle crossing neutrinos, being approximately equal to $(2.5 - 3.0)$. Thus, on the basis of the above results we can expect that at small mixing angles the Earth matter effect in the solar ν_e survival probability, $P_\oplus(\nu_e \rightarrow \nu_e)$, will be substantially smaller (roughly by a factor of $\sim (2.5 - 4.0)$) for the $\nu_e \rightarrow \nu_s$ solution of the solar neutrino problem than for the $\nu_e \rightarrow \nu_{\mu(\tau)}$ one.

Further important implications of equation (5) for the magnitude of the D-N effect if the solar ν_e undergo transitions into a sterile neutrino will be discussed in the next Section. Here we would like to add one more remark only. Following the detailed discussion of the uncertainties in the knowledge of the chemical composition and the bulk matter density of the Earth core and the method chosen to effectively account for these uncertainties in [1], we use two values of Y_e in the core in the present analysis: the reference Earth model value $Y_e(core) = 0.467$ which has been used also in refs. [1, 2, 9, 10], and the value $Y_e(core) = 0.500$, which represents a conservative upper limit for $Y_e(core)$ [22]. In all calculations performed for the present study the value of $Y_e = 0.49$ in the mantle has been utilized.

---

[6] The $\nu_e \rightarrow \nu_s$ transition SMA solution region in the $\Delta m^2 - \sin^2 2\theta$ plane is shifted on average by a factor of 1.2 to smaller values of Δm^2 with respect to the analogous region of the $\nu_e \rightarrow \nu_{\mu(\tau)}$ solution [16].

3 The Time-Averaged Probabilities

The relevant probabilities for the problem of interest, in addition to the probability of solar ν_e survival in the Sun, $\bar{P}_{\odot}$, and the instantaneous $\nu_2 \rightarrow \nu_e$ transition probability in the Earth,P_{e2}, are the time averaged of P_{e2} over the full night or part of it, $< P_{e2} >^s$, where the index s indicates over which time period of the night (or equivalently, over which neutrino trajectories in the Earth) P_{e2} is averaged, and the time averaged ν_e survival probability when the solar neutrinos cross the Earth, $P^s_{\oplus}(\nu_e \rightarrow \nu_e)$. As in [1, 2], we will consider three types of time averaging which correspond to three different selections of events in the Super-Kamiokande detector: those due to neutrinos which cross only the mantle, due to the core crossing neutrinos, and the events collected during the full night. We shall call these event samples respectively *Mantle*, *Core* and *Night* samples and will denote them by M, C and N: $s = M, C, N$.

It proves useful to study the D-N asymmetry in the probability of solar ν_e survival:

$$\mathcal{A}^s_P(E_\nu/\Delta m^2) \equiv \mathcal{A}^s_P = 2\,\frac{P^s_{\oplus} - \bar{P}_{\odot}}{P^s_{\oplus} + \bar{P}_{\odot}}, \quad s = M, C, N. \tag{13}$$

The values of the asymmetry $\mathcal{A}^s_P$ give an idea about the magnitude of the D-N effect to be expected in the corresponding sample of events.

The calculation of the probabilities $< P_{e2} >^s$ and $P^s_{\oplus}$ is performed using the methods described in [2]. For a rather large set of values of $\sin^2 2\theta_V$ our results for $< P_{e2} >^s$, $\bar{P}_{\odot}$, $P^s_{\oplus}$ and the probability asymmetries $\mathcal{A}^s_P$, $s = N, M, C$, are presented graphically in Figs. 3.1 - 3.12.

In Figs. 3.1a - 3.12a we show $< P_{e2} >^s$, $s = N, M, C$, as a function of the density parameter

$$\rho_r = \frac{\Delta m^2 \cos 2\theta_V}{2E_\nu\sqrt{2}G_F 0.25} \tag{14}$$

for fixed values of $\sin^2 2\theta_V$. This parameter would coincide with the resonance density if Y_e were equal to 1/2 both in the mantle and in the core; it is equivalent to $E_\nu/\Delta m^2$, but gives an idea about the densities at which one has an enhancement of the Earth matter effect. In sub-figures 3.1b - 3.12b, 3.1c - 3.12c and 3.1d - 3.12d the probabilities $\bar{P}_\odot$, $< P_{e2} >^s$, $P^s_\oplus$ (upper frames) and the related asymmetries $\mathcal{A}^s_P$ (lower frames) are shown as functions of $E_\nu/\Delta m^2$.

The enhancement of $< P_{e2} >^s$ due to the Earth matter effect is clearly seen in the figures. The dependence of $< P_{e2} >^s$ on $E_\nu/\Delta m^2$ at small and at large mixing angles is quite different. The most remarkable feature, as in the case of transitions into an active neutrino [1, 2], is the enhancement at small mixing angles, $\sin^2 2\theta_V \lesssim 0.03$, of $< P_{e2} >$ for the core-crossing neutrinos, $< P_{e2} >^C$, with respect to $< P_{e2} >$ for the only mantle crossing neutrinos, $< P_{e2} >^M$, and with respect to $< P_{e2} >^N$ (core enhancement). As a quantitative measure of the enhancement one can consider the ratio of $< P_{e2} >^C$ and $< P_{e2} >^N$ at their maxima: $\max(< P_{e2} >^C)/\max(< P_{e2} >^N)$. In the case of $\nu_e \rightarrow \nu_s$ transitions one typically has $3.3 \lesssim \max(< P_{e2} >^C)/\max(< P_{e2} >^N) \lesssim 3.8$ for $0.001 \leq \sin^2 2\theta_V \leq 0.03$, which is of the same order of magnitude as in the case of $\nu_e \rightarrow \nu_{\mu(\tau)}$ transitions. In contrast, at large mixing angles, $\sin^2 2\theta_V \sim (0.1 - 0.6)$, we have: $\max(< P_{e2} >^C)/\max(< P_{e2} >^N) \lesssim 1.5$. Thus, as like for the $\nu_e \rightarrow \nu_{\mu(\tau)}$ transitions, the core enhancement is significant only at small mixing angles.

At large mixing angles, $\sin^2 2\theta_V \sim (0.1 - 0.6)$, we note the existence of a substantial negative D-N asymmetry in the *Core* sample (Figs. 3.11 - 3.12). Physically, a negative D-N asymmetry means that the Earth effect suppresses the solar ν_e flux instead of enhancing it, so that the solar neutrino signal is smaller at night than during the day. At small mixing angles a negative D-N effect occurs when the survival probability in the Sun, $\bar{P}_\odot$, is larger than 1/2. In the case of $\nu_e \rightarrow \nu_s$ transitions this happens at large mixing angles because for certain values of ρ_r (or equivalently of $E_\nu/\Delta m^2$) we have $< P_{e2} >^C < \sin^2 \theta_V$ [7].

Let us discuss next briefly the behavior of the probabilities $< P_{e2} >^s$ and the corresponding asymmetries $\mathcal{A}^s_P$ as $\sin^2 2\theta_V$ changes from 0.001 to 0.6. For values of $\sin^2 2\theta_V$ from the interval (0.001 - 0.006) there are two clear "peaks" in the D-N asymmetry in the probabilities, $\mathcal{A}^s_P$, but the only physically relevant "peak" is the "negative" ($\mathcal{A}^s_P < 0$) one: the "positive" ($\mathcal{A}^s_P > 0$) peak located at smaller values of $E_\nu/\Delta m^2$ (see Figs. 3.1 - 3.7) is caused [2] essentially by the small value of the adiabatic minimum of the probability $\bar{P}_\odot$, $min\ \bar{P}_\odot = \sin^2 \theta_V$. As $\sin^2 2\theta$ increases the negative "peak" in $\mathcal{A}_P^C$ ($\mathcal{A}_P^N$) increases in absolute value and reaches a maximum approximately at $\sin^2 2\theta \cong 0.007$; when $\sin^2 2\theta$ increases further its significance begins to diminish, as physically relevant positive "peaks" preceding it along the $E_\nu/\Delta m^2$ axis appear and become prominent. For $\sin^2 2\theta \approx 0.007$, the negative "peak" corresponds to $\mathcal{A}_P^C \approx -2.8\%$ while the dominant positive one is approximately equal to 1%; at $\sin^2 2\theta \approx 0.009$ the two "peaks" in $\mathcal{A}_P^C$ are practically equal in absolute value.

---

[7] The negative D-N effect takes place at large mixing angles also in the $\nu_e \rightarrow \nu_{\mu(\tau)}$ case, but it is much smaller in magnitude and the integration over the recoil-electron energy makes it negligible [1, 2].

Actually, the dominant physically relevant "positive" peak appears in $\mathcal{A}_P^C$ because for $0.006 \lesssim \sin^2 2\theta \lesssim 0.01$ the region of resonance enhancement of $< P_{e2} >^C$ is divided into two parts by the $\bar{P}_\odot = 1/2$ zero Earth effect ($\mathcal{A}_P^s = 0$) line located in the $E_\nu/\Delta m^2-$region where $\bar{P}_\odot$ is non adiabatic. As a consequence, one has in the resonance region, i.e., in the region of the absolute maximum of $< P_{e2} >^C$: $\mathcal{A}_P^C < 0$ if $E_\nu/\Delta m^2 > (E_\nu/\Delta m^2)_0$ and $\mathcal{A}_P^C > 0$ for $E_\nu/\Delta m^2 < (E_\nu/\Delta m^2)_0$, where $(E_\nu/\Delta m^2)_0$ is the point at which $\bar{P}_\odot = 1/2$ and $\mathcal{A}_P^C = 0$. The contributions from the regions of positive and negative $\mathcal{A}_P^C$ to the energy-integrated D-N *Core* asymmetry can partially compensate each other. The degree of compensation depends on the value of Δm^2. For $0.014 \lesssim \sin^2 2\theta \lesssim 0.03$ the $\bar{P}_\odot = 1/2$ (i.e., zero Earth effect) line is outside the region of resonance enhancement of $< P_{e2} >^C$ and $\mathcal{A}_P^C > 0$ in this region. The maximal value of $|\mathcal{A}_P^C|$ (i.e., the value at the relevant negative "peak") is nearly constant for $0.004 \lesssim \sin^2 2\theta \lesssim 0.007$ because of the interplay between the change of $< P_{e2} >^C$ and the change of the position of the $\bar{P}_\odot = 1/2$ line with respect to the position of the $< P_{e2} >^C$ resonance maximum (Figs. 3.4 - 3.6).

It is important to note that the value $(E_\nu/\Delta m^2)_0$, at which $\bar{P}_\odot = 1/2$ and the ν_e transitions in the Sun are nonadiabatic, is practically the same for the $\nu_e \rightarrow \nu_s$ and the $\nu_e \rightarrow \nu_{\mu(\tau)}$ transitions [16]. However, since the dominating absolute maximum of $< P_{e2} >^C$ occurs in the two cases for values of $E_\nu/\Delta m^2$ which differ by approximately a factor of two, $(E_\nu/\Delta m^2)_s^{res} \cong 2\ (E_\nu/\Delta m^2)_a^{res}$, the zero Earth effect point $(E_\nu/\Delta m^2)_0$ in the case of solar ν_e transitions into an active neutrino "leaves" the region of the absolute maximum of $< P_{e2} >^C$ as $sin^2 2\theta$ increases at a considerably smaller value of $sin^2 2\theta$ than in the case of $\nu_e \rightarrow \nu_s$ transitions, namely at $sin^2 2\theta \cong 0.006$ [2]. Therefore, in contrast to the possibility described above for the $\nu_e \rightarrow \nu_s$ transitions, a partial or complete compensation between the negative and positive contributions to the energy-integrated D-N *Core* asymmetry can occur for the $\nu_e \rightarrow \nu_{\mu(\tau)}$ transitions only at $sin^2 2\theta \lesssim 0.005$. This together with the observations made in the previous Section implies that for values of $\sin^2 2\theta$ from the interval $0.006 \lesssim \sin^2 2\theta \lesssim 0.03$, in which the reference and most of the "conservative" regions of the SMA nonadiabatic $\nu_e \rightarrow \nu_s$ and $\nu_e \rightarrow \nu_{\mu(\tau)}$ solutions lie, the energy-integrated D-N *Core* asymmetry corresponding to the $\nu_e \rightarrow \nu_s$

transitions should be much smaller than the asymmetry due to $\nu_e \rightarrow \nu_{\mu(\tau)}$ transitions. Similar considerations apply to the *Mantle* and *Night* asymmetries as well.

As $\sin^2 2\theta_V$ increases from $\sin^2 2\theta_V \approx 0.007$, the asymmetry $\mathcal{A}^s_P$ steadily increases for all the samples until $\sin^2 2\theta_V$ reaches approximately the value of $\sim (0.1-0.2)$. At larger values the dominant positive "peak" in $\mathcal{A}^C_P$ is followed, as $E_\nu/\Delta m^2$ increases, by a prominent negative "peak" and several smaller maxima. The negative "peak" is due to the inequality $< P_{e2} >^C < \sin^2\theta_V$ taking place in a specific region of values of $E_\nu/\Delta m^2$. For $\sin^2 2\theta_V \cong 0.4$ the probability D-N asymmetries for the *Night* and *Core* samples are roughly equal, the ratio $< P_{e2} >^C / < P_{e2} >^N$ varying between 1.0 and 1.5, except in the narrow region of the indicated negative "peak" in $< P_{e2} >^C$. As $\sin^2 2\theta_V$ increases further we have $< P_{e2} >^C / < P_{e2} >^N < 1$ in a relatively large interval of values of $E_\nu/\Delta m^2$ (Fig. 3.12).

Changing $Y_e(core)$ from 0.467 to 0.50, which accounts to large extent for the uncertainties in the knowledge of the core chemical composition and density (see [1, 22]) shifts the position of the absolute (resonance) maximum of $< P_{e2} >^C$ ($< P_{e2} >^N$) to a smaller by a factor of 1.25 value of $E_\nu/\Delta m^2$. As a consequence, the zero Earth effect point $(E_\nu/\Delta m^2)_0$ falls outside the region of resonance enhancement of $< P_{e2} >^C$ (as $sin^2 2\theta$ increases) at smaller value of $sin^2 2\theta$ than in the $Y_e = 0.467$ case. Accordingly, for $0.008 \lesssim sin^2 2\theta \lesssim 0.03$, the D-N *Core* asymmetry in the probability $\mathcal{A}^C_P$ for $Y_e = 0.50$ is bigger than the asymmetry for $Y_e = 0.467$ by a substantial factor varying approximately between 1.3 and 4.0. This also leads to a bigger (by a factor $\sim (1.5 - 2.0)$) *Night* asymmetry $\mathcal{A}^N_P$ for the indicated values of $sin^2 2\theta$. Thus, the *Core* asymmetry $\mathcal{A}^C_P$ at small mixing angles is considerably more sensitive to the value of Y_e in the Earth core when the solar ν_e transitions are into sterile neutrino than if the transitions were of the type $\nu_e \rightarrow \nu_{\mu(\tau)}$ [1].

4 D-N Effect Related Observables

As explained in the preceding Section, following the analyzes performed in [1, 2] we consider four possible groups or samples of solar neutrino events in the Super-Kamiokande experiment depending on their detection time: *Day*, *Night*, *Core* and *Mantle*. The recoil-e^- spectra associated with the four samples are denoted by $\mathcal{S}^s(T_e)$, where $s = D$, N, C, M, and T_e is the recoil-e^- kinetic energy, while for the event rates we will use the notation $\mathcal{R}^s$. The symbols $\mathcal{S}_0(T_e)$ and $\mathcal{R}_0$ will be used to denote the recoil-e^- spectrum and event rates for massless ("conventionally" behaving) neutrinos, computed using the predictions of a given reference standard solar model. Obviously, $\mathcal{S}_0(T_e)$ and $\mathcal{R}_0$

are the same for the four event samples of interest. The spectra $\mathcal{S}_0(T_e)$, $\mathcal{S}^s(T_e)$ and the event rates $\mathcal{R}_0$, $\mathcal{R}^s$ considered in the present article are one year averaged spectra and event rates.

The spectra $\mathcal{S}_0(T_e)$ and $\mathcal{S}^s(T_e)$ are given by the well-known expressions:

$$\mathcal{S}_0(T_e) = \Phi_B \int_{T_e\left(1+\frac{m_e}{2T_e}\right)} dE_\nu \, n(E_\nu) \, \frac{d\,\sigma_{\nu_e}(T_e, E_\nu)}{d\,T_e}, \tag{15}$$

and

$$\mathcal{S}^s(T_e) = \Phi_B \int_{T_e\left(1+\frac{m_e}{2T_e}\right)} dE_\nu \, n(E_\nu) \, \frac{d\,\sigma_{\nu_e}(T_e, E_\nu)}{d\,T_e} P^s_\oplus\left(\nu_e \rightarrow \nu_e\right). \tag{16}$$

Here Φ_B is the total ^{8}B neutrino flux, E_ν is the incoming ^{8}B neutrino energy, m_e is the electron mass, $n(E_\nu)$ is the normalized to one ^{8}B neutrino spectrum [23], $P^s_\oplus(\nu_e \rightarrow \nu_e)$ is the one year averaged solar ν_e survival probability for *Day*, *Night*, *Core*, and *Mantle* samples, and $d\,\sigma_{\nu_e}(T_e, E_\nu)/d\,T_e$ is the differential $\nu_e \; - e^-$ elastic scattering cross section [24]. Note the absence in eq. (16) of an analog of the neutral current $\nu_{\mu(\tau)} - e^-$ elastic scattering term which plays an important role in the case of $\nu_e \rightarrow \nu_{\mu(\tau)}$ transitions. For the corresponding energy integrated event rates we have:

$$\begin{aligned} \mathcal{R}_0(T_{e,th}) &= \int_{T_{e,th}} dT_e \, \mathcal{S}_0(T_e), \\ \mathcal{R}^s(T_{e,th}) &= \int_{T_{e,th}} dT_e \, \mathcal{S}^s(T_e), \end{aligned} \tag{17}$$

where $T_{e,th}$ is the recoil-e^- kinetic energy threshold of the Super - Kamiokande detector. In order to assess the dependence of the magnitude of D-N effect in the three event samples on $T_{e,th}$ we report here results obtained for two values of $T_{e,th}$: $T_{e,th} = 5$ MeV and 7.5 MeV.

As like in [1], we have studied three observables relevant to D-N effect which can be measured with the Super - Kamiokande detector. The first is the distortion of the recoil-e^- spectrum due to the MSW effect for the four different event samples:

$$N^s(T_e) = \frac{\mathcal{S}^s(T_e)}{\mathcal{S}_0(T_e)}, \qquad s = D,\, N,\, C,\, M. \tag{18}$$

In the absence of the MSW effect, or in the case of energy - independent (constant) reduction of the ^{8}B ν_e flux at $E_\nu \geq 5$ MeV, we would have $N^s(T_e) =$ *const*. The spectrum ratio $N^s(T_e)$ shows the magnitude and the shape of the e^- spectrum deformations (with respect to the standard spectrum) due to the MSW effect taking place in the Sun only, as well as in the Sun and when the solar ν_e cross the Earth mantle only, the Earth core, or the mantle only + the core.

The second observable we consider is the D-N asymmetry in the recoil-e^- spectrum for the three solar neutrino event samples, associated with the MSW effect in the Earth:

$$\mathcal{A}^s_{D-N}(T_e) = 2\,\frac{\mathcal{S}^s(T_e) - \mathcal{S}^D(T_e)}{\mathcal{S}^s(T_e) + \mathcal{S}^D(T_e)}, \qquad s = N,\, C,\, M. \tag{19}$$

The third observable is the energy integrated event rate asymmetry [8]:

$$A^s_{D-N}(T_{e,th}) \equiv A^s_{D-N} = 2\,\frac{\mathcal{R}^s - \mathcal{R}^D}{\mathcal{R}^s + \mathcal{R}^D}, \qquad s = N,\, C,\, M. \tag{20}$$

The shape of the ^{8}B neutrino spectrum and the asymmetries $\mathcal{A}^s_{D-N}(T_e)$ and $A^s_{D-N}(T_{e,th})$ are solar model independent observables.

The observation of a nonzero D-N asymmetry $\mathcal{A}^s_{D-N}(T_e) \neq 0$ and/or $A^s_{D-N}(T_{e\ th}) \neq 0$ would be a very strong evidence (if not a proof) that solar neutrinos undergo MSW transitions. If, for instance, nonzero *Core* and *Mantle* (or *Night*) asymmetries will be observed, the magnitudes of these asymmetries can indicate, in particular, whether the solar ν_e undergo transitions into active or sterile neutrinos (see further).

The one year averaged spectrum ratio $N^s(T_e)$, $s = D,\, N,\, C,\, M$, and the spectrum and event rate D-N asymmetries $\mathcal{A}^s_{D-N}(T_e)$ and A^s_{D-N}, $s = N,\, C,\, M$, for the Super - Kamiokande detector have been calculated for 39 pairs of values of Δm^2 and $\sin^2 2\theta_V$ distributed evenly in the "conservative" MSW $\nu_e \rightarrow \nu_s$ transition solution regions, eqs. (3) - (4) and (5) - (6). These values together with the corresponding results for $A^{N,C,M}_{D-N}$ and for the ratio A^C_{D-N}/A^N_{D-N}, are given in Tables I - VII. The predicted event rates for the *Day*, *Night*, *Core* and *Mantle* samples for the two values of Y_e in the Earth core considered by us, $Y_e(core) = 0.467$ and 0.50, are given in Tables I, V, VI and VII in units of the rates, calculated in the standard solar model [14] with "conventionally" behaving solar neutrinos and multiplied by the ^{8}B neutrino flux factor $f_B = \Phi_B/\Phi_B^{BP}$ (see, e.g., [16] and [2]) given in the Tables. Tables II - IV contain the results for the D-N asymmetries A^s_{D-N}, $s = N,\, C,\, M$, and for the ratio A^C_{D-N}/A^N_{D-N} for $Y_e(core) = 0.467$ *and* 0.50. The asymmetries given in Tables II - IV have been calculated for two values of the threshold recoil$-e^-$ kinetic energy: $T_{e,th} = 5.0$ MeV *and* 7.5 MeV. Some of the results obtained for $N^s(T_e)$ and $\mathcal{A}^s_{D-N}(T_e)$ are presented graphically in Figs. 4.1 - 4.16. Finally, Figs. 5a - 5b, Figs. 6a - 6d, and Figs. 7a - 7b contain plots of contours in the Δm^2 - $\sin^2 2\theta_V$ plane, corresponding respectively to fixed values of the event rate asymmetries A^N_{D-N}, A^C_{D-N}, and A^M_{D-N} (iso - (D-N) asymmetry contours) in the region of $\sin^2 2\theta_V \geq 10^{-4}$, 10^{-7} eV$^2 \leq \Delta m^2 \leq 10^{-4}$ eV^2. The iso-(D-N) asymmetry contour plots are derived for electron number fraction in the core $Y_e(core) = 0.467$ (Figs. 5a, 5b, 6a and 6c) and $Y_e(core) = 0.50$ (Figs. 5a, 5b, 6b and 6d), and for $T_{e,th} = 5.0$ MeV (Figs. 5a, 6a, 6b, and 7a) and $T_{e,th} = 7.5$ MeV (Figs. 5b, 6c, 6d and 7b).

---

[8] Note the difference between the definitions of the event rate D-N asymmetry used by us and that employed by the Super-Kamiokande collaboration, eq. (7).

5 The Earth Matter Effect and the Recoil$-e^-$ Spectrum

We shall discuss first the relation between the structures ("peaks") present in the probability asymmetries $\mathcal{A}^s_P$ (due to the Earth matter effect) and the structures in the corresponding spectrum D-N asymmetries $\mathcal{A}^s_{D-N}(T_e)$. For a given $\sin^2 2\theta$ the probabilities $< P_{e2} >^s$ and $P^s_\oplus$ and the asymmetries $\mathcal{A}^s_P$ are functions of $E_\nu/\Delta m^2$. If Δm^2 is given, a structure or "peak" in $\mathcal{A}^s_P(E_\nu/\Delta m^2)$ taking place at $E_\nu/\Delta m^2 = (E_\nu/\Delta m^2)_p$, would correspond to a structure in the solar neutrino distorted spectrum at $E_{\nu p} = \Delta m^2 (E_\nu/\Delta m^2)_p$. Qualitatively the effect of a "peak" in $\mathcal{A}^s_P$ will be maximal if the corresponding $E_{\nu p}$ is near the maximum in the neutrino spectrum, which for ^{8}B neutrinos is located at approximately 6.5 MeV. A necessary condition for the structure to appear in the solar neutrino spectrum obviously is $E^{min}_\nu \leq E_{\nu p} \leq E^{max}_\nu$, where E^{max}_ν (E^{min}_ν) is the maximal (minimal) solar ν_e energy to which a given detector is sensitive. In the case of the Super-Kamiokande experiment one has: $E^{max}_\nu \cong 14.4$ MeV, which is the maximal energy of the ^{8}B neutrino flux, and $E^{min}_\nu \cong 5.26$ MeV (7.76 MeV) if the threshold recoil-e^- kinetic energy is 5 MeV (7.5 MeV). Further, in the indicated energy intervals, the cross-section $d\sigma_{\nu_e}(T_e, E_\nu)/dT_e$, which enters into eq. (18) and is proportional to the probability that a solar neutrino having an energy E_ν will produce a recoil electron with a kinetic energy T_e, is practically T_e-independent and depends linearly on E_ν. This can lead, in particular, to a reduction in magnitude or disappearance ("filling") of the "peaks" present in the probability asymmetries $\mathcal{A}^s_P(E_\nu/\Delta m^2)$ when one calculates the D-N asymmetries in the recoil-e$^-$ spectrum, $\mathcal{A}^s_{D-N}(T_e)$. To illustrate this point consider two "peaks" in $\mathcal{A}^s_P$ located at $E_\nu/\Delta m^2 = (E_\nu/\Delta m^2)_1$ and at $E_\nu/\Delta m^2 = (E_\nu/\Delta m^2)_2$, with $(E_\nu/\Delta m^2)_2 < (E_\nu/\Delta m^2)_1$. Let us assume that $\mathcal{A}^s_P((E_\nu/\Delta m^2)_2) > 0$ and $\mathcal{A}^s_P((E_\nu/\Delta m^2)_1) < 0$. If for a chosen fixed Δm^2 one has, say, $E_2 < 14$ MeV and 15 MeV $< E_1$, where $E_{2,1} = \Delta m^2 (E_\nu/\Delta m^2)_{2,1}$, the asymmetry $\mathcal{A}^s_{D-N}(T_e)$ will also exhibit a "peak" at T_e located in the interval determined by the inequality:

$0.5T_e(1+\sqrt{1+2m_e/T_e}) < E_2$. However, if Δm^2 is such that $E_{1,2} < 14$ MeV, the integration over E_ν in eq. (18) can lead to a partial (or complete compensation) between the contributions in $\mathcal{A}^s_{D-N}(T_e)$ from the regions of the positive and the negative "peaks" in $\mathcal{A}^s_P(E_\nu/\Delta m^2)$ when T_e lies in the indicated interval. As a consequence, in such intervals $|\mathcal{A}^s_{D-N}(T_e)|$ can be considerably smaller than the corresponding $|\mathcal{A}^s_P(E_\nu/\Delta m^2)|$. It should be obvious from the above and the preceding discussions that the asymmetry $\mathcal{A}^s_{D-N}(T_e)$ can exhibit a strong dependence on the value of Δm^2, and that, in general, one can expect the extrema and the bulk of $\mathcal{A}^s_{D-N}(T_e)$ to be located at relatively large values of T_e, $T_e \gtrsim (8-9)$ MeV. Let us add that due to the differences between the $E_\nu/\Delta m^2$-dependence of the probabilities $P^s_\oplus$ corresponding to $\nu_e \rightarrow \nu_s$ and to $\nu_e \rightarrow \nu_{\mu(\tau)}$ transitions, discussed in Section 3, at small mixing angles these considerations are much more relevant for the $\nu_e \rightarrow \nu_s$ case than for the $\nu_e \rightarrow \nu_{\mu(\tau)}$ one.

The above remarks are well illustrated by Figs. 4.1 - 4.16, in which we show the recoil$-e^-$ spectrum distortions $N^s(T_e)$ (upper frames) and D-N asymmetries $\mathcal{A}^s_{D-N}(T_e)$ (lower frames) for selected representative sets of the parameters Δm^2 and $\sin^2 2\theta_V$, as functions of the recoil-e$^-$ kinetic energy T_e. The *short - dashed*, *solid* and *dotted* lines correspond to spectrum distortions or D-N asymmetries for the *Night*, *Core* and *Mantle* samples respectively, while the *long - dashed* lines correspond to the spectrum distortion for the *Day* sample. Figures 4.1 - 4.12 and figures 4.13 - 4.16 have been obtained for $Y_e(core) = 0.467$ and for $Y_e(core) = 0.50$, respectively.

At small mixing angles, $\sin^2 2\theta_V < 0.014$, the spectrum D-N asymmetry for the *Night* sample, $\mathcal{A}^N_{D-N}(T_e)$, is very small, $|\mathcal{A}^N_{D-N}(T_e)| \lesssim 0.01$ for 5 MeV $\leq T_e \leq$ 14 MeV, and seems hardly observable with the Super-Kamiokande detector. This conclusion is valid both for $Y_e(core) = 0.467$ and $Y_e(core) = 0.50$. For $\sin^2 2\theta \geq 0.014$ the spectrum deformations due to the Earth matter effect and the asymmetry $\mathcal{A}^N_{D-N}(T_e)$ increase with the increasing of $\sin^2 2\theta$ and become nonnegligible at large mixing angles. For $0.4 \lesssim \sin^2 2\theta \lesssim 0.5$, for instance, the asymmetry $\mathcal{A}^N_{D-N}(T_e)$ is typically bigger than (15 - 20)% and for $Y_e(core) = 0.467$ ($Y_e(core) = 0.50$) it can be as large as 40% (50%) in the interval of values of $T_e = (5-14)$ MeV of interest.

In the case of the *Core* sample, the effect of the core enhancement is evident both in the $e^-$$-$spectrum distortions and in the corresponding D-N spectrum asymmetry $\mathcal{A}^C_{D-N}(T_e)$, but at small mixing angles both are hardly detectable with the Super-Kamiokande detector. Because of the effect of "spectrum filling" discussed above, the largest value of $|\mathcal{A}^C_{D-N}(T_e)|$ is typically smaller than the largest value of $|\mathcal{A}^C_P(E_\nu/\Delta m^2)|$. For $Y_e(core) = 0.467$ and at $\sin^2 2\theta_V \leq 0.007$ the negative D-N effect is the only relevant feature and for $\sin^2 2\theta_V > 0.001$ the negative spectrum asymmetry can be larger in absolute value than 1% and can reach a maximum of 3%, provided the Δm^2 value does not "push" the region of the negative "peak" in $\mathcal{A}_P^C$ above the ^{8}B neutrino spectrum upper end. The latter typically occurs for $\Delta m^2 \gtrsim (7-8) \times 10^{-6}$ eV^2. Due to the "spectrum filling", positive values of $\mathcal{A}_{D-N}^C(T_e) \gtrsim 1\%$ do not appear in the interval $T_e = (5-14)$ MeV as long as $\sin^2 2\theta_V < 0.008$. At $\sin^2 2\theta_V = 0.009$, for instance, $\mathcal{A}_{D-N}^C(T_e)$ takes both positive and negative values going through zero in the indicated interval if $\Delta m^2 = 4 \times 10^{-6}$ eV^2 (Figs. 4.6 and 4.13), while for $\Delta m^2 = 5 \times 10^{-6}$ eV^2 (Figs. 4.7 and 4.14) the "filling" is less relevant since the negative " peak" in $\mathcal{A}_P^C$ is located (in E_ν) above the upper limit of the ^{8}B neutrino spectrum. For $\sin^2 2\theta_V \cong 0.014$ we have $\mathcal{A}_{D-N}^C(T_e) > 0$ and the spectrum asymmetry can be as large as 16% for $Y_e(core) = 0.467$.

At large mixing angles (Figs. 4.10 - 4.12), the presence of a negative D-N effect in $\mathcal{A}_P^C(E_\nu/\Delta m^2)$ (Figs. 3.11 - 3.12) is reflected in $\mathcal{A}_{D-N}^C(T_e)$. However, together with the dominant positive "peak" in $\mathcal{A}_P^C(E_\nu/\Delta m^2)$, it is located (in E_ν) beyond the ^{8}B neutrino spectrum upper limit if $\Delta m^2 > 8.5 \times 10^{-6}$ eV^2, and therefore both have little effect on any of the D-N effect observables for $\Delta m^2 > 8.5 \times 10^{-6}$ eV^2 (see, e.g., Fig. 4.10). The "spectrum filling" effect is evident at $\sin^2 2\theta_V = 0.4$, for instance, if we compare the two $\mathcal{A}_{D-N}^C(T_e)$ plots, Figs. 4.10 and 4.11, obtained for $\Delta m^2 = 6 \times 10^{-6}$ eV^2 and for $\Delta m^2 = 8 \times 10^{-6}$ eV^2. At $\Delta m^2 = 6 \times 10^{-6}$ eV^2, the spectrum asymmetry $\mathcal{A}_{D-N}^C(T_e)$ changes from (+50%) at $T_e \cong 7$ MeV to (-50%) at $T_e \cong 12$ MeV. For $\sin^2 2\theta_V = 0.5$, the asymmetry $\mathcal{A}_{D-N}^C(T_e)$ is maximal at $\Delta m^2 \cong 8 \times 10^{-6}$ eV^2, reaching approximately the value of +70% at $T_e \cong 11.5$ MeV. The *Night* and *Mantle* spectrum asymmetries, $\mathcal{A}_{D-N}^N(T_e)$ and $\mathcal{A}_{D-N}^M(T_e)$, are positive at large mixing angles, having values between 15% and 45%.

Changing the value of $Y_e(core)$ from 0.467 to 0.50 leads to small (insignificant) changes of the spectrum asymmetries $\mathcal{A}_{D-N}^C(T_e)$ and $\mathcal{A}_{D-N}^N(T_e)$ as long as $\sin^2 2\theta \lesssim 0.007$. However, for $\sin^2 2\theta_V \geq 0.008$, the asymmetry $|\mathcal{A}_{D-N}^C(T_e)|$ increases by a factor which can be as large as 2. For $\sin^2 2\theta_V = 0.5$ and, e.g., $\Delta m^2 = 8 \times 10^{-6}$ eV^2, $\mathcal{A}_{D-N}^C(T_e)$ reaches 85%, so that a 7% increase in $Y_e(core)$ produces nearly a 20% increase in the maximal value of $\mathcal{A}_{D-N}^C(T_e)$.

6 Event Rate D-N Asymmetries

Our results for the magnitudes of the event rate D-N asymmetries in the *Night*, *Core* and *Mantle* samples are collected in Tables II - IV and in Figs. 5a - 5b, 6a - 6d and 7a - 7b. In what follows we will comment on these results.

We begin with a discussion of the *Night* and *Mantle* sample asymmetries to be expected for Δm^2 and $\sin^2 2\theta$ from the "conservative" $\nu_e \rightarrow \nu_s$ solution regions. For $\sin^2 2\theta \ \leq 0.010$ the *Night* asymmetry is never bigger than approximately 1.25%: $|A^N_{D-N}| \lesssim 1.25\%$. Actually, the value of 1.25% is reached for $Y_e(core) = 0.50$ and $T_{e,th} = 7.5$ MeV at $\sin^2 2\theta = 0.010$ (Table IV). For $T_{e,th} = 5.0$ MeV and $Y_e(core) = 0.467$ (0.50), we have in the indicated small mixing angle region (Table II): $|A^N_{D-N}| \lesssim 0.70\%$ (1.17%), the maximal values corresponding again to $\sin^2 2\theta = 0.010$. The asymmetry in the *Mantle* sample, A^M_{D-N}, is typically smaller in absolute value than the *Night* sample asymmetry, $|A^N_{D-N}|$, by a factor of (1.5 - 2.0).

At $\sin^2 2\theta \cong 0.014$ the asymmetry A^N_{D-N} is considerably larger: for $Y_e(core) = 0.467$ and $T_{e,th} =$ 5.0 (7.5) MeV, it varies approximately between 1.8% (2.0%) and 3.0% (3.7%) depending on the solution value of Δm^2. The change of the threshold energy from 5.0 MeV to 7.5 MeV leads to an increase of A^N_{D-N}. The increase is much more dramatic - approximately by a factor of (1.5 - 2.0), if $Y_e(core) = 0.50$ instead of 0.467 (Table II). The *Mantle* asymmetry continues to be 1.5 to 2.0 times smaller than the *Night* asymmetry and changes insignificantly when $T_{e,th} = 5.0$ MeV is replaced by $T_{e,th} = 7.5$ MeV.

It should be noted that as a result of the differences between the Earth matter effect in the cases of the $\nu_e \rightarrow \nu_s$ and the $\nu_e \rightarrow \nu_{\mu(\tau)}$ solutions of the solar neutrino problem discussed in detail in Sections 2, 3 and 5, at small mixing angles, $0.006 \lesssim \sin^2 2\theta \lesssim 0.01$, the *Night* and the *Mantle* D-N asymmetries under study are substantially smaller than the asymmetries predicted for the $\nu_e \rightarrow \nu_{\mu(\tau)}$ solution [1]. For $\sin^2 2\theta = 0.008$ (0.01), for instance, and for $Y_e(core) = 0.467$ and $T_{e,th} = 5.0$ MeV, the *Night* sample asymmetry corresponding to the $\nu_e \rightarrow \nu_{\mu(\tau)}$ solution, $A^N_{D-N}(active)$, exceeds the asymmetry $|A^N_{D-N}(sterile)|$ in the case of the $\nu_e \rightarrow \nu_s$ solution by a factor which, depending on the chosen values of Δm^2 from the corresponding solution regions, varies between [9] approximately 4 and 25 (see Table II in [1] and Table II in this article). The analogous factor for the *Mantle* asymmetry is smaller: it varies typically between 2 and 9.

At large mixing angles, $\sin^2 2\theta \cong (0.40 - 0.50)$, the *Night* and the *Mantle* asymmetries are of the same order, both exceeding 18% and having maximal values of $\sim$ 40%. Both asymmetries A^N_{D-N} and A^M_{D-N} increase by 10% to 20%, depending on the value of Δm^2 from the solution region, when $Y_e(core) = 0.467$ is changed to $Y_e(core) = 0.50$ and/or when $T_{e,th} = 7.5$ MeV is used instead of

---

[9] For the same Δm^2 values from the overlapping region of the two solutions the factor ranges between approximately 4 and 15.

$T_{e,th} = 5.0$ MeV. Both A^N_{D-N} and A^M_{D-N} have their smaller values in the considered $\sin^2 2\theta$ interval for $Y_e(core) = 0.467$ and $T_{e,th} = 5.0$ MeV.

Adding the systematic and the statistical errors in eq. (7) in quadratures, we find that at 95% C.L. the Super-Kamiokande result on the D-N asymmetry in the *Night* sample implies: $A^N_{D-N} \leq 17.4\%$. This rules out (at the indicated confidence level) the "conservative" adiabatic region (eqs. (5) - (6)) of the $\nu_e \rightarrow \nu_s$ transition solution. The large mixing angle $\nu_e \rightarrow \nu_s$ adiabatic solution was possible only for rather large values of the ^{8}B neutrino flux [16].

Consider next the *Core* asymmetry, A^C_{D-N}. At small mixing angles and for values of Δm^2 from the "conservative" solution region, $|A^C_{D-N}|$ is bigger (due to the core enhancement) than $|A^N_{D-N}|$ by a factor of approximately (3 - 4) if $\Delta m^2 \; < 5 \times 10^{-6}$ eV^2, and by a factor of $\sim (1.5 - 2.5)$ for $\Delta m^2 \; \gtrsim 5 \times 10^{-6}$ eV^2 (Table II). In the solution region where $0.0012 \lesssim \; \sin^2 2\theta \lesssim 0.008$ and $\Delta m^2 \lesssim 4 \times 10^{-6}$ eV^2, one has $(-2\%) \lesssim A^C_{D-N} \lesssim (-1\%)$. For $\sin^2 2\theta \; \gtrsim 0.009$ and $\Delta m^2 \lesssim 4.4 \times 10^{-6}$ eV^2 the asymmetry is positive and $A^C_{D-N} \geq 1\%$. The asymmetry A^C_{D-N} has a minimum in the interval $0.008 \lesssim \; \sin^2 2\theta \lesssim 0.03$ at $\Delta m^2 \cong 6.0 \times 10^{-6}$ eV^2 and for this value of Δm^2 we have $A^C_{D-N} \geq 1\%$ only when $\sin^2 2\theta \geq 0.012$. Changing the threshold energy $T_{e,th}$ from 5 MeV to 7.5 MeV typically increases $|A^C_{D-N}|$ for $\sin^2 2\theta \lesssim 0.03$ by a factor of $\sim (1.2 - 1.5)$ if $\Delta m^2 \lesssim 5 \times 10^{-6}$ eV^2, decreases somewhat $|A^C_{D-N}|$ if $\Delta m^2 \; \cong \; (6 - 7) \times 10^{-6}$ eV^2, and practically does not change the asymmetry when $\Delta m^2 \; \sim 5.5 \times 10^{-6}$ eV^2 (Table III). In the region $0.0012 \lesssim \; \sin^2 2\theta \lesssim 0.008$, $\Delta m^2 \lesssim 4 \times 10^{-6}$ eV^2, for instance, for $T_{e,th} = 7.5$ MeV we get $(-3\%) \lesssim A^C_{D-N} \lesssim (-1\%)$. The asymmetry A^C_{D-N}, however, is rather sensitive to the value of Y_e(core). The dependence of A^C_{D-N} on Y_e(core) is particularly strong in the solution interval $0.0075 \lesssim \; \sin^2 2\theta \lesssim 0.030$, where a change of the value of Y_e(core) from 0.467 to 0.50 leads to an increase of A^C_{D-N} by a factor of $\sim (2 - 4)$.

The *Core* sample asymmetry in the case of the $\nu_e \rightarrow \nu_s$ solution under study, A^C_{D-N}(sterile), is substantially smaller than the *Core* asymmetry, A^C_{D-N}(active), predicted for the $\nu_e \rightarrow \nu_{\mu(\tau)}$ transition solution (see Table II in [1] and Table II in this article): the ratio of the absolute values of the two *Core* asymmetries $|A^C_{D-N}(active)/A^C_{D-N}(sterile)|$ in the small mixing angle region $0.006 \lesssim \; \sin^2 2\theta \lesssim 0.014$ where A^C_{D-N}(active) $\; \geq 1\%$, is always greater than 3.5, can be as large as 40 (for, e.g., $\Delta m^2 = 7 \times 10^{-6}$ eV^2 and $\sin^2 2\theta = 0.008$) and is typically [10] between 5 and 10.

The specific features of the three energy-integrated event rate D-N asymmetries, A^N_{D-N}, A^C_{D-N}

---

[10] As our results show, the naive suggestion that $|A^s_{D-N}(sterile)| > |A^s_{D-N}(active)|$, made e.g. in ref. [25] and the discussion based on it, are incorrect.

and A^{M}_{D-N}, discussed above can also be seen on the iso-(D-N) asymmetry contour plots derived in the region 10^{-7} eV$^2 \leq \Delta m^2 \leq 10^{-4}$ eV^2, $10^{-4} \leq \sin^2 2\theta \leq 1.0$ and shown in Figs. 5a - 5b, 6a - 6d and 7a - 7b [11].

It follows from the above results that probing experimentally the region of the SMA solution via the D-N effect with the Super-Kamiokande detector will require a much higher precision in the case of solar neutrino transitions into sterile neutrino than if the solar ν_e transitions were into an active neutrino.

7 D-N Asymmetry Measurements: Discriminating Between the $\nu_e \rightarrow \nu_{\mu(\tau)}$ and the $\nu_e \rightarrow \nu_s$ Transition Solutions

If two-neutrino MSW transitions of the solar neutrinos are at the origin of the solar neutrino problem, it will be of fundamental importance to determine whether the transitions are into active or into sterile neutrinos, or into a mixture of active and sterile neutrinos. The solar $\nu_e \rightarrow \nu_s$ transitions produce (for given Δm^2 and $\sin^2 2\theta$) larger distortions of the recoil-e$^-$ spectrum which is being measured in the Super-Kamiokande experiment, than the $\nu_e \rightarrow \nu_{\mu(\tau)}$ transitions [16] (see also [26]). The two MSW solutions of the solar neutrino problem imply very different values of the ratio of the charged current (CC) and the neutral current (NC) event rates, $R_{CC/NC}$, to be measured with the SNO detector [4]. An unambiguous proof that the solar neutrinos undergo transitions into sterile neutrino would be the observation of a nonzero D-N asymmetry in the NC signal due to the solar neutrinos in the SNO detector [16]: the indicated asymmetry is zero in the case of $\nu_e \rightarrow \nu_{\mu(\tau)}$ transitions. Other possible tests of the hypothesis of $\nu_e \rightarrow \nu_s$ conversion of solar neutrinos which can be performed utilizing the Super-Kamiokande and SNO data were considered in ref. [27].

If the solar neutrinos undergo two-neutrino matter-enhanced transitions generated by the existence of nonzero neutrino masses and mixing, the measurement of the D-N asymmetries in the *Core* and the *Mantle* samples of events, which are two independent observables, can also give information about the type of the transitions: $\nu_e \to \nu_s$ or $\nu_e \to \nu_{\mu(\tau)}$. In the brief qualitative discussion which follows we neglect the uncertainties in the Earth core density and chemical composition, consider the case of $T_{e,th} = 5$ MeV and analyze the small mixing angle solutions only. A complete quantitative study of the indicated possibility is beyond the scope of the present paper and will be given elsewhere [28].

---

[11] Let us note that the most interesting feature in A^{C}_{D-N} at large mixing angles is the negative D-N effect producing a "hole", i.e., a deep minimum, in A^{C}_{D-N} at $\sin^2 2\theta_V \approx 0.5$, $\Delta m^2 \approx 3.5 \times 10^{-6}$ eV^2. The "hole" is clearly seen in Figs. 6a - 6b (Figs. 6c - 6d) where for graphical reasons only the iso-asymmetry contour lines for $A^{C}_{D-N} \geq -0.02$ (-0.03) are displayed in the region of the "hole". The value of the asymmetry reached at the "bottom" of the "hole" for $Y_e(core) = 0.467$ is $A^{C}_{D-N} = -49\%$ (-51%) for $T_{e,th} = 5.0$ (7.5) MeV, while if $Y_e(core) = 0.5$ the minimum value reads -51% (-91%).

The mean event rate data from the different solar neutrino experiments determine the $\nu_e \to \nu_s$ and $\nu_e \to \nu_{\mu(\tau)}$ solution regions in the $\Delta m^2 - \sin^2 2\theta_V$ plane. With the improvement of the data the regions will diminish in size. The values of the two D-N effect asymmetries A^C_{D-N} and A^M_{D-N}, derived from the data, must correspond to one and the same set (or range) of values Δm^2 and $\sin^2 2\theta_V$. Suppose, for instance, that the measurement of the *Mantle* sample asymmetry gives the upper limit: $A^M_{D-N} < 2.5\%$. For the small mixing angle solution values of Δm^2 and $\sin^2 2\theta_V$, which are compatible with the above limit, the asymmetries $A^C_{D-N}(active)$ and $A^C_{D-N}(sterile)$ corresponding to the $\nu_e \to \nu_s$ and $\nu_e \to \nu_{\mu(\tau)}$ transitions are also limited from above: $A^C_{D-N}(active) \leq 30\%$ and $A^C_{D-N}(sterile) \leq 20\%$ (see Figs. 3b and 3c in ref. [2] and Figs. 6a and 7a). An observation of a *Core* sample asymmetry which is definitely greater than 20% would imply that the solar ν_e transitions are of the type $\nu_e \to \nu_{\mu(\tau)}$, while if the measured value of A^C_{D-N} is smaller than 20%, no unambiguous conclusion about the type of the transition can be drawn. Similarly, an experimental upper limit on A^M_{D-N} of 1% and a measured value of the *Core* sample asymmetry bigger than 10% would mean that the solar neutrinos undergo transitions into an active neutrino since in this case $A^C_{D-N}(sterile) \leq 10\%$. It should be obvious that if only upper limits on the *Core* and the *Mantle* sample asymmetries would be obtained from the data, no definite conclusion concerning the type of the solar neutrino transitions could be made.

8 Conclusions

In the present article we have performed a rather detailed quantitative study of the D-N effect for the Super-Kamiokande detector for the solution of the solar neutrino problem involving two-neutrino matter-enhanced transitions of the solar neutrinos into a sterile neutrino, $\nu_e \to \nu_s$. The one year average D-N asymmetry, A^s_{D-N}, has been calculated (using the high precision methods developed in refs. [1, 2]) for three samples of events, *Mantle* (M) , *Core* (C) and *Night* (N), produced respectively by the solar neutrinos crossing the Earth mantle only, the Earth core, and by the only mantle crossing + the core crossing neutrinos (the full night sample). The asymmetry calculations require the knowledge of the one year averaged spectrum of the recoil electrons and energy-integrated even rate, produced by the solar neutrinos during the day (the *Day* sample). Results for the D-N asymmetry in the recoil-e$^-$ spectrum for the same three samples of events, $\mathcal{A}^s_{D-N}(T_e)$, s=N,C,M, have also been obtained. The asymmetries have been calculated for a large representative set of values of the neutrino transition parameters Δm^2 and $\sin^2 2\theta$ from the "conservative" $\nu_e \rightarrow \nu_s$ transition solution regions (eqs. (3) - (6)), derived by taking into account the possible uncertainties in the predictions for the ^{8}B and ^{7}Be neutrino fluxes. We have investigated the dependence of the three D-N asymmetries studied, on the recoil-e$^-$ kinetic energy threshold $T_{e,th}$, which can be varied in the Super-Kamiokande experiment, by performing calculations of all the indicated D-N asymmetries for $T_{e,th} = 5.0$ MeV and $T_{e,th} = 7.5$ MeV. The effect of the estimated uncertainties in the knowledge of the bulk matter density and the chemical composition of the Earth core [20, 21, 22] on the predictions for the D-N asymmetries, has been studied as well by deriving results for $\mathcal{A}^s_{D-N}(T_e)$ and A^s_{D-N} both for the standard value of the electron number fraction in the core $Y_e(core) = 0.467$ and for the estimated conservative upper limit on $Y_e(core)$, $Y_e(core) = 0.50$ (see [22] and [1]). Iso-(D-N) asymmetry contour plots for the *Night*, *Core* and *Mantle* samples of events in the region 10^{-7} eV^2 $\leq$ Δm^2 $\leq 10^{-4}$ eV^2, 10^{-4} $\leq$ $\sin^2 2\theta_V$ $\leq$ 1, have been obtained for $T_{e,th} = 5.0$ MeV and $T_{e,th} = 7.5$ MeV, and for the *Night* and *Core* samples - for $Y_e(core) = 0.467$ and $Y_e(core) = 0.50$. The main results of this study are collected in Tables I - VII and are shown graphically in Figs. 4 - 7.

We have found that, as like in the case of the $\nu_e \rightarrow \nu_{\mu(\tau)}$ solution, the division of the data collected at night into a *Core* and *Mantle* samples is a rather effective method of enhancing the D-N asymmetry at small mixing angles, $0.001 \lesssim \sin^2 2\theta_V \lesssim 0.03$: the asymmetry in the *Core* sample $|A^C_{D-N}|$ is larger than the asymmetry in the *Night* sample $|A^N_{D-N}|$ typically by a factor of (3 - 4) if $\Delta m^2 < 5 \times 10^{-6}$ eV^2, and by a factor of $\sim (1.5 - 2.5)$ for 5×10^{-6} eV^2 $\lesssim \Delta m^2 \lesssim 8 \times 10^{-6}$ eV^2 (Table II). However, the enhancement is not as strong as in the case of the $\nu_e \rightarrow \nu_{\mu(\tau)}$ transition solution [1]. Moreover, in the interesting region $0.005 \lesssim \sin^2 2\theta_V \lesssim 0.014$ the D-N asymmetries in the *Core* and *Night* samples found for the $\nu_e \rightarrow \nu_s$ solution, $|A^C_{D-N}(sterile)|$ and $|A^N_{D-N}(sterile)|$, are substantially smaller - at least by a factor of 4 and typically by a factor of 5 to 10, than the asymmetries corresponding to the $\nu_e \rightarrow \nu_{\mu(\tau)}$ solution, $A^C_{D-N}(\text{active})$ and $A^N_{D-N}(\text{active})$. Similar conclusion is valid for the *Mantle* sample asymmetries. This remarkable difference in the magnitudes of the asymmetries $|A^s_{D-N}(sterile)|$ and $|A^s_{D-N}(active)|$ in the corresponding small mixing angle solution regions is a consequence of the different roles the neutron number density distribution in the Earth $n_n(r)$ plays in the solar neutrino transitions in the two cases: the $\nu_e \rightarrow \nu_{\mu(\tau)}$ transitions, as is well-known, depend only on the electron number density distribution, $n_e(r)$, while the $\nu_e \rightarrow \nu_s$ transitions depend on the difference $(n_e(r) - 0.5\ n_n(r))$. In the Sun one has [14] $0.5\ n_n(r) \ll n_e(r)$ and $n_n(r)$ influences little the $\nu_e \rightarrow \nu_s$ transitions. In contrast, due to the neutrality and approximate isotopic symmetry of the Earth matter, one has in the Earth: $n_e(r) - 0.5\ n_n(r) \cong 0.5\ n_e(r)$. This difference between the number density distributions $n_e(r)$ and $(n_e(r) - 0.5\ n_n(r))$ in the Earth is at the origin of the dramatic difference between the magnitudes of the D-N asymmetries corresponding to the small mixing angle $\nu_e \rightarrow \nu_s$ and $\nu_e \rightarrow \nu_{\mu(\tau)}$ transition solutions discussed above. Correspondingly, it leads to a shift towards smaller (by a factor of ~ 2) values of Δm^2 and larger values of $\sin^2 2\theta_V$ of the iso - D-N asymmetry contours in the $\Delta m^2 - \sin^2 2\theta_V$ plane corresponding to the $\nu_e \rightarrow \nu_s$ solution with respect to the analogous contours for the $\nu_e \rightarrow \nu_{\mu(\tau)}$ solution (compare Figs. 3a - 3c in [1] with Figs. 5a, 6a and 7a).

At small mixing angles even the *Core* asymmetry corresponding to the $\nu_e \rightarrow \nu_s$ solution is rather small (Table II, Fig. 6a): for $0.0012 \lesssim \sin^2 2\theta_V \lesssim 0.008$ and $2.8 \times 10^{-6}\ \mathrm{eV}^2 \lesssim \Delta m^2 \lesssim 4 \times 10^{-6}\ \mathrm{eV}^2$ we find $(-2\%) \lesssim A^C_{D-N}(sterile) \lesssim (-1\%)$. For other values of Δm^2 from the small mixing angle "conservative" solution region $0.001 \lesssim \sin^2 2\theta_V \lesssim 0.009$ one obtains $|A^C_{D-N}(sterile)| \leq 1\%$. We have $A^C_{D-N}(sterile) \gtrsim 1\%$ in the solution region $\sin^2 2\theta_V \gtrsim 0.009$ and $3.0 \times 10^{-6}\ \mathrm{eV}^2 \lesssim \Delta m^2 \lesssim 4.4 \times 10^{-6}\ \mathrm{eV}^2$. In addition, $A^C_{D-N}(\mathrm{sterile})$ has a minimum in the interval $0.008 \lesssim \sin^2 2\theta_V \lesssim 0.03$ at $\Delta m^2 \cong 6.0 \times 10^{-6}\ \mathrm{eV}^2$ and for this value of Δm^2 one has $A^C_{D-N} \geq 1\%$ only when $\sin^2 2\theta_V \geq 0.012$. The *Night* and *Mantle* asymmetries are larger than 1% in absolute value only if $\sin^2 2\theta > 0.010$ (Table II, Figs. 5a and 7a).

Replacing the threshold energy $T_{e,th} = 5$ MeV with 7.5 MeV can, depending on the SMA solution value of Δm^2, increase $|A^C_{D-N}|$ (by a factor $\sim (1.2 - 1.5)$), decrease it somewhat or leave the asymmetry practically the same; it changes little the magnitudes of A^N_{D-N} and A^M_{D-N}(Tables III and IV, Figs. 5b, 6c and 7b).

The asymmetries A^C_{D-N} and A^N_{D-N}, however, are rather sensitive to the value of Y_e(core) (Tables II - IV and Figs. 5a, 5b and 6a - 6d). The dependence of A^C_{D-N} and A^N_{D-N} on Y_e(core) is particularly strong in the "conservative" solution interval $0.0075 \lesssim \sin^2 2\theta_V < 0.030$, where a change of the value of Y_e(core) from 0.467 to 0.50 leads to an increase of $|A^C_{D-N}|$ and $|A^N_{D-N}|$ by factors of $\sim (2 - 4)$.

The predicted D-N asymmetries in the recoil-e^- spectrum for the three samples of events are small in the SMA solution region (Figs. 4.1 - 4.16). The spectrum asymmetry for the *Night* sample, for instance, at $\sin^2 2\theta_V < 0.014$ satisfies $|\mathcal{A}^N_{D-N}(T_e)| \lesssim 1\%$ for $5 \text{ MeV} \leq T_e \leq 14$ MeV, and is hardly observable with the Super-Kamiokande detector. This conclusion is valid both for $Y_e(core) = 0.467$ and $Y_e(core) = 0.50$. Analogous results are valid for the *Core* sample spectrum asymmetry $\mathcal{A}^C_{D-N}(T_e)$: one has $|\mathcal{A}^C_{D-N}(T_e)| \geq 4\%$ only if $\sin^2 2\theta_V \geq 0.01$; at $\sin^2 2\theta_V \cong 0.014$ the asymmetry $\mathcal{A}^C_{D-N}(T_e)$ reaches 16%.

The upper limit on the D-N asymmetry A^N_{D-N} following from the Super-Kamiokande data (eq. (7)) rules out (at 95% C.L.) the "conservative" large mixing angle (adiabatic) solution possible in the case of solar $\nu_e \rightarrow \nu_s$ transitions for unrealistically large values of the ^{8}B neutrino flux [16].

A qualitative analysis performed by us indicates that the measurement of the *Core* and *Mantle* sample asymmetries, which are independent observables, can help to discriminate between the $\nu_e \rightarrow \nu_{\mu(\tau)}$ and the $\nu_e \rightarrow \nu_s$ transition solutions of the solar neutrino problem.

The results obtained in the present study suggest that it will be difficult to probe the small mixing angle nonadiabatic $\nu_e \rightarrow \nu_s$ transition solution of the solar neutrino problem at $\sin^2 2\theta_V \lesssim 0.01$ by performing high precision measurements of the event rate and the recoil-e^- spectrum D-N asymmetries with the Super-Kamiokande detector. The precision required to test the indicated solution region exceeds, for most values of the parameters Δm^2 and $\sin^2 2\theta_V$ from the region, the precision in the D-N asymmetry measurements which is planned to be achieved in the Super-Kamiokande experiment.

Acknowledgments

We are indebted to the ICARUS group of the University of Pavia and INFN, Sezione di Pavia, and especially to Prof. E. Calligarich, for allowing the use of their computing facilities for the present study. M.M. wishes to thank Prof. A. Piazzoli for constant interest in the work and support and the International School for Advanced Studies, Trieste, where most of the work for this study has been done, for financial support. The work of S.T.P. was supported in part by the EEC grant ERBFMRXCT960090 and by Grant PH-510 from the Bulgarian Science Foundation.

References

[1] M. Maris and S.T. Petcov, Phys. Rev. D **56**, 7444 (1997).

[2] Q.Y. Liu, M. Maris and S.T. Petcov, Phys. Rev. D **56**, 5991 (1997).

[3] P.I. Krastev and S.T. Petcov, reported by S.T. Petcov in *"Neutrino '96"*, Proceedings of the Int. Conference on Neutrino Physics and Astrophysics, June 13 - 19, 1996, Helsinki, Finland (eds. K. Enqvist, K. Huitu and J. Maalampi, World Scientific, Singapore, 1997), p. 106; J.N. Bahcall, P.I. Krastev and A.Yu. Smirnov, work in progress; S.T. Petcov, in Proceedings of the 4th Int. Conference on Solar Neutrinos, April 8 - 11, 1997, Heidelberg, Germany (ed. W. Hampel, Max-Planck-Institut fur Kernphysik, Heidelberg, 1997), p. 309.

[4] P.I. Krastev and S.T. Petcov, unpublished.

[5] P.I. Krastev and A.Yu. Smirnov, Phys. Lett. 338B (1994) 282; V. Berezinsky, G. Fiorentini and M. Lissia, Phys. Lett. B **341**, 38 (1995); N. Hata and P. Langacker, Phys. Rev. D **52**, 420 (1995).

[6] A.J. Baltz and J. Weneser, Phys. Rev. D **50**, 5971 (1994).

[7] N. Hata and P. Langacker, Phys. Rev. D **50**, 632 (1994).

[8] J.M. Gelb, W. Kwong and S.P. Rosen, Phys. Rev. Lett. **78**, 2296 (1997).

[9] E. Lisi and D. Montanino, Phys. Rev. D **56**, 1792 (1997).

[10] J.N. Bahcall and P.I. Krastev, Phys. Rev. C **56**, 2839 (1997).

[11] N. Hata, Talk given at the Conference on Solar Neutrinos: News About SNUs, December 2 - 6, 1997, Institute of Theoretical Physics, University of California, Santa Barbara, U. S. A.

[12] M. Maris, in Proceedings of the 4th Int. Conference on Solar Neutrinos, April 8 - 11, 1997, Heidelberg, Germany (ed. W. Hampel, Max-Planck-Institut fur Kernphysik, Heidelberg, 1997), p. 342.

[13] M. Maris and S.T. Petcov, E-archive report hep-ph/9703207.

[14] J.N. Bahcall and M.H. Pinsonneault, Rev. Mod. Phys. **67**, 781 (1995).

[15] P.I. Krastev and S.T. Petcov, Nucl. Phys. B **449**, 605 (1995).

[16] P.I. Krastev, Q.Y. Liu and S.T. Petcov, Phys. Rev. D **54**, 7057 (1996).

[17] K.S. Hirata et al., Phys. Rev. D **44**, 2241 (1991) and Phys. Rev. Lett. **66**, 9 (1991).

[18] R. Svoboda (Super-Kamiokande collaboration), Talk given at the Conference on Solar Neutrinos: News About SNUs, December 2 - 6, 1997, Institute of Theoretical Physics, University of California, Santa Barbara, U. S. A.

[19] P. Langacker et al., Nucl. Phys. B **282**, 589 (1986).

[20] F.D. Stacey, *Physics of the Earth, 2^{nd} edition*, John Wiley and Sons, London, New York, 1977.

[21] A.D. Dziewonski and D.L. Anderson, Physics of the Earth and Planetary Interiors **25**, 297 (1981).

[22] R. Jeanloz, Annu. Rev. Earth Planet. Sci. **18**, 356 (1990); C.J. Allègre et al., Earth Planet. Sci. Lett. **134**, 515 (1995); W.F. McDonough and S.-s. Sun, Chemical Geology **120**, 223 (1995).

[23] J.N. Bahcall et al., Phys. Rev. D **54**, 411 (1996).

[24] J.N. Bahcall, M. Kamionkowski and A. Sirlin, Phys. Rev. D **51**, 6146 (1995).

[25] Q.Y. Liu and A.Yu. Smirnov, E-archive report hep-ph/9712493.

[26] W. Kwong and S.P. Rosen, Phys. Rev. D**51**, 6159 (1995).

[27] S.M. Bilenky and C. Giunti, Phys. Lett. B**320**, 323 (1994); Z. Phys. C**68**, 495 (1995).

[28] M. Maris and S.T. Petcov, in preparation.

Figure Captions

Figure 1. The dependence of the probability P_{e2} on ρ_r for $\sin^2 2\theta_V = 0.01$. The five plots are obtained for $0.1 \text{ gr/cm}^3 \leq \rho_r \leq 30.0 \text{ gr/cm}^3$ ($Y_e(mantle) = 0.49$, $Y_e(core) = 0.467$) and five different solar neutrino trajectories in the Earth determined by the Nadir angle $\hat{h}$: a) center crossing ($\hat{h} = 0°$), b) winter solstice for the Super - Kamiokande detector ($\hat{h} = 13°$), c) half core for the Super - Kamiokande detector ($\hat{h} = 23°$), d) core/mantle boundary ($\hat{h} = 33°$), e) half mantle ($\hat{h} = 51°$).

Figure 2. The dependence of the probability P_{e2} on ρ_r for $\sin^2 2\theta_V = 0.5$. The five plots were obtained for the same range of values of ρ_r and neutrino trajectories as in figure 1.

Figure 3.1 - 3.12 The probabilities $< P_{e2} >$, $\bar{P}_\odot$and $P_\oplus$ and the probability asymmetries $\mathcal{A}^s_P$ as functions of ρ_r and $E_\nu/\Delta m^2$. Each figure represents $< P_{e2} >$, $\bar{P}_\odot$, $P_\oplus$ and $\mathcal{A}^s_P$ for the value of $\sin^2 2\theta_V$ indicated in the figure. The frames (a) show the probability $< P_{e2} >$ as a function of the density ρ_r for the *Night* (*short - dashed line*), *Mantle* (*dotted line*) and *Core* (*solid line*) samples. In all calculations Y_e in the mantle and in the core was assumed to be equal respectively to 0.49 and 0.467. The frames (b), (c) and (d) represent the probabilities (upper parts) $\bar{P}_\odot$ (*dotted line*), $< P_{e2} >$ (*dashed line*) and $P_\oplus$ (*solid line*), and the probability asymmetry $\mathcal{A}^s_P$ (lower parts) corresponding to the *Night*, *Core* and *Mantle* samples as functions of $E_\nu/\Delta m^2$. In some cases $< P_{e2} >$ is multiplied by a factor of 10, which is indicated in the corresponding figure.

Figures 4.1 - 4.16. Recoil - e$^-$ spectrum distortion $N^s(T_e)$ (upper frame) and D-N asymmetry in the spectrum $\mathcal{A}^s_{D-N}$ (lower frame) (see eqs. 18 and 19) for the *Day* (*long-dashed line*), *Night* (*short-dashed line*), *Core* (*solid line*) and *Mantle* (*dotted line*) samples for $Y_e(mantle) = 0.49$, $Y_e(core) = 0.467$ (Figs. 4.1 - 4.12) and $Y_e(core) = 0.50$ (Figs. 4.13 - 4.16). The values of Δm^2 and $\sin^2 2\theta_V$ are indicated between the upper and the lower frames.

Figures 5a - 5b. One year average event rate iso - (D-N) asymmetry contour plots for the *Night* sample for the Super - Kamiokande detector for $T_{e,th} = 5.0$ (a) and $T_{e,th} = 7.5$ MeV (b). The *solid* (*dash-dotted*) lines correspond to $Y_e(core) = 0.467$ (0.50). The two light-grey areas limited by the dashed lines represent the "conservative" $\nu_e \rightarrow \nu_s$ solution regions, while the dark-grey area limited by the solid line represents the reference solution region obtained in the second study quoted in ref. [3] within the standard solar model [14].

Figures 6a - 6d. One year average event rate iso - (D-N) asymmetry contour plots for the *Core* sample for the Super - Kamiokande detector: figures (a) and (c) (b and d) correspond to $Y_e(core) =$

0.467 ($Y_e(core) = 0.5$), while figures (a) and (b) (c and d) were obtained for $T_{e,th} = 5$ MeV ($T_{e,th} = 7.5$ MeV). The light-grey and dark-grey regions are the same as in Figs. 5a - 5b.

Figures 7a - 7b. One year averaged event-rates iso - (D-N) asymmetry contour plots for the *Mantle* sample for the Super - Kamiokande detector: figure (a) was obtained for $T_{e,th} = 5$ MeV, while figure (b) corresponds to $T_{e,th} = 7.5$ MeV. The light-grey and dark-grey regions are the same as in Figs. 5a - 5b and 6a - 6d.

Table I. Event Rates for the Super - Kamiokande Detector for $Y_e(core) = 0.467$, $T_{e,th} = 5$ MeV.

N.	$\sin^2 2\theta_V$	Δm^2 [eV^2]	f_B	*Day*	*Night*	*Core*	*Mantle*
1	0.001	3×10^{-6}	0.35	0.9188	0.9167	0.9107	0.9177
2	0.001	5×10^{-6}	0.35	0.8721	0.8718	0.8712	0.8719
3	0.001	7×10^{-6}	0.35	0.8274	0.8273	0.8273	0.8273
4	0.002	3×10^{-6}	0.40	0.8446	0.8412	0.8311	0.8428
5	0.002	5×10^{-6}	0.40	0.7612	0.7608	0.7598	0.7610
6	0.002	7×10^{-6}	0.50	0.6858	0.6857	0.6856	0.6857
7	0.002	8×10^{-6}	0.50	0.6506	0.6505	0.6504	0.6505
8	0.003	3×10^{-6}	0.50	0.7765	0.7723	0.7601	0.7743
9	0.003	5×10^{-6}	0.50	0.6646	0.6642	0.6630	0.6644
10	0.003	7×10^{-6}	0.50	0.5691	0.5690	0.5690	0.5690
11	0.004	4×10^{-6}	0.50	0.6439	0.6422	0.6369	0.6431
12	0.004	5×10^{-6}	0.50	0.5809	0.5805	0.5795	0.5807
13	0.005	4×10^{-6}	0.50	0.5775	0.5762	0.5716	0.5769
14	0.005	6×10^{-6}	0.70	0.4472	0.4473	0.4473	0.4473
15	0.005	7×10^{-6}	0.70	0.3937	0.3939	0.3940	0.3938
16	0.007	3.3×10^{-6}	0.70	0.5270	0.5254	0.5206	0.5262
17	0.007	4×10^{-6}	0.70	0.4652	0.4649	0.4638	0.4651
18	0.007	5×10^{-6}	0.70	0.3896	0.3899	0.3901	0.3898
19	0.007	6×10^{-6}	1.00	0.3266	0.3270	0.3272	0.3270
20	0.008	3×10^{-6}	0.70	0.5121	0.5108	0.5075	0.5113
21	0.008	4×10^{-6}	0.70	0.4178	0.4183	0.4195	0.4181
22	0.008	5×10^{-6}	1.00	0.3416	0.3421	0.3430	0.3420
23	0.008	6×10^{-6}	1.00	0.2796	0.2802	0.2805	0.2801
24	0.008	7×10^{-6}	1.50	0.2292	0.2297	0.2302	0.2296
25	0.009	3×10^{-6}	0.70	0.4717	0.4718	0.4731	0.4716
26	0.009	4×10^{-6}	1.00	0.3755	0.3769	0.3808	0.3762
27	0.009	5×10^{-6}	1.00	0.2997	0.3007	0.3021	0.3004
28	0.009	6×10^{-6}	1.50	0.2397	0.2404	0.2408	0.2403
29	0.010	3×10^{-6}	1.00	0.4345	0.4364	0.4429	0.4354
30	0.010	4×10^{-6}	1.00	0.3377	0.3400	0.3468	0.3389
31	0.010	5×10^{-6}	1.00	0.2633	0.2645	0.2668	0.2642
32	0.014	4×10^{-6}	2.00	0.2221	0.2289	0.2493	0.2255
33	0.014	5×10^{-6}	2.00	0.1582	0.1611	0.1665	0.1601
34	0.400	6×10^{-6}	3.00	0.1130	0.1649	0.1704	0.1640
35	0.400	8×10^{-6}	3.00	0.1133	0.1513	0.1798	0.1466
36	0.400	1×10^{-5}	3.00	0.1137	0.1393	0.1467	0.1381
37	0.500	7×10^{-6}	2.00	0.1470	0.2017	0.2368	0.1960
38	0.500	8×10^{-6}	2.00	0.1471	0.1926	0.2222	0.1877
39	0.500	1×10^{-5}	2.00	0.1476	0.1787	0.1864	0.1774

Table II. D - N Asymmetries for the Super - Kamiokande Detector for $T_{e,th} = 5$ MeV.

				$Y_e(core) = 0.467$				$Y_e(core) = 0.500$			
				$A^s_{D-N} \times 100$			$\frac{\|A^C_{D-N}\|}{\|A^N_{D-N}\|}$	$A^s_{D-N} \times 100$			$\frac{\|A^C_{D-N}\|}{\|A^N_{D-N}\|}$
N.	$\sin^2 2\theta_V$	Δm^2	f_B	*Night*	*Core*	*Mantle*		*Night*	*Core*	*Mantle*	
1	0.001	3×10^{-6}	0.35	-0.22	-0.88	-0.12	3.97	-0.25	-1.08	-0.12	4.31
2	0.001	5×10^{-6}	0.35	-0.03	-0.11	-0.02	3.33	-0.07	-0.36	-0.02	5.25
3	0.001	7×10^{-6}	0.35	-0.01	-0.02	-0.01	1.60	-0.02	-0.06	-0.01	3.72
4	0.002	3×10^{-6}	0.40	-0.41	-1.60	-0.21	3.95	-0.45	-1.93	-0.21	4.28
5	0.002	5×10^{-6}	0.40	-0.06	-0.19	-0.03	3.47	-0.11	-0.61	-0.03	5.37
6	0.002	7×10^{-6}	0.50	-0.02	-0.02	-0.01	1.52	-0.02	-0.09	-0.01	3.72
7	0.002	8×10^{-6}	0.50	-0.02	-0.03	-0.01	1.79	-0.02	-0.07	-0.01	3.71
8	0.003	3×10^{-6}	0.50	-0.54	-2.13	-0.28	3.93	-0.60	-2.52	-0.28	4.23
9	0.003	5×10^{-6}	0.50	-0.07	-0.24	-0.04	3.63	-0.14	-0.74	-0.04	5.40
10	0.003	7×10^{-6}	0.50	-0.01	-0.01	-0.01	1.23	-0.02	-0.07	-0.01	3.71
11	0.004	4×10^{-6}	0.50	-0.25	-1.09	-0.12	4.29	-0.37	-1.90	-0.12	5.16
12	0.004	5×10^{-6}	0.50	-0.06	-0.24	-0.03	3.77	-0.13	-0.71	-0.03	5.51
13	0.005	4×10^{-6}	0.50	-0.24	-1.02	-0.11	4.35	-0.33	-1.68	-0.11	5.12
14	0.005	6×10^{-6}	0.70	0.01	0.02	0.01	1.80	0.01	0.02	0.01	1.32
15	0.005	7×10^{-6}	0.70	0.03	0.07	0.02	2.20	0.04	0.15	0.02	3.75
16	0.007	3.3×10^{-6}	0.70	-0.31	-1.24	-0.16	3.94	-0.30	-1.18	-0.16	3.86
17	0.007	4×10^{-6}	0.70	-0.06	-0.30	-0.02	5.35	-0.02	-0.06	-0.02	2.77
18	0.007	5×10^{-6}	0.70	0.07	0.12	0.06	1.75	0.15	0.69	0.06	4.60
19	0.007	6×10^{-6}	1.00	0.11	0.18	0.10	1.69	0.19	0.73	0.10	3.95
20	0.008	3×10^{-6}	0.70	-0.26	-0.90	-0.16	3.43	-0.20	-0.46	-0.16	2.28
21	0.008	4×10^{-6}	0.70	0.12	0.41	0.07	3.41	0.26	1.42	0.07	5.39
22	0.008	5×10^{-6}	1.00	0.17	0.41	0.13	2.43	0.36	1.74	0.13	4.84
23	0.008	6×10^{-6}	1.00	0.18	0.29	0.17	1.61	0.33	1.34	0.17	4.02
24	0.008	7×10^{-6}	1.50	0.23	0.43	0.20	1.87	0.35	1.25	0.20	3.58
25	0.009	3×10^{-6}	0.70	0.04	0.31	-0.01	8.20	0.16	1.17	-0.01	7.33
26	0.009	4×10^{-6}	1.00	0.36	1.39	0.19	3.82	0.66	3.42	0.19	5.20
27	0.009	5×10^{-6}	1.00	0.31	0.81	0.23	2.57	0.64	3.14	0.23	4.89
28	0.009	6×10^{-6}	1.50	0.29	0.46	0.26	1.58	0.53	2.16	0.26	4.06
29	0.010	3×10^{-6}	1.00	0.44	1.91	0.20	4.31	0.64	3.27	0.20	5.11
30	0.010	4×10^{-6}	1.00	0.69	2.68	0.35	3.90	1.17	5.98	0.35	5.10
31	0.010	5×10^{-6}	1.00	0.48	1.32	0.34	2.73	1.01	4.95	0.34	4.89
32	0.014	4×10^{-6}	2.00	3.00	11.52	1.52	3.84	4.75	22.27	1.52	4.69
33	0.014	5×10^{-6}	2.00	1.78	5.10	1.21	2.86	3.66	17.18	1.21	4.70
34	0.400	6×10^{-6}	3.00	37.34	40.50	36.81	1.08	40.05	57.23	36.81	1.43
35	0.400	8×10^{-6}	3.00	28.71	45.38	25.60	1.58	31.53	60.29	25.60	1.91
36	0.400	1×10^{-5}	3.00	20.23	25.36	19.37	1.25	21.13	31.19	19.37	1.48
37	0.500	7×10^{-6}	2.00	31.41	46.79	28.57	1.49	33.87	60.07	28.57	1.77
38	0.500	8×10^{-6}	2.00	26.74	40.63	24.21	1.52	28.65	51.38	24.21	1.79
39	0.500	1×10^{-5}	2.00	19.09	23.26	18.38	1.22	19.76	27.72	18.38	1.40

Table III. Threshold Energy Dependence of the D - N Asymmetries for $Y_e(core) = 0.467$.

				$T_{e,th} = 5$ MeV				$T_{e,th} = 7.5$ MeV			
				$A^s_{D-N} \times 100$			$\frac{\lvert A^C_{D-N}\rvert}{\lvert A^N_{D-N}\rvert}$	$A^s_{D-N} \times 100$			$\frac{\lvert A^C_{D-N}\rvert}{\lvert A^N_{D-N}\rvert}$
N.	$\sin^2 2\theta_V$	Δm^2	f_B	*Night*	*Core*	*Mantle*		*Night*	*Core*	*Mantle*	
1	0.001	3×10^{-6}	0.35	-0.22	-0.88	-0.12	3.97	-0.28	-1.06	-0.15	3.80
2	0.001	5×10^{-6}	0.35	-0.03	-0.11	-0.02	3.33	-0.05	-0.19	-0.03	3.95
3	0.001	7×10^{-6}	0.35	-0.01	-0.02	-0.01	1.60	-0.01	-0.02	-0.01	1.39
4	0.002	3×10^{-6}	0.40	-0.41	-1.60	-0.21	3.95	-0.51	-1.92	-0.28	3.80
5	0.002	5×10^{-6}	0.40	-0.06	-0.19	-0.03	3.47	-0.08	-0.33	-0.04	3.88
6	0.002	7×10^{-6}	0.50	-0.02	-0.02	-0.01	1.52	-0.02	-0.02	-0.02	1.17
7	0.002	8×10^{-6}	0.50	-0.02	-0.03	-0.01	1.79	-0.02	-0.03	-0.01	1.97
8	0.003	3×10^{-6}	0.50	-0.54	-2.13	-0.28	3.93	-0.68	-2.58	-0.37	3.79
9	0.003	5×10^{-6}	0.50	-0.07	-0.24	-0.04	3.63	-0.10	-0.41	-0.05	3.96
10	0.003	7×10^{-6}	0.50	-0.01	-0.01	-0.01	1.23	-0.01	-0.01	-0.01	1.02
11	0.004	4×10^{-6}	0.50	-0.25	-1.09	-0.12	4.29	-0.39	-1.69	-0.18	4.34
12	0.004	5×10^{-6}	0.50	-0.06	-0.24	-0.03	3.77	-0.10	-0.42	-0.05	4.05
13	0.005	4×10^{-6}	0.50	-0.24	-1.02	-0.11	4.35	-0.37	-1.59	-0.17	4.33
14	0.005	6×10^{-6}	0.70	0.01	0.02	0.01	1.80	0.00	-0.02	0.00	5.22
15	0.005	7×10^{-6}	0.70	0.03	0.07	0.02	2.20	0.02	0.05	0.02	2.44
16	0.007	3.3×10^{-6}	0.70	-0.31	-1.24	-0.16	3.94	-0.50	-1.95	-0.27	3.86
17	0.007	4×10^{-6}	0.70	-0.06	-0.30	-0.02	5.35	-0.14	-0.58	-0.06	4.25
18	0.007	5×10^{-6}	0.70	0.07	0.12	0.06	1.75	0.05	0.10	0.04	2.03
19	0.007	6×10^{-6}	1.00	0.11	0.18	0.10	1.69	0.08	0.07	0.08	0.90
20	0.008	3×10^{-6}	0.70	-0.26	-0.90	-0.16	3.43	-0.49	-1.72	-0.28	3.52
21	0.008	4×10^{-6}	0.70	0.12	0.41	0.07	3.41	0.09	0.41	0.04	4.44
22	0.008	5×10^{-6}	1.00	0.17	0.41	0.13	2.43	0.16	0.51	0.11	3.11
23	0.008	6×10^{-6}	1.00	0.18	0.29	0.17	1.61	0.14	0.14	0.14	1.00
24	0.008	7×10^{-6}	1.50	0.23	0.43	0.20	1.87	0.20	0.34	0.18	1.67
25	0.009	3×10^{-6}	0.70	0.04	0.31	-0.01	8.20	-0.19	-0.54	-0.13	2.94
26	0.009	4×10^{-6}	1.00	0.36	1.39	0.19	3.82	0.41	1.75	0.18	4.30
27	0.009	5×10^{-6}	1.00	0.31	0.81	0.23	2.57	0.32	1.06	0.20	3.28
28	0.009	6×10^{-6}	1.50	0.29	0.46	0.26	1.58	0.23	0.24	0.23	1.06
29	0.010	3×10^{-6}	1.00	0.44	1.91	0.20	4.31	0.23	1.02	0.09	4.52
30	0.010	4×10^{-6}	1.00	0.69	2.68	0.35	3.90	0.82	3.49	0.37	4.26
31	0.010	5×10^{-6}	1.00	0.48	1.32	0.34	2.73	0.53	1.79	0.32	3.38
32	0.014	4×10^{-6}	2.00	3.00	11.52	1.52	3.84	3.68	14.82	1.71	4.03
33	0.014	5×10^{-6}	2.00	1.78	5.10	1.21	2.86	2.00	6.82	1.18	3.41
34	0.400	6×10^{-6}	3.00	37.34	40.50	36.81	1.08	40.28	27.51	42.21	0.68
35	0.400	8×10^{-6}	3.00	28.71	45.38	25.60	1.58	34.15	57.48	29.53	1.68
36	0.400	1×10^{-5}	3.00	20.23	25.36	19.37	1.25	23.82	33.08	22.19	1.39
37	0.500	7×10^{-6}	2.00	31.41	46.79	28.57	1.49	36.10	52.94	32.94	1.47
38	0.500	8×10^{-6}	2.00	26.74	40.63	24.21	1.52	31.72	51.71	27.88	1.63
39	0.500	1×10^{-5}	2.00	19.09	23.26	18.38	1.22	22.37	30.19	21.01	1.35

Table IV. Threshold Energy Dependence of the D - N Asymmetries for $Y_e(core) = 0.5$.

				$T_{e,th} = 5$ MeV				$T_{e,th} = 7.5$ MeV			
				$A^s_{D-N} \times 100$			$\frac{\lvert A^C_{D-N}\rvert}{\lvert A^N_{D-N}\rvert}$	$A^s_{D-N} \times 100$			$\frac{\lvert A^C_{D-N}\rvert}{\lvert A^N_{D-N}\rvert}$
N.	$\sin^2 2\theta_V$	Δm^2	f_B	*Night*	*Core*	*Mantle*		*Night*	*Core*	*Mantle*	
1	0.001	3×10^{-6}	0.35	-0.25	-1.08	-0.12	4.31	-0.28	-1.07	-0.15	3.82
2	0.001	5×10^{-6}	0.35	-0.07	-0.36	-0.02	5.25	-0.10	-0.56	-0.03	5.50
3	0.001	7×10^{-6}	0.35	-0.02	-0.06	-0.01	3.72	-0.02	-0.08	-0.01	3.80
4	0.002	3×10^{-6}	0.40	-0.45	-1.93	-0.21	4.28	-0.51	-1.94	-0.28	3.80
5	0.002	5×10^{-6}	0.40	-0.11	-0.61	-0.03	5.37	-0.17	-0.96	-0.04	5.57
6	0.002	7×10^{-6}	0.50	-0.02	-0.09	-0.01	3.72	-0.03	-0.11	-0.02	3.78
7	0.002	8×10^{-6}	0.50	-0.02	-0.07	-0.01	3.71	-0.02	-0.09	-0.01	3.63
8	0.003	3×10^{-6}	0.50	-0.60	-2.52	-0.28	4.23	-0.68	-2.58	-0.37	3.79
9	0.003	5×10^{-6}	0.50	-0.14	-0.74	-0.04	5.40	-0.21	-1.17	-0.05	5.60
10	0.003	7×10^{-6}	0.50	-0.02	-0.07	-0.01	3.71	-0.03	-0.10	-0.01	3.83
11	0.004	4×10^{-6}	0.50	-0.37	-1.90	-0.12	5.16	-0.53	-2.68	-0.18	5.08
12	0.004	5×10^{-6}	0.50	-0.13	-0.71	-0.03	5.51	-0.21	-1.15	-0.05	5.55
13	0.005	4×10^{-6}	0.50	-0.33	-1.68	-0.11	5.12	-0.49	-2.45	-0.17	5.04
14	0.005	6×10^{-6}	0.70	0.01	0.02	0.01	1.32	-0.02	-0.11	0.00	7.01
15	0.005	7×10^{-6}	0.70	0.04	0.15	0.02	3.75	0.03	0.12	0.02	4.02
16	0.007	3.3×10^{-6}	0.70	-0.30	-1.18	-0.16	3.86	-0.51	-2.02	-0.27	3.92
17	0.007	4×10^{-6}	0.70	-0.02	-0.06	-0.02	2.77	-0.13	-0.57	-0.06	4.22
18	0.007	5×10^{-6}	0.70	0.15	0.69	0.06	4.60	0.13	0.68	0.04	5.16
19	0.007	6×10^{-6}	1.00	0.19	0.73	0.10	3.95	0.16	0.64	0.08	4.07
20	0.008	3×10^{-6}	0.70	-0.20	-0.46	-0.16	2.28	-0.45	-1.49	-0.28	3.27
21	0.008	4×10^{-6}	0.70	0.26	1.42	0.07	5.39	0.20	1.17	0.04	5.86
22	0.008	5×10^{-6}	1.00	0.36	1.74	0.13	4.84	0.38	2.02	0.11	5.32
23	0.008	6×10^{-6}	1.00	0.33	1.34	0.17	4.02	0.31	1.28	0.14	4.21
24	0.008	7×10^{-6}	1.50	0.35	1.25	0.20	3.58	0.33	1.22	0.18	3.69
25	0.009	3×10^{-6}	0.70	0.16	1.17	-0.01	7.33	-0.14	-0.24	-0.13	1.69
26	0.009	4×10^{-6}	1.00	0.66	3.42	0.19	5.20	0.66	3.50	0.18	5.30
27	0.009	5×10^{-6}	1.00	0.64	3.14	0.23	4.89	0.72	3.81	0.20	5.29
28	0.009	6×10^{-6}	1.50	0.53	2.16	0.26	4.06	0.50	2.14	0.23	4.26
29	0.010	3×10^{-6}	1.00	0.64	3.27	0.20	5.11	0.28	1.40	0.09	5.00
30	0.010	4×10^{-6}	1.00	1.17	5.98	0.35	5.10	1.25	6.43	0.37	5.13
31	0.010	5×10^{-6}	1.00	1.01	4.95	0.34	4.89	1.16	6.09	0.32	5.26
32	0.014	4×10^{-6}	2.00	4.75	22.27	1.52	4.69	5.29	24.50	1.71	4.63
33	0.014	5×10^{-6}	2.00	3.66	17.18	1.21	4.70	4.21	20.77	1.18	4.93
34	0.400	6×10^{-6}	3.00	40.05	57.23	36.81	1.43	42.11	41.51	42.21	0.99
35	0.400	8×10^{-6}	3.00	31.53	60.29	25.60	1.91	38.17	76.15	29.53	2.00
36	0.400	1×10^{-5}	3.00	21.13	31.19	19.37	1.48	25.29	41.97	22.19	1.66
37	0.500	7×10^{-6}	2.00	33.87	60.07	28.57	1.77	39.06	68.28	32.94	1.75
38	0.500	8×10^{-6}	2.00	28.65	51.38	24.21	1.79	34.46	65.56	27.88	1.90
39	0.500	1×10^{-5}	2.00	19.76	27.72	18.38	1.40	23.51	37.28	21.01	1.59

Table V. Event Rates for the Super - Kamiokande Detector for $Y_e(core) = 0.5$, $T_{e,th} = 5$ MeV.

N.	$\sin^2 2\theta_V$	Δm^2 [eV^2]	f_B	*Day*	*Night*	*Core*	*Mantle*
1	0.001	3×10^{-6}	0.35	0.9188	0.9165	0.9090	0.9177
2	0.001	5×10^{-6}	0.35	0.8721	0.8715	0.8690	0.8719
3	0.001	7×10^{-6}	0.35	0.8274	0.8273	0.8269	0.8273
4	0.002	3×10^{-6}	0.40	0.8446	0.8408	0.8285	0.8428
5	0.002	5×10^{-6}	0.40	0.7612	0.7604	0.7566	0.7610
6	0.002	7×10^{-6}	0.50	0.6858	0.6856	0.6852	0.6857
7	0.002	8×10^{-6}	0.50	0.6506	0.6505	0.6502	0.6505
8	0.003	3×10^{-6}	0.50	0.7765	0.7719	0.7572	0.7743
9	0.003	5×10^{-6}	0.50	0.6646	0.6637	0.6597	0.6644
10	0.003	7×10^{-6}	0.50	0.5691	0.5690	0.5687	0.5690
11	0.004	4×10^{-6}	0.50	0.6439	0.6415	0.6318	0.6431
12	0.004	5×10^{-6}	0.50	0.5809	0.5802	0.5768	0.5807
13	0.005	4×10^{-6}	0.50	0.5775	0.5756	0.5679	0.5769
14	0.005	6×10^{-6}	0.70	0.4472	0.4473	0.4473	0.4473
15	0.005	7×10^{-6}	0.70	0.3937	0.3939	0.3943	0.3938
16	0.007	3.3×10^{-6}	0.70	0.5270	0.5254	0.5209	0.5262
17	0.007	4×10^{-6}	0.70	0.4652	0.4651	0.4649	0.4651
18	0.007	5×10^{-6}	0.70	0.3896	0.3902	0.3923	0.3898
19	0.007	6×10^{-6}	1.00	0.3266	0.3272	0.3290	0.3270
20	0.008	3×10^{-6}	0.70	0.5121	0.5111	0.5098	0.5113
21	0.008	4×10^{-6}	0.70	0.4178	0.4189	0.4238	0.4181
22	0.008	5×10^{-6}	1.00	0.3416	0.3428	0.3475	0.3420
23	0.008	6×10^{-6}	1.00	0.2796	0.2806	0.2834	0.2801
24	0.008	7×10^{-6}	1.50	0.2292	0.2300	0.2321	0.2296
25	0.009	3×10^{-6}	0.70	0.4717	0.4724	0.4772	0.4716
26	0.009	4×10^{-6}	1.00	0.3755	0.3780	0.3886	0.3762
27	0.009	5×10^{-6}	1.00	0.2997	0.3016	0.3093	0.3004
28	0.009	6×10^{-6}	1.50	0.2397	0.2410	0.2449	0.2403
29	0.010	3×10^{-6}	1.00	0.4345	0.4373	0.4490	0.4354
30	0.010	4×10^{-6}	1.00	0.3377	0.3416	0.3585	0.3389
31	0.010	5×10^{-6}	1.00	0.2633	0.2659	0.2766	0.2642
32	0.014	4×10^{-6}	2.00	0.2221	0.2329	0.2778	0.2255
33	0.014	5×10^{-6}	2.00	0.1582	0.1641	0.1879	0.1601
34	0.400	6×10^{-6}	3.00	0.1130	0.1696	0.2037	0.1640
35	0.400	8×10^{-6}	3.00	0.1133	0.1558	0.2111	0.1466
36	0.400	1×10^{-5}	3.00	0.1137	0.1406	0.1557	0.1381
37	0.500	7×10^{-6}	2.00	0.1470	0.2069	0.2732	0.1960
38	0.500	8×10^{-6}	2.00	0.1471	0.1964	0.2489	0.1877
39	0.500	1×10^{-5}	2.00	0.1476	0.1799	0.1951	0.1774

Table VI. Event Rates for the Super - Kamiokande Detector for $Y_e(core) = 0.467$, $T_{e,th} = 7.5$ MeV.

N.	$\sin^2 2\theta_V$	Δm^2 [eV^2]	f_B	*Day*	*Night*	*Core*	*Mantle*
1	0.001	$3{\times}10^{-6}$	0.35	0.9284	0.9258	0.9187	0.9270
2	0.001	$5{\times}10^{-6}$	0.35	0.8873	0.8869	0.8856	0.8871
3	0.001	$7{\times}10^{-6}$	0.35	0.8479	0.8478	0.8478	0.8479
4	0.002	$3{\times}10^{-6}$	0.40	0.8623	0.8579	0.8458	0.8599
5	0.002	$5{\times}10^{-6}$	0.40	0.7875	0.7869	0.7850	0.7872
6	0.002	$7{\times}10^{-6}$	0.50	0.7194	0.7193	0.7192	0.7193
7	0.002	$8{\times}10^{-6}$	0.50	0.6872	0.6871	0.6870	0.6871
8	0.003	$3{\times}10^{-6}$	0.50	0.8008	0.7954	0.7805	0.7979
9	0.003	$5{\times}10^{-6}$	0.50	0.6989	0.6982	0.6961	0.6985
10	0.003	$7{\times}10^{-6}$	0.50	0.6104	0.6103	0.6103	0.6103
11	0.004	$4{\times}10^{-6}$	0.50	0.6792	0.6766	0.6679	0.6781
12	0.004	$5{\times}10^{-6}$	0.50	0.6205	0.6199	0.6180	0.6202
13	0.005	$4{\times}10^{-6}$	0.50	0.6170	0.6147	0.6072	0.6159
14	0.005	$6{\times}10^{-6}$	0.70	0.4926	0.4925	0.4925	0.4925
15	0.005	$7{\times}10^{-6}$	0.70	0.4403	0.4404	0.4405	0.4403
16	0.007	$3.3{\times}10^{-6}$	0.70	0.5684	0.5656	0.5574	0.5669
17	0.007	$4{\times}10^{-6}$	0.70	0.5091	0.5084	0.5062	0.5087
18	0.007	$5{\times}10^{-6}$	0.70	0.4351	0.4353	0.4355	0.4353
19	0.007	$6{\times}10^{-6}$	1.00	0.3721	0.3724	0.3723	0.3724
20	0.008	$3{\times}10^{-6}$	0.70	0.5539	0.5512	0.5445	0.5524
21	0.008	$4{\times}10^{-6}$	0.70	0.4626	0.4630	0.4645	0.4628
22	0.008	$5{\times}10^{-6}$	1.00	0.3868	0.3874	0.3887	0.3872
23	0.008	$6{\times}10^{-6}$	1.00	0.3236	0.3241	0.3241	0.3241
24	0.008	$7{\times}10^{-6}$	1.50	0.2709	0.2715	0.2719	0.2714
25	0.009	$3{\times}10^{-6}$	0.70	0.5148	0.5138	0.5120	0.5141
26	0.009	$4{\times}10^{-6}$	1.00	0.4205	0.4222	0.4279	0.4213
27	0.009	$5{\times}10^{-6}$	1.00	0.3439	0.3451	0.3476	0.3446
28	0.009	$6{\times}10^{-6}$	1.50	0.2817	0.2823	0.2823	0.2823
29	0.010	$3{\times}10^{-6}$	1.00	0.4784	0.4795	0.4833	0.4789
30	0.010	$4{\times}10^{-6}$	1.00	0.3823	0.3854	0.3959	0.3837
31	0.010	$5{\times}10^{-6}$	1.00	0.3060	0.3076	0.3115	0.3070
32	0.014	$4{\times}10^{-6}$	2.00	0.2619	0.2717	0.3038	0.2664
33	0.014	$5{\times}10^{-6}$	2.00	0.1926	0.1965	0.2062	0.1949
34	0.400	$6{\times}10^{-6}$	3.00	0.1129	0.1699	0.1490	0.1734
35	0.400	$8{\times}10^{-6}$	3.00	0.1131	0.1597	0.2044	0.1524
36	0.400	$1{\times}10^{-5}$	3.00	0.1134	0.1441	0.1584	0.1417
37	0.500	$7{\times}10^{-6}$	2.00	0.1468	0.2115	0.2525	0.2047
38	0.500	$8{\times}10^{-6}$	2.00	0.1469	0.2023	0.2494	0.1946
39	0.500	$1{\times}10^{-5}$	2.00	0.1472	0.1843	0.1996	0.1818

Table VII. Event Rates for the Super - Kamiokande Detector for $Y_e(core) = 0.5$, $T_{e,th} = 7.5$ MeV.

N.	$\sin^2 2\theta_V$	Δm^2 [eV^2]	f_B	*Day*	*Night*	*Core*	*Mantle*
1	0.001	3×10^{-6}	0.35	0.9284	0.9258	0.9185	0.9270
2	0.001	5×10^{-6}	0.35	0.8873	0.8864	0.8823	0.8871
3	0.001	7×10^{-6}	0.35	0.8479	0.8478	0.8473	0.8479
4	0.002	3×10^{-6}	0.40	0.8623	0.8579	0.8457	0.8599
5	0.002	5×10^{-6}	0.40	0.7875	0.7862	0.7800	0.7872
6	0.002	7×10^{-6}	0.50	0.7194	0.7192	0.7186	0.7193
7	0.002	8×10^{-6}	0.50	0.6872	0.6870	0.6866	0.6871
8	0.003	3×10^{-6}	0.50	0.8008	0.7954	0.7804	0.7979
9	0.003	5×10^{-6}	0.50	0.6989	0.6974	0.6908	0.6985
10	0.003	7×10^{-6}	0.50	0.6104	0.6102	0.6097	0.6103
11	0.004	4×10^{-6}	0.50	0.6792	0.6757	0.6613	0.6781
12	0.004	5×10^{-6}	0.50	0.6205	0.6193	0.6135	0.6202
13	0.005	4×10^{-6}	0.50	0.6170	0.6140	0.6020	0.6159
14	0.005	6×10^{-6}	0.70	0.4926	0.4925	0.4920	0.4925
15	0.005	7×10^{-6}	0.70	0.4403	0.4404	0.4408	0.4403
16	0.007	3.3×10^{-6}	0.70	0.5684	0.5655	0.5571	0.5669
17	0.007	4×10^{-6}	0.70	0.5091	0.5084	0.5062	0.5087
18	0.007	5×10^{-6}	0.70	0.4351	0.4357	0.4381	0.4353
19	0.007	6×10^{-6}	1.00	0.3721	0.3727	0.3745	0.3724
20	0.008	3×10^{-6}	0.70	0.5539	0.5514	0.5457	0.5524
21	0.008	4×10^{-6}	0.70	0.4626	0.4635	0.4681	0.4628
22	0.008	5×10^{-6}	1.00	0.3868	0.3882	0.3947	0.3872
23	0.008	6×10^{-6}	1.00	0.3236	0.3246	0.3278	0.3241
24	0.008	7×10^{-6}	1.50	0.2709	0.2718	0.2743	0.2714
25	0.009	3×10^{-6}	0.70	0.5148	0.5140	0.5135	0.5141
26	0.009	4×10^{-6}	1.00	0.4205	0.4233	0.4354	0.4213
27	0.009	5×10^{-6}	1.00	0.3439	0.3464	0.3573	0.3446
28	0.009	6×10^{-6}	1.50	0.2817	0.2831	0.2878	0.2823
29	0.010	3×10^{-6}	1.00	0.4784	0.4798	0.4852	0.4789
30	0.010	4×10^{-6}	1.00	0.3823	0.3871	0.4077	0.3837
31	0.010	5×10^{-6}	1.00	0.3060	0.3096	0.3252	0.3070
32	0.014	4×10^{-6}	2.00	0.2619	0.2762	0.3351	0.2664
33	0.014	5×10^{-6}	2.00	0.1926	0.2009	0.2373	0.1949
34	0.400	6×10^{-6}	3.00	0.1129	0.1732	0.1721	0.1734
35	0.400	8×10^{-6}	3.00	0.1131	0.1665	0.2523	0.1524
36	0.400	1×10^{-5}	3.00	0.1134	0.1463	0.1737	0.1417
37	0.500	7×10^{-6}	2.00	0.1468	0.2181	0.2991	0.2047
38	0.500	8×10^{-6}	2.00	0.1469	0.2081	0.2903	0.1946
39	0.500	1×10^{-5}	2.00	0.1472	0.1865	0.2147	0.1818

Figure 1

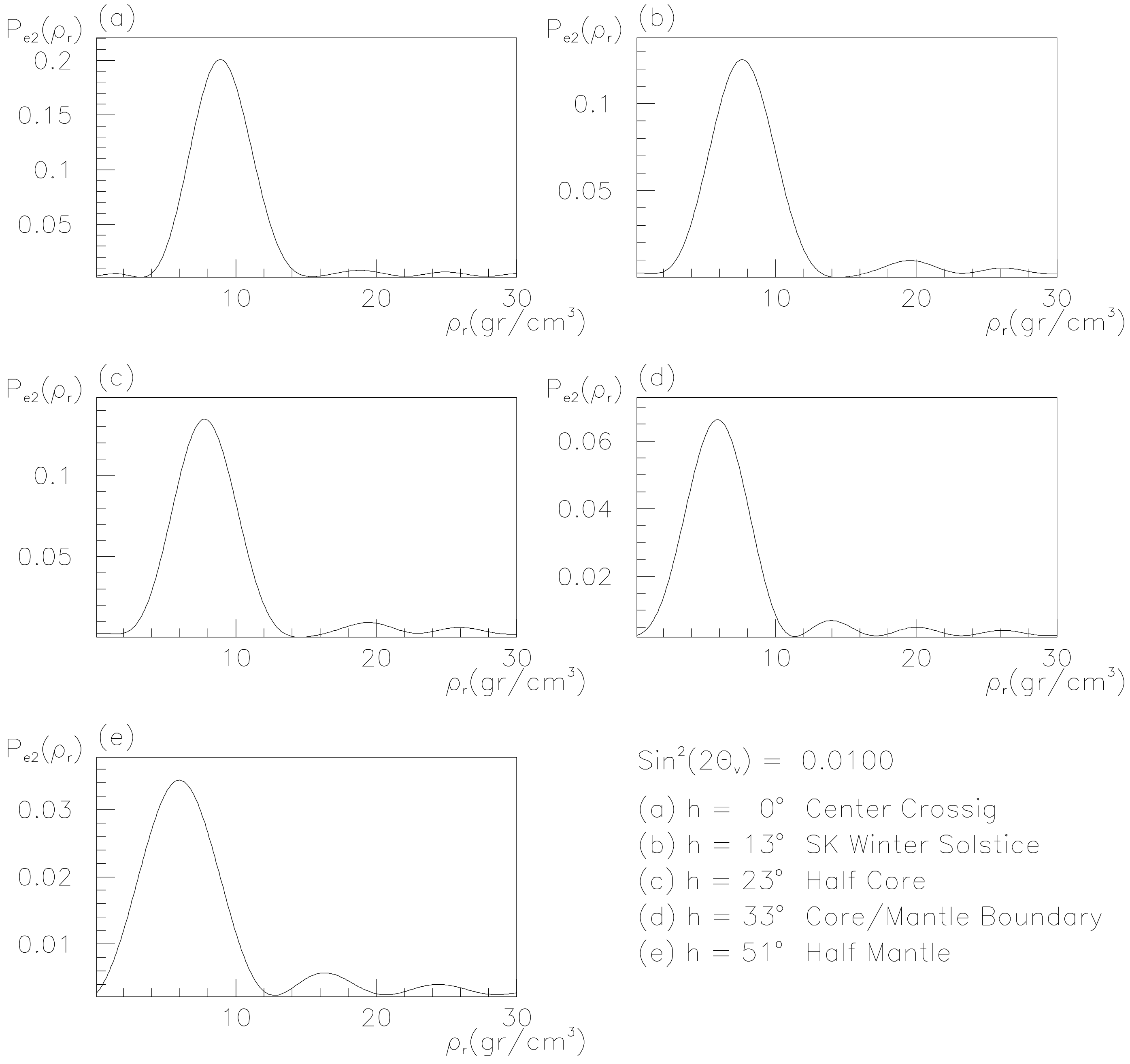

(a)
$P_{e2}(\rho_r)$
0.2
0.15
0.1
0.05
10
20
30
$\rho_r(gr/cm^3)$
(b)
$P_{e2}(\rho_r)$
0.1
0.05
10
20
30
$\rho_r(gr/cm^3)$
(c)
$P_{e2}(\rho_r)$
0.1
0.05
10
20
30
$\rho_r(gr/cm^3)$
(d)
$P_{e2}(\rho_r)$
0.06
0.04
0.02
10
20
30
$\rho_r(gr/cm^3)$
(e)
$P_{e2}(\rho_r)$
0.03
0.02
0.01
10
20
30
$\rho_r(gr/cm^3)$
$Sin^2(2\Theta_v) =$ 0.0100
(a) h = 0° Center Crossig
(b) h = 13° SK Winter Solstice
(c) h = 23° Half Core
(d) h = 33° Core/Mantle Boundary
(e) h = 51° Half Mantle

Fig. 3.1 $Y_e=0.467$ $\sin^2(2\Theta_v) = 0.0010$

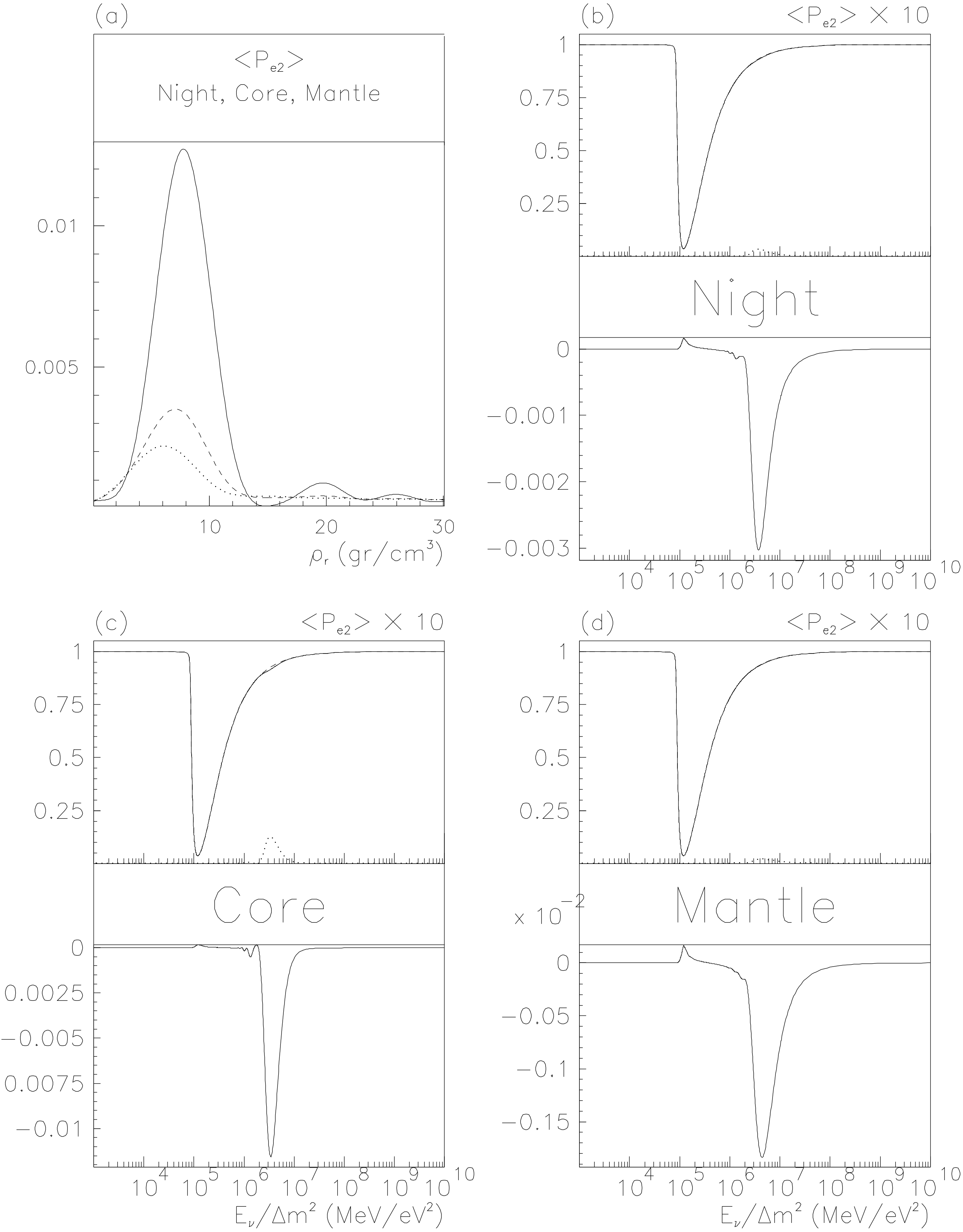

Figure 2

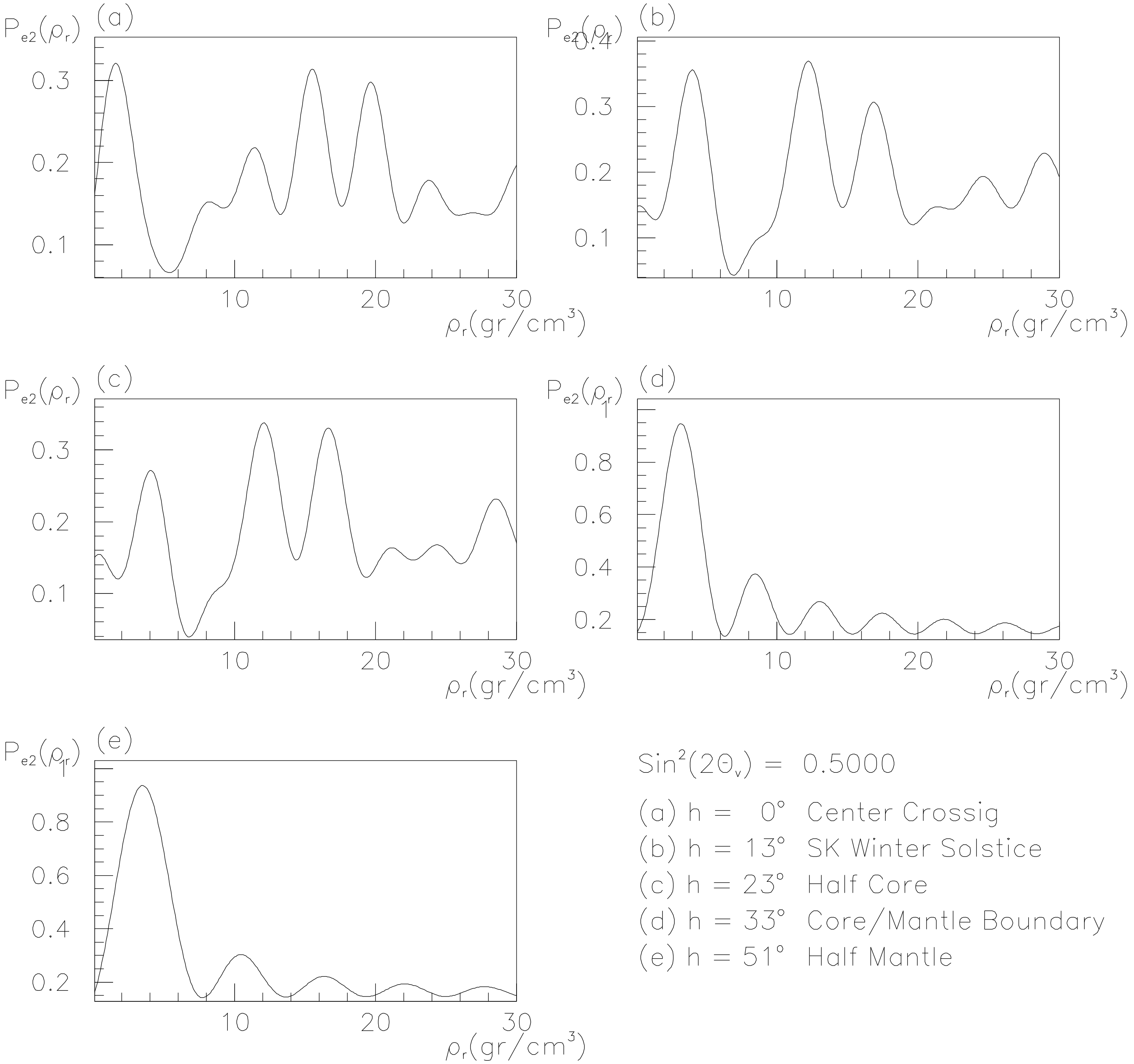
(a)
$P_{e2}(\rho_r)$
0.1
0.2
0.3
10
20
30
$\rho_r(gr/cm^3)$
(b)
$P_{e2}(\rho_r)$
0.1
0.2
0.3
0.4
10
20
30
$\rho_r(gr/cm^3)$
(c)
$P_{e2}(\rho_r)$
0.1
0.2
0.3
10
20
30
$\rho_r(gr/cm^3)$
(d)
$P_{e2}(\rho_r)$
0.2
0.4
0.6
0.8
1
10
20
30
$\rho_r(gr/cm^3)$
(e)
$P_{e2}(\rho_r)$
0.2
0.4
0.6
0.8
1
10
20
30
$\rho_r(gr/cm^3)$
$Sin^2(2\Theta_v) = 0.5000$
(a) h = 0° Center Crossig
(b) h = 13° SK Winter Solstice
(c) h = 23° Half Core
(d) h = 33° Core/Mantle Boundary
(e) h = 51° Half Mantle

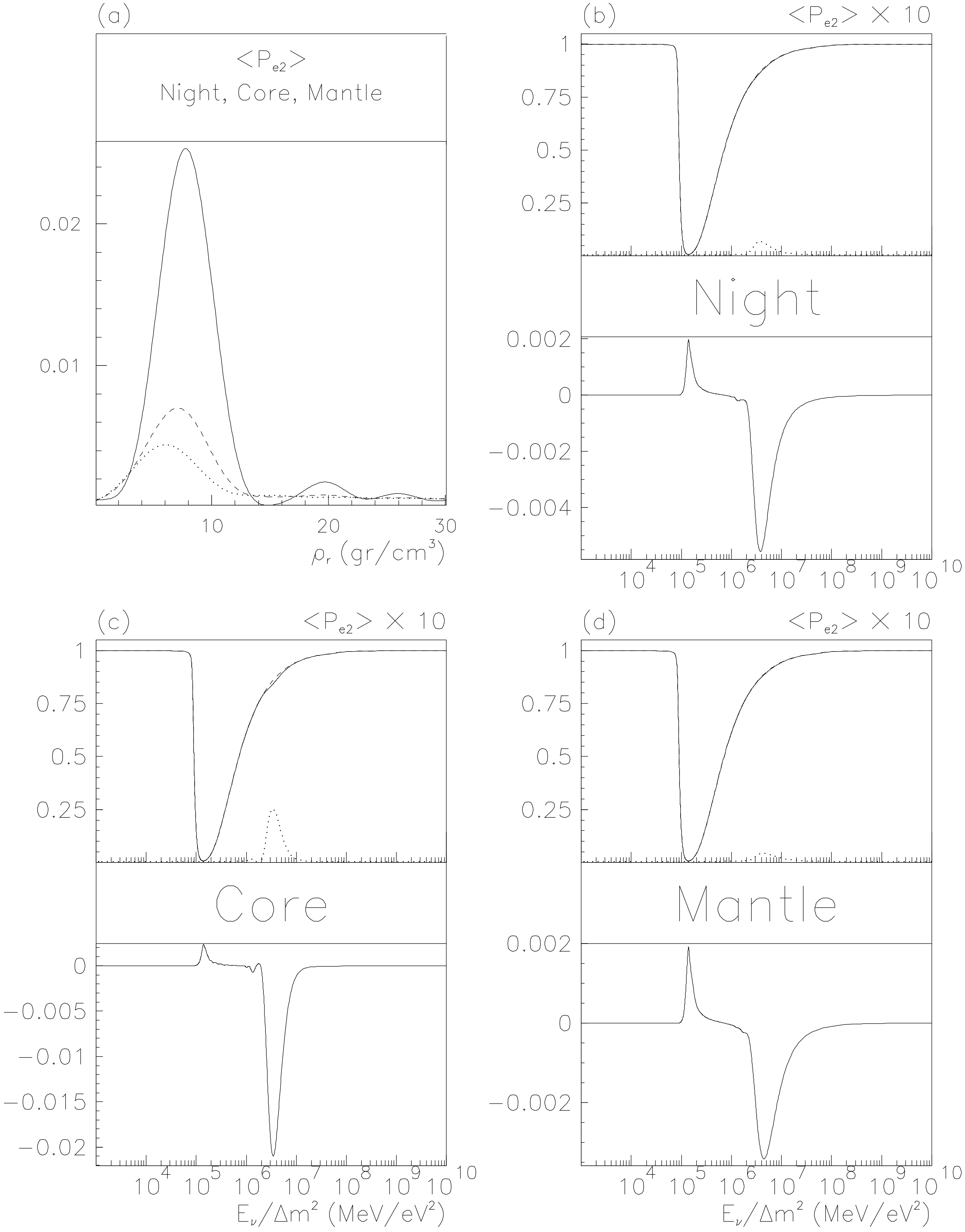

Fig. 3.2 $Y_e=0.467$ $\sin^2(2\Theta_v) = 0.0020$

Fig. 3.3 $Y_e=0.467$ $\sin^2(2\Theta_v) = 0.0030$

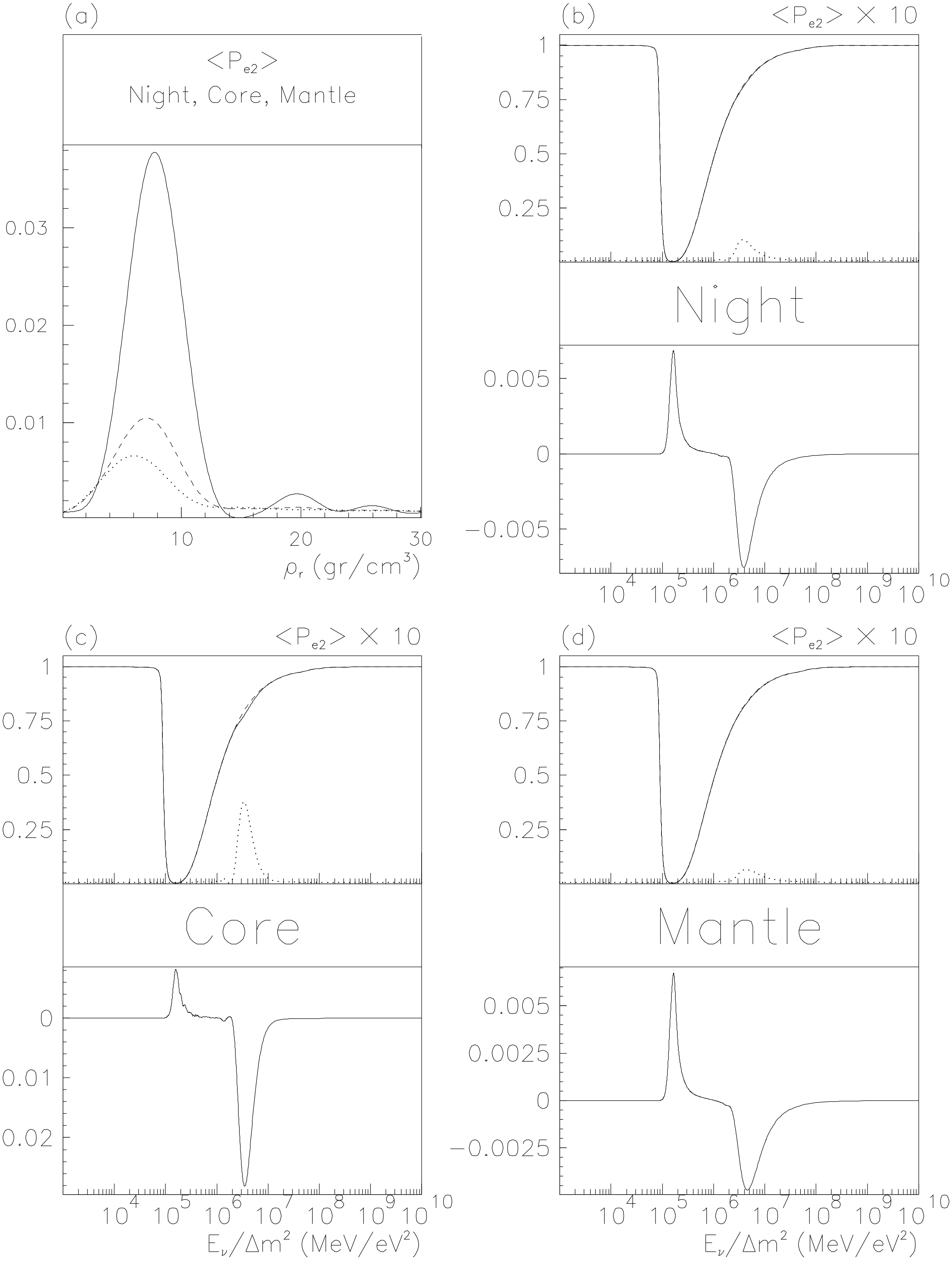

Fig. 3.4 $Y_e=0.467$ $\sin^2(2\Theta_v) = 0.0040$

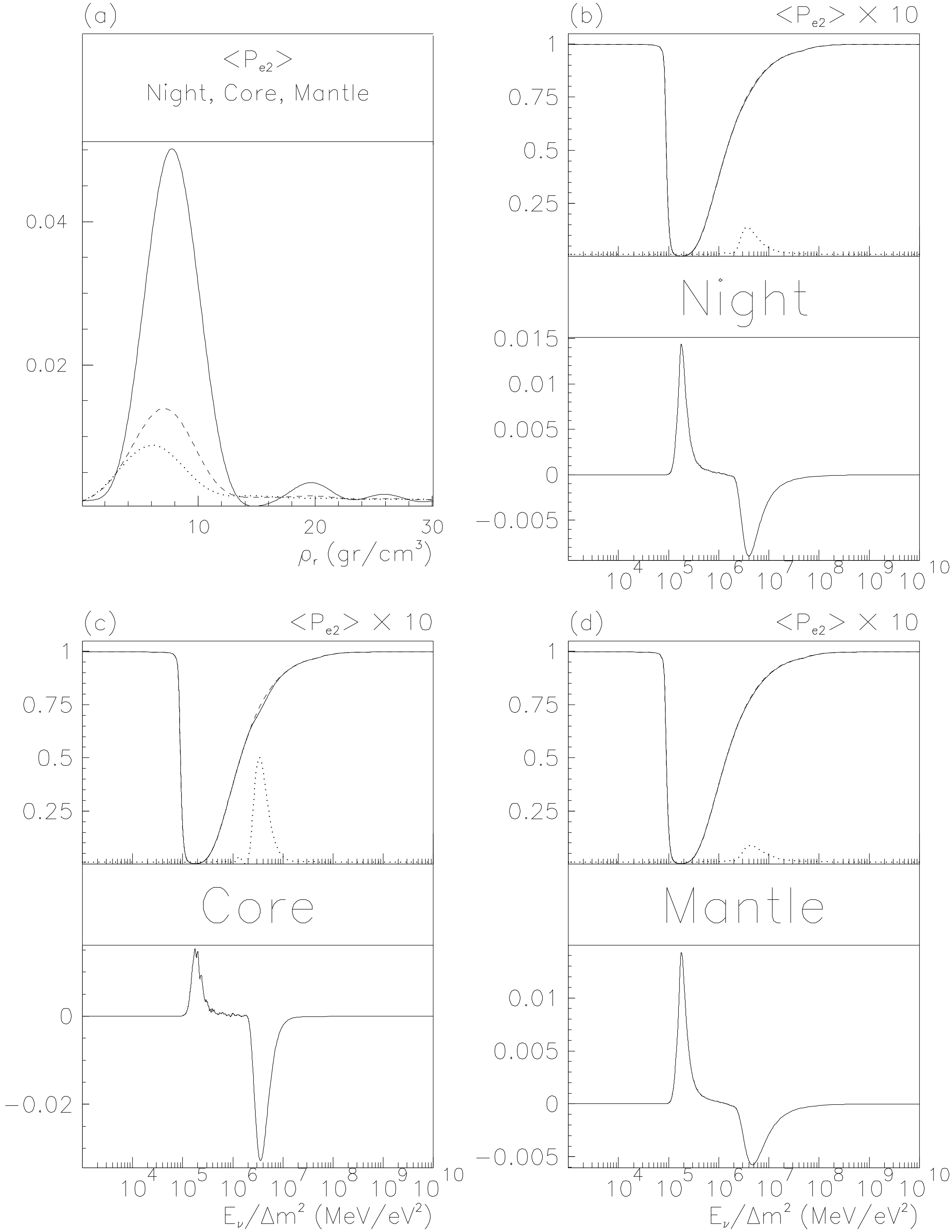

(4.1)

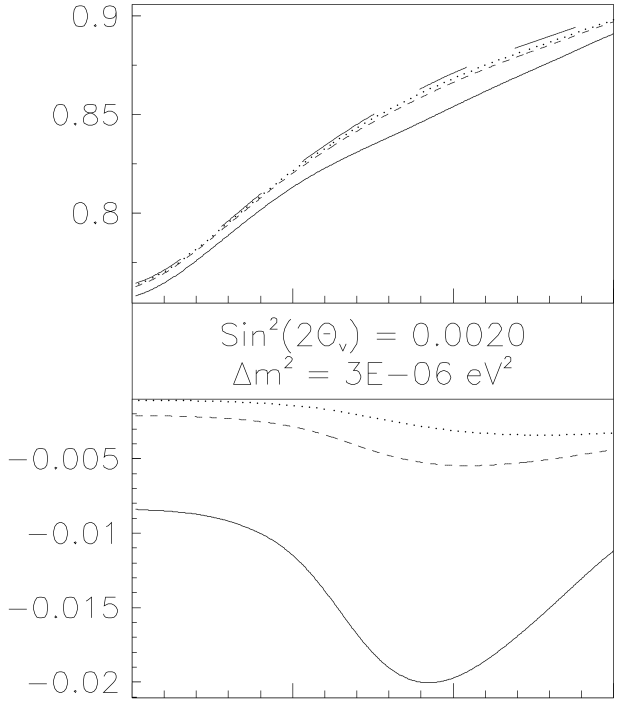

0.9
0.85
0.8
Sin²(2Θᵥ) = 0.0020
Δm² = 3E−06 eV²
−0.005
−0.01
−0.015
−0.02

(4.2)

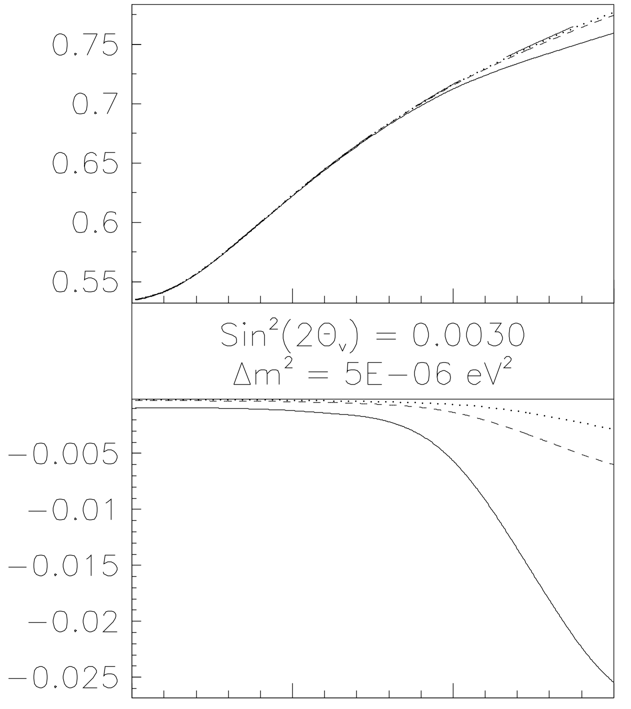

0.75
0.7
0.65
0.6
0.55
Sin²(2Θᵥ) = 0.0030
Δm² = 5E−06 eV²
−0.005
−0.01
−0.015
−0.02
−0.025

(4.3)

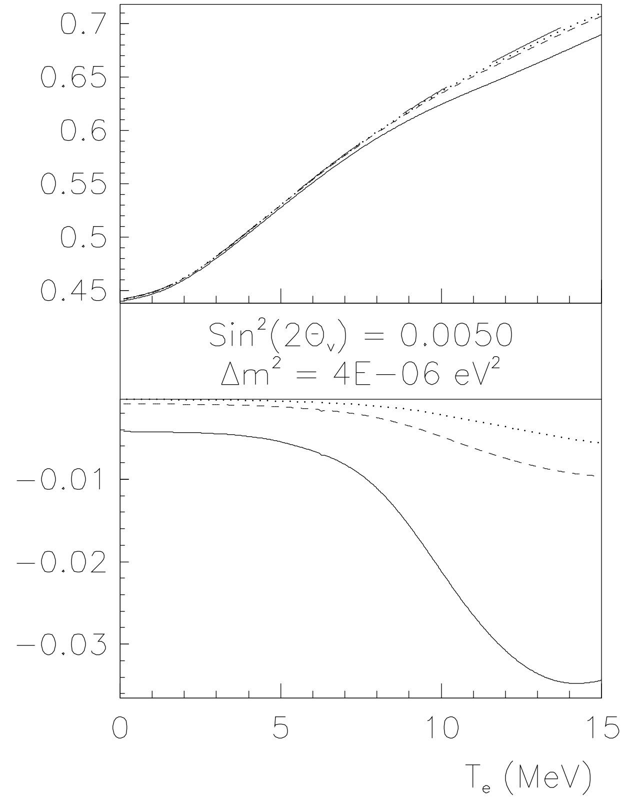

0.7
0.65
0.6
0.55
0.5
0.45
Sin²(2Θᵥ) = 0.0050
Δm² = 4E−06 eV²
−0.01
−0.02
−0.03
0
5
10
15
Tₑ (MeV)

(4.4)

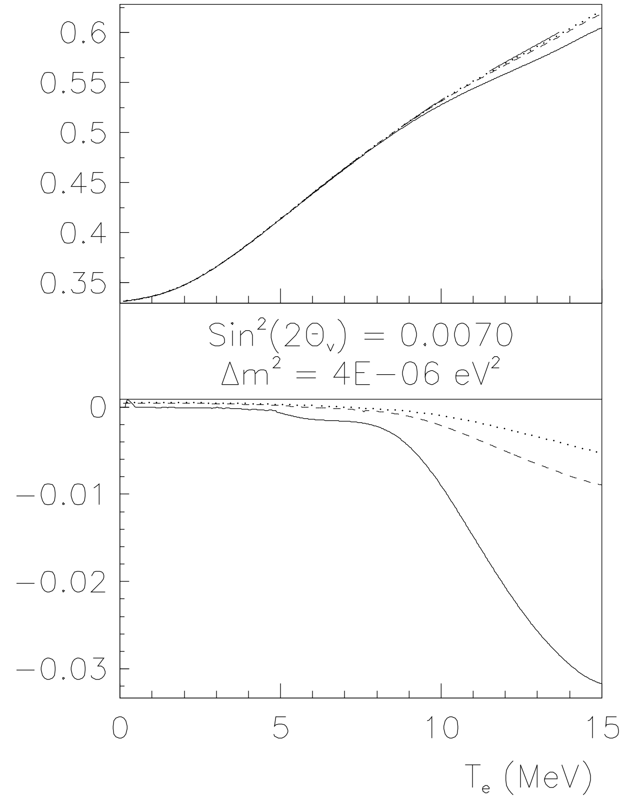

0.6
0.55
0.5
0.45
0.4
0.35
Sin²(2Θᵥ) = 0.0070
Δm² = 4E−06 eV²
0
−0.01
−0.02
−0.03
0
5
10
15
Tₑ (MeV)

Fig. 3.5 $Y_e=0.467$ $\sin^2(2\Theta_v) = 0.0050$

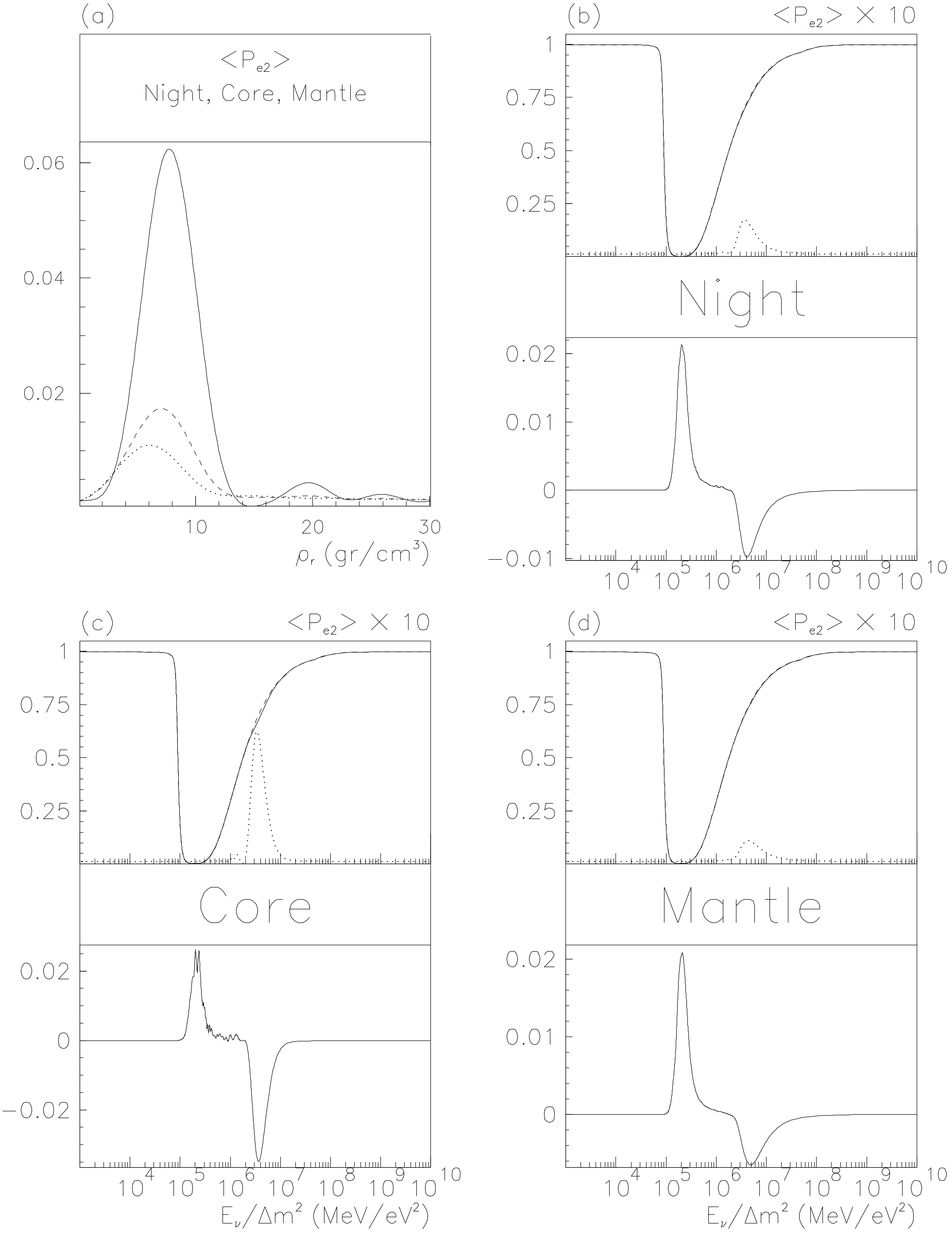

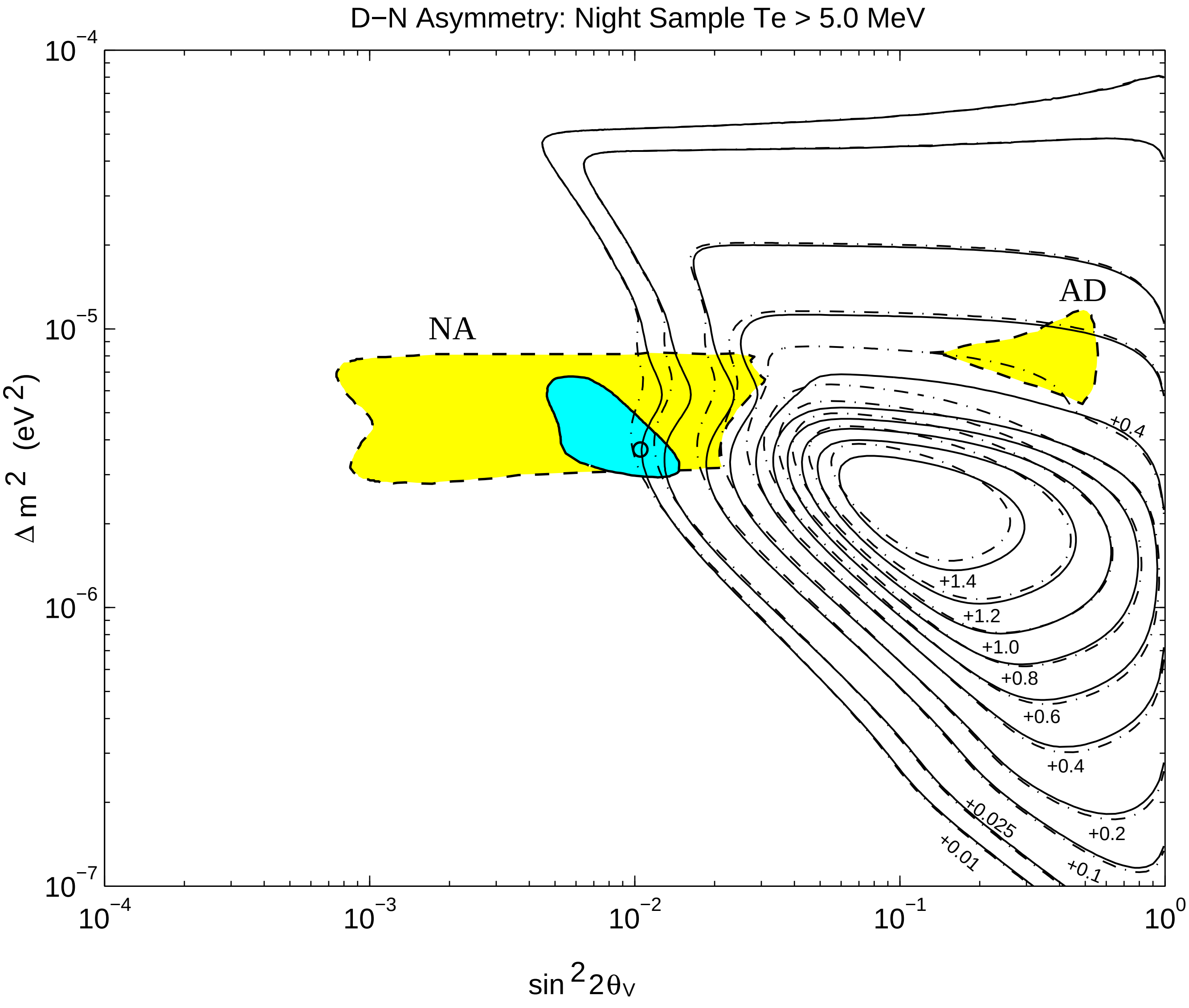
D−N Asymmetry: Night Sample Te > 5.0 MeV
NA
AD
+0.4
+1.4
+1.2
+1.0
+0.8
+0.6
+0.4
+0.2
+0.1
+0.025
+0.01
Δm^2 (eV^2)
10^{-4}
10^{-5}
10^{-6}
10^{-7}
10^{-4}
10^{-3}
10^{-2}
10^{-1}
10^{0}
$\sin^2 2\theta_V$

Figure 5a

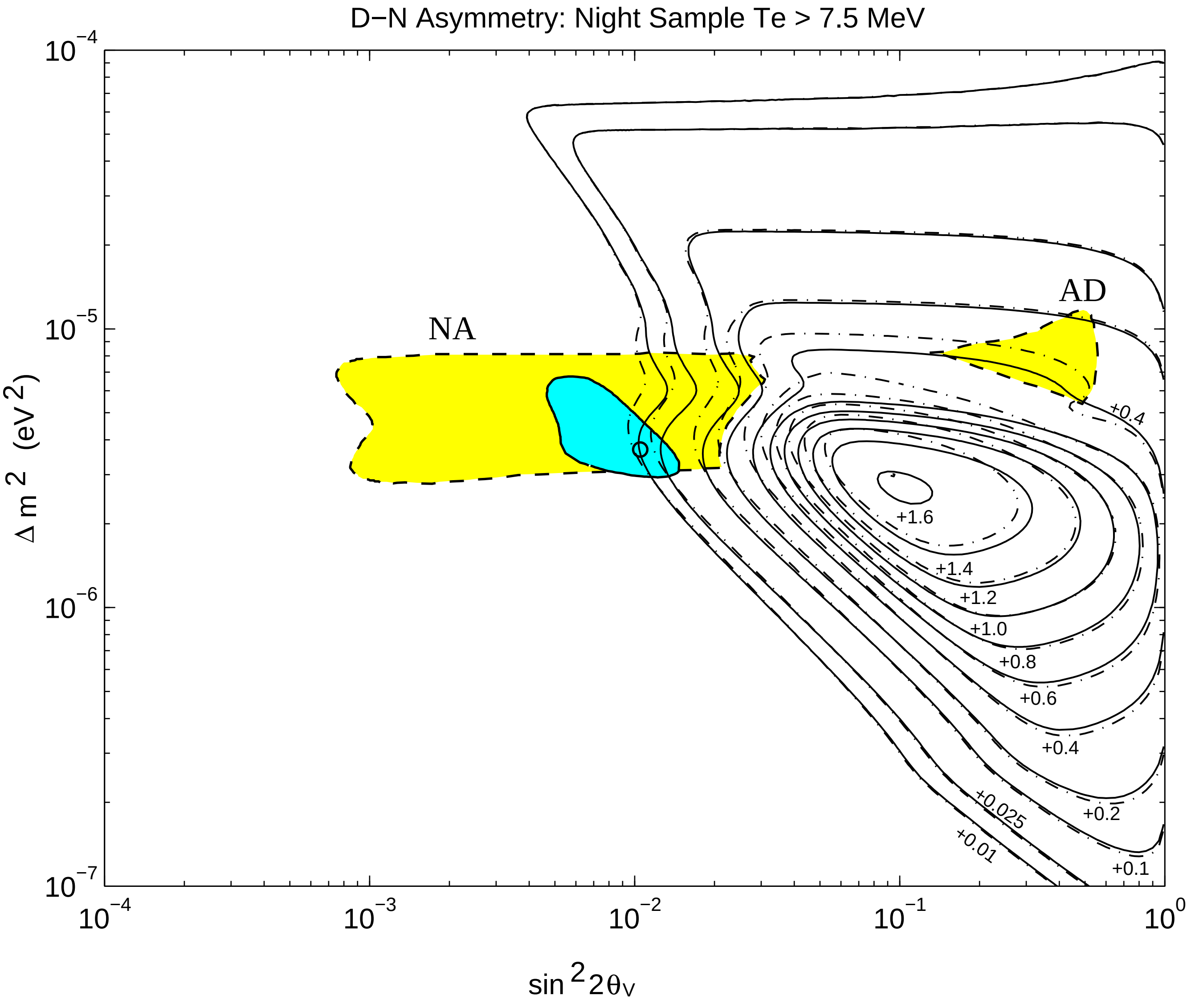
D−N Asymmetry: Night Sample Te > 7.5 MeV
10^−4
10^−5
10^−6
10^−7
Δ m 2 (eV 2)
10^−4
10^−3
10^−2
10^−1
10^0
sin 2 2θV
NA
AD
+0.4
+1.6
+1.4
+1.2
+1.0
+0.8
+0.6
+0.4
+0.2
+0.1
+0.025
+0.01

Figure 5b

Fig. 3.6 $Y_e=0.467$ $\sin^2(2\Theta_v) = 0.0070$

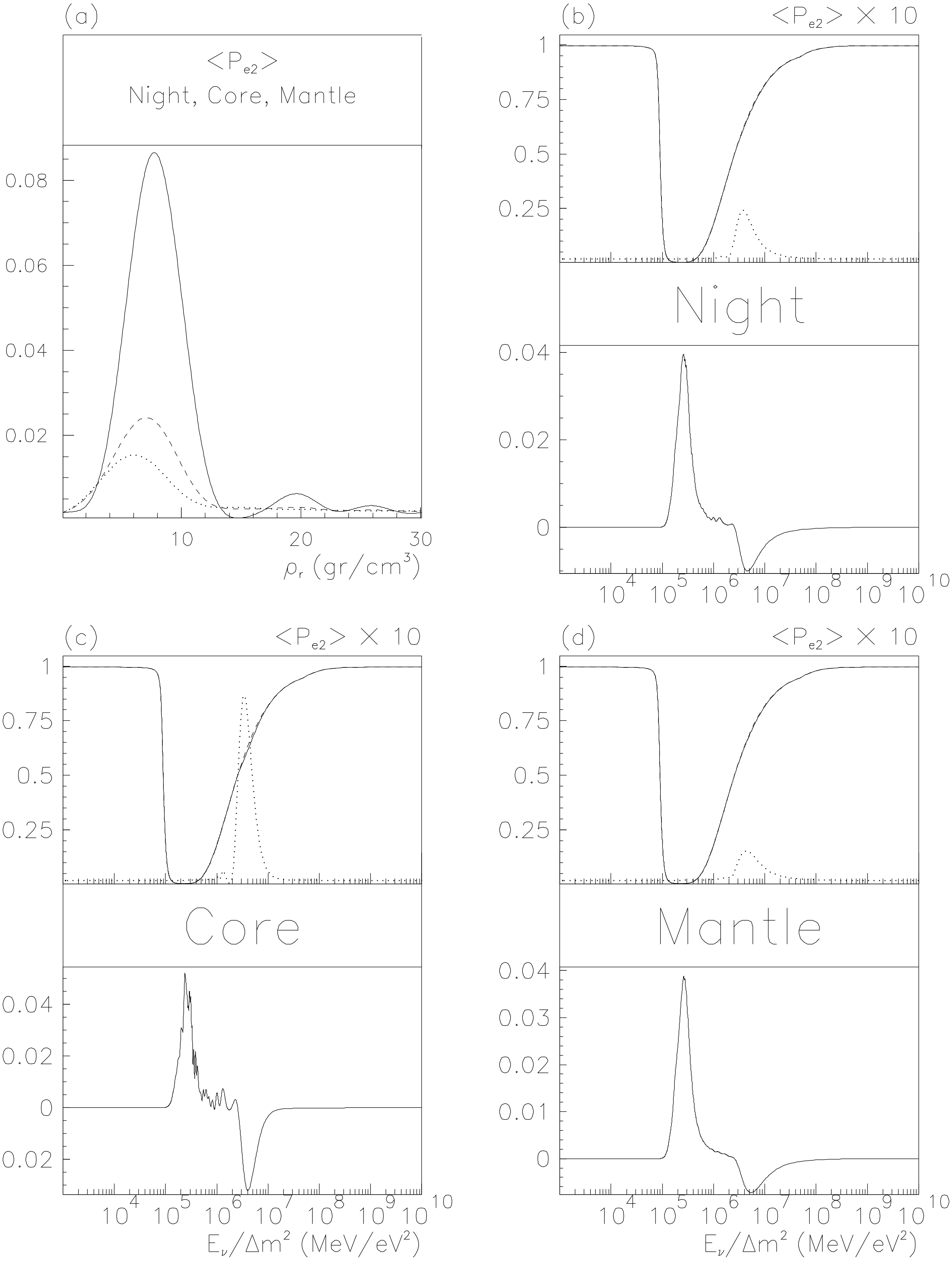

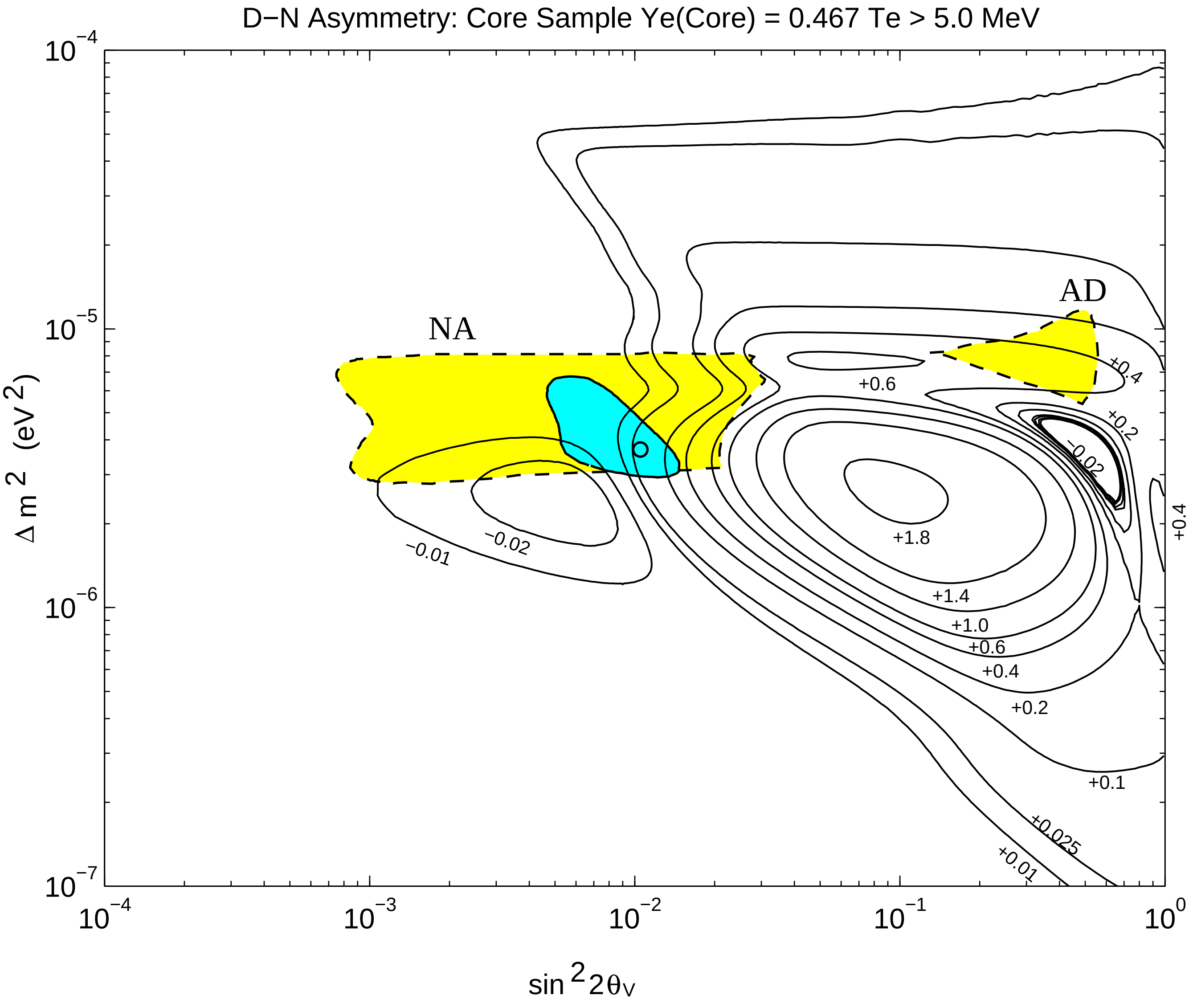
D−N Asymmetry: Core Sample Ye(Core) = 0.467 Te > 5.0 MeV
10^{-4}
10^{-5}
10^{-6}
10^{-7}
Δm^2 (eV^2)
NA
AD
+0.6
+0.4
+0.2
−0.02
+0.4
+1.8
+1.4
+1.0
+0.6
+0.4
+0.2
+0.1
+0.025
+0.01
−0.01
−0.02
10^{-4}
10^{-3}
10^{-2}
10^{-1}
10^{0}
$\sin^2 2\theta_V$

Figure 6a

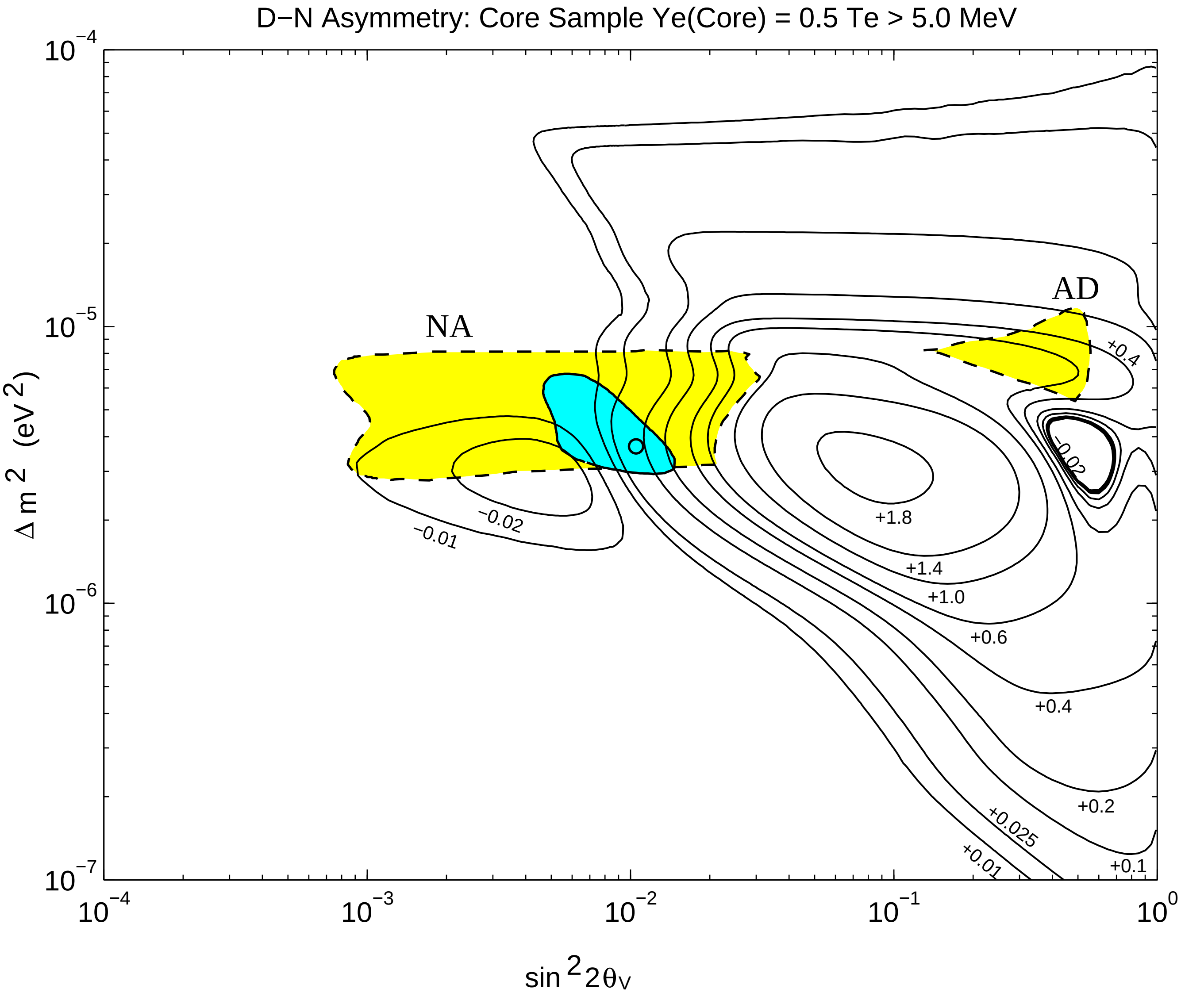

D−N Asymmetry: Core Sample Ye(Core) = 0.5 Te > 5.0 MeV

Figure 6b

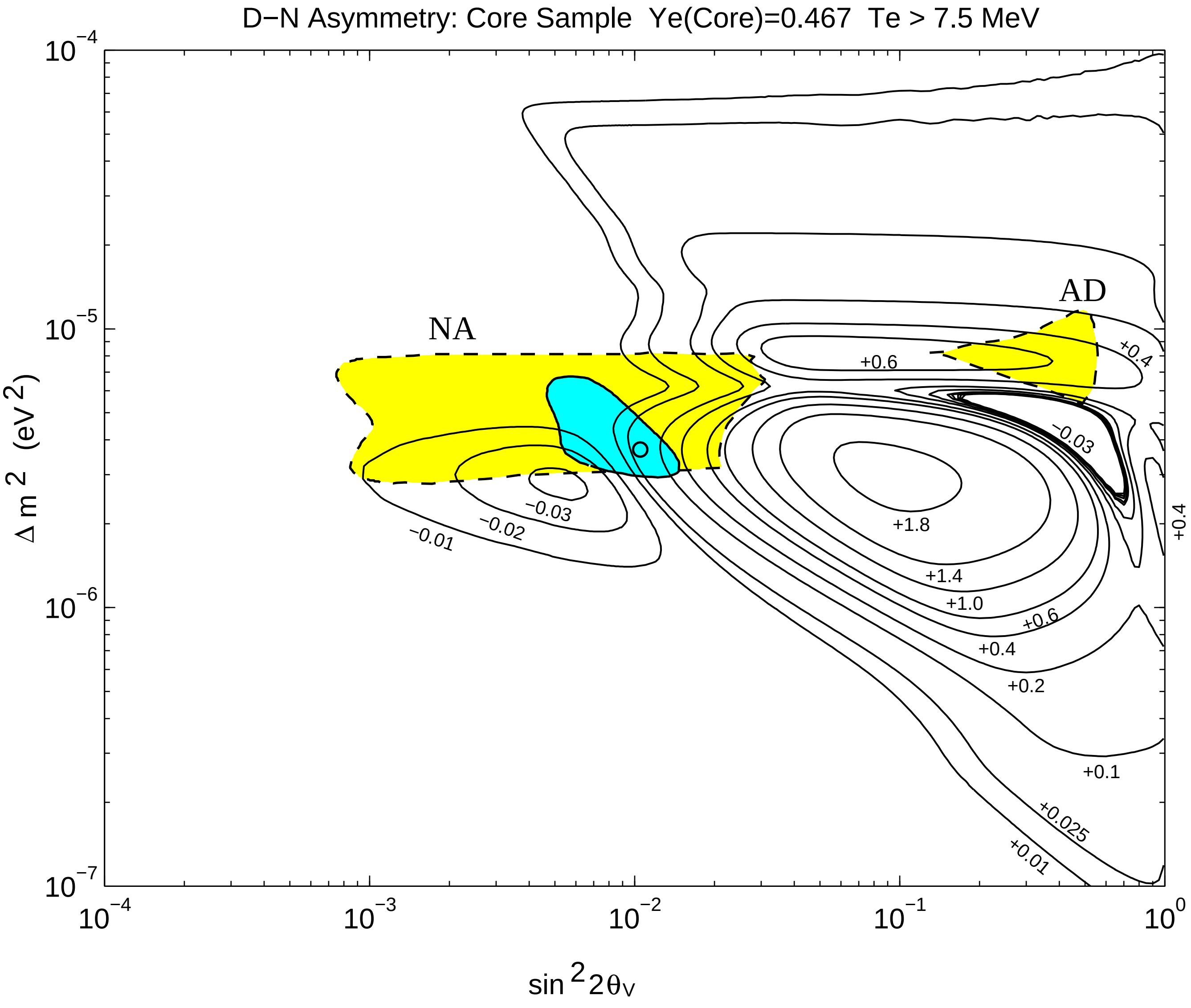
D−N Asymmetry: Core Sample Ye(Core)=0.467 Te > 7.5 MeV

Figure 6c

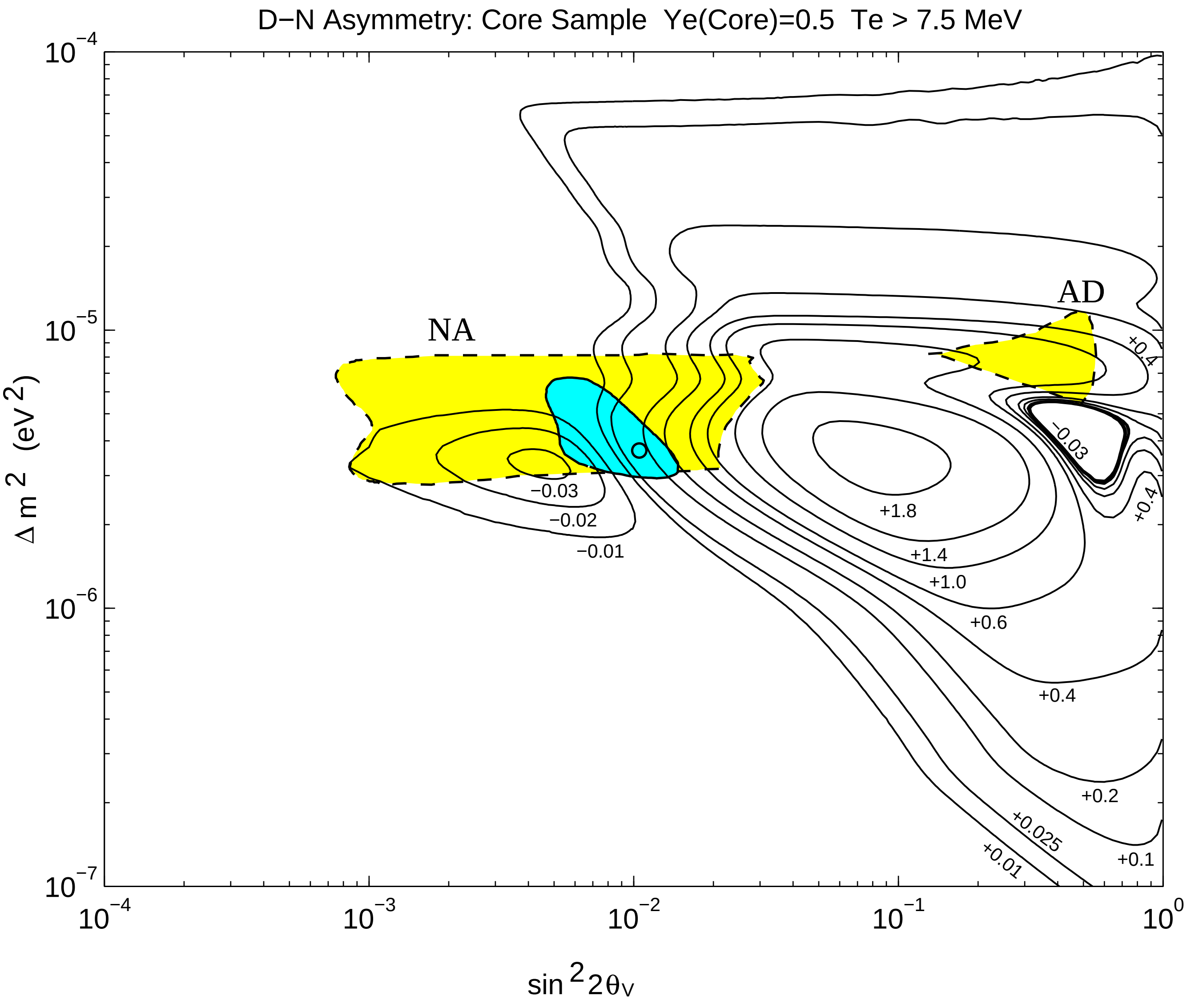
D−N Asymmetry: Core Sample Ye(Core)=0.5 Te > 7.5 MeV
Δm^2 (eV^2)
$\sin^2 2\theta_V$
10^{-4}
10^{-5}
10^{-6}
10^{-7}
10^{-4}
10^{-3}
10^{-2}
10^{-1}
10^{0}
NA
AD
−0.03
−0.02
−0.01
+1.8
+1.4
+1.0
+0.6
+0.4
+0.2
+0.1
+0.025
+0.01
+0.4
−0.03
+0.4

Figure 6d

Fig. 3.7 $Y_e=0.467$ $\sin^2(2\Theta_v) = 0.0080$

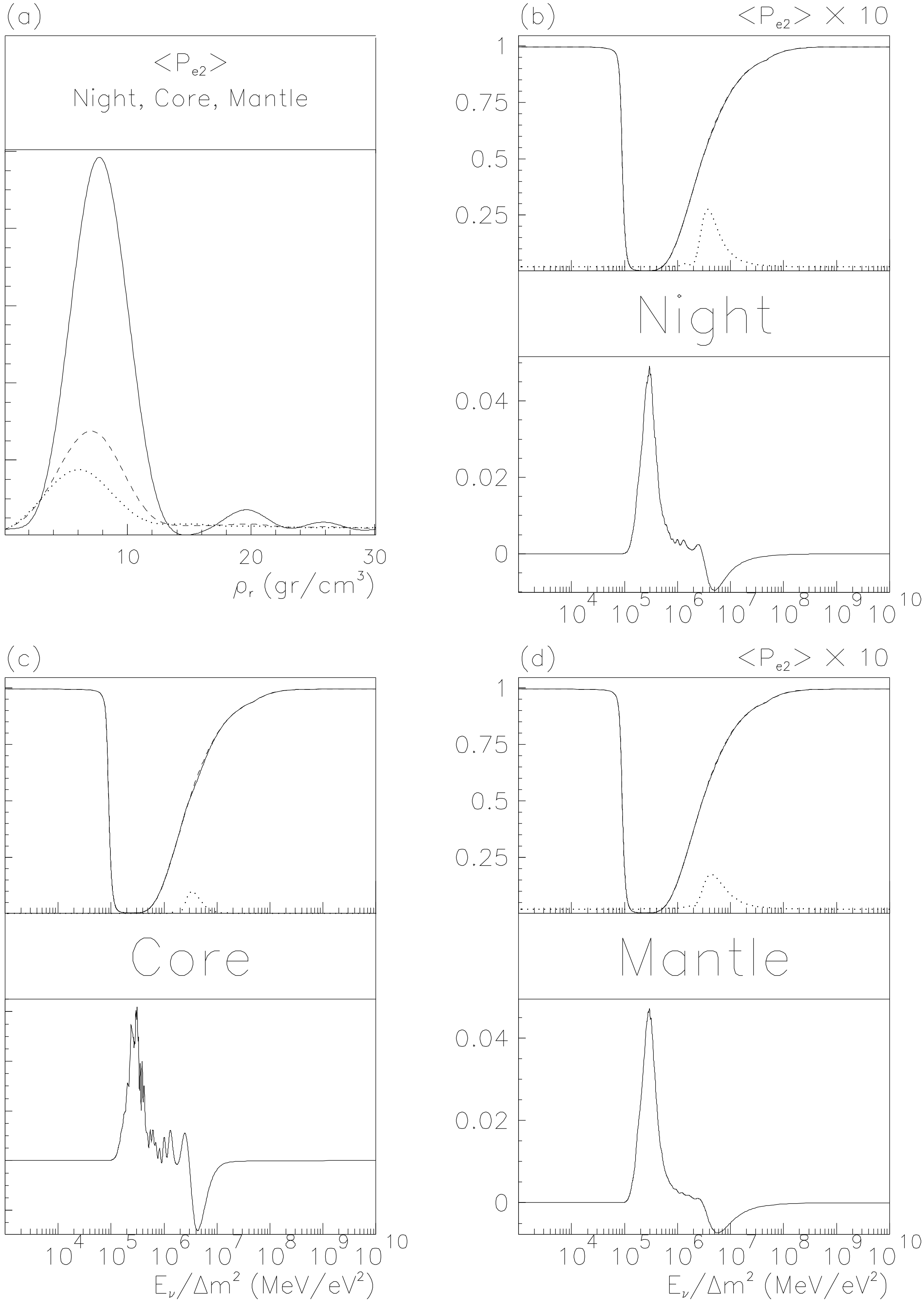

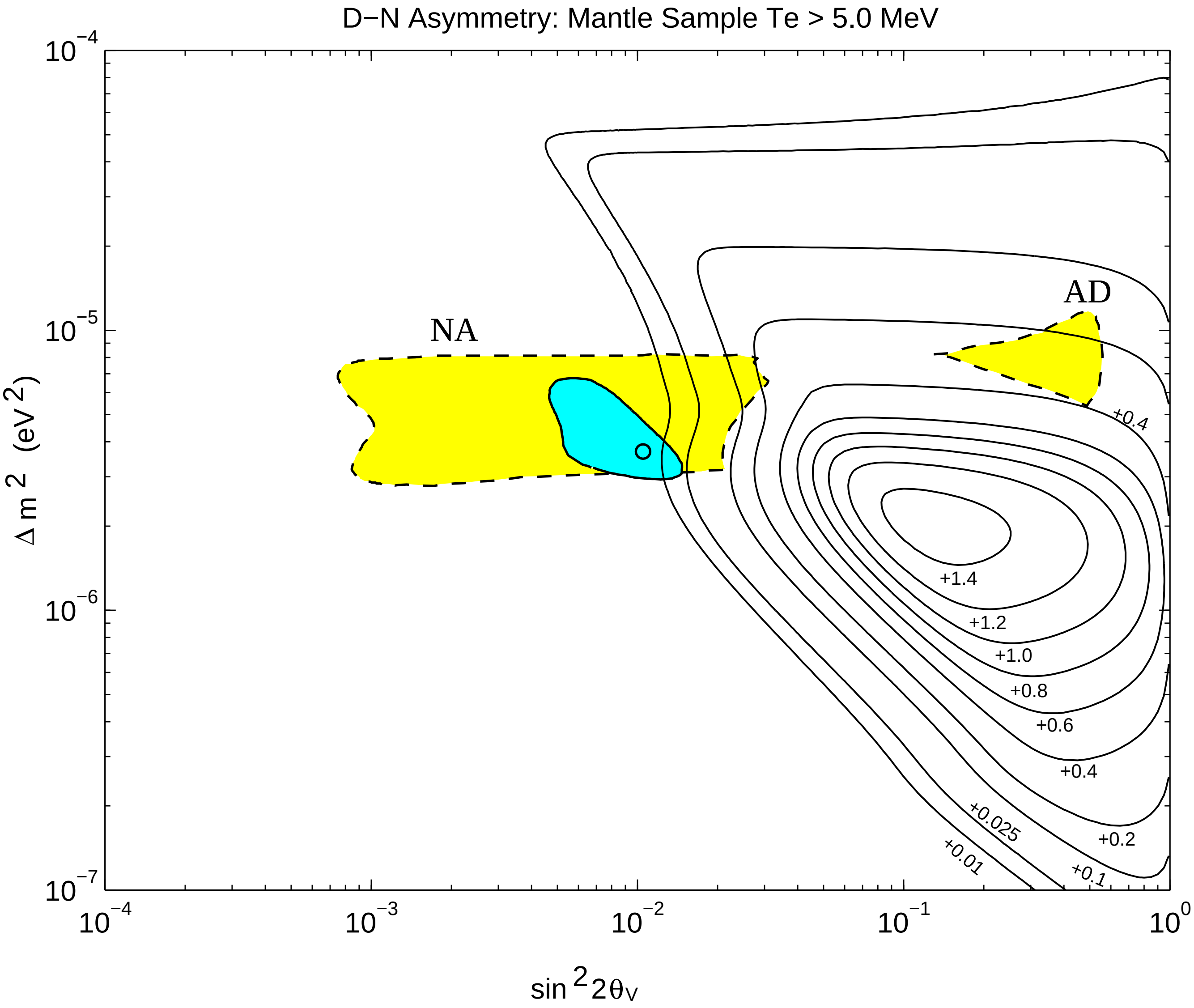
D−N Asymmetry: Mantle Sample Te > 5.0 MeV
NA
AD
+1.4
+1.2
+1.0
+0.8
+0.6
+0.4
+0.4
+0.2
+0.1
+0.025
+0.01
10^{-4}
10^{-5}
10^{-6}
10^{-7}
10^{-3}
10^{-2}
10^{-1}
10^{0}
Δm^2 (eV^2)
$\sin^2 2\theta_V$

Figure 7a

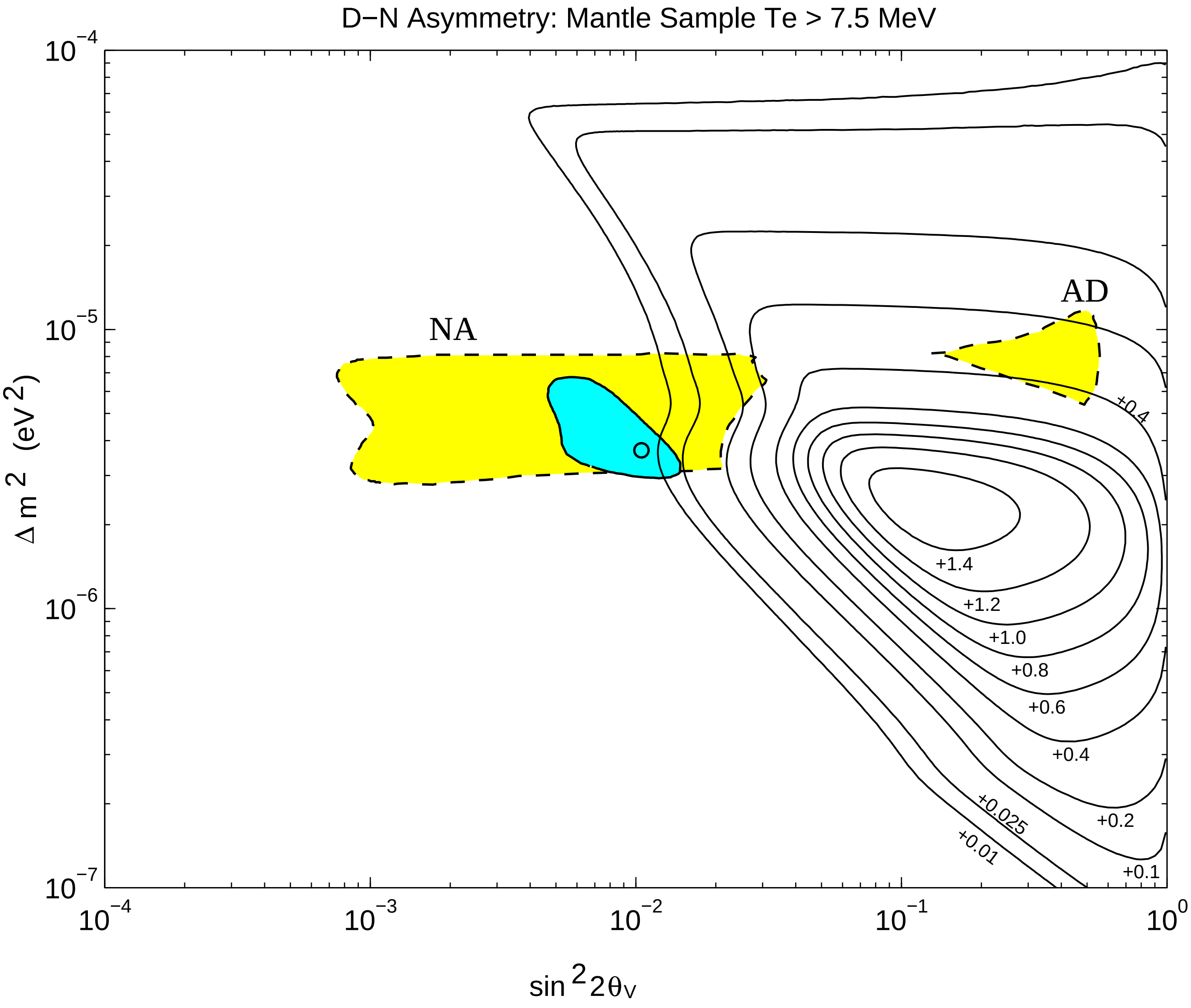
D−N Asymmetry: Mantle Sample Te > 7.5 MeV
NA
AD
+0.4
+1.4
+1.2
+1.0
+0.8
+0.6
+0.4
+0.2
+0.1
+0.025
+0.01
10^{-4}
10^{-5}
10^{-6}
10^{-7}
Δm^2 (eV^2)
10^{-4}
10^{-3}
10^{-2}
10^{-1}
10^{0}
$\sin^2 2\theta_V$

Figure 7b

Fig. 3.8 $Y_e=0.467$ $\sin^2(2\Theta_v) = 0.0090$

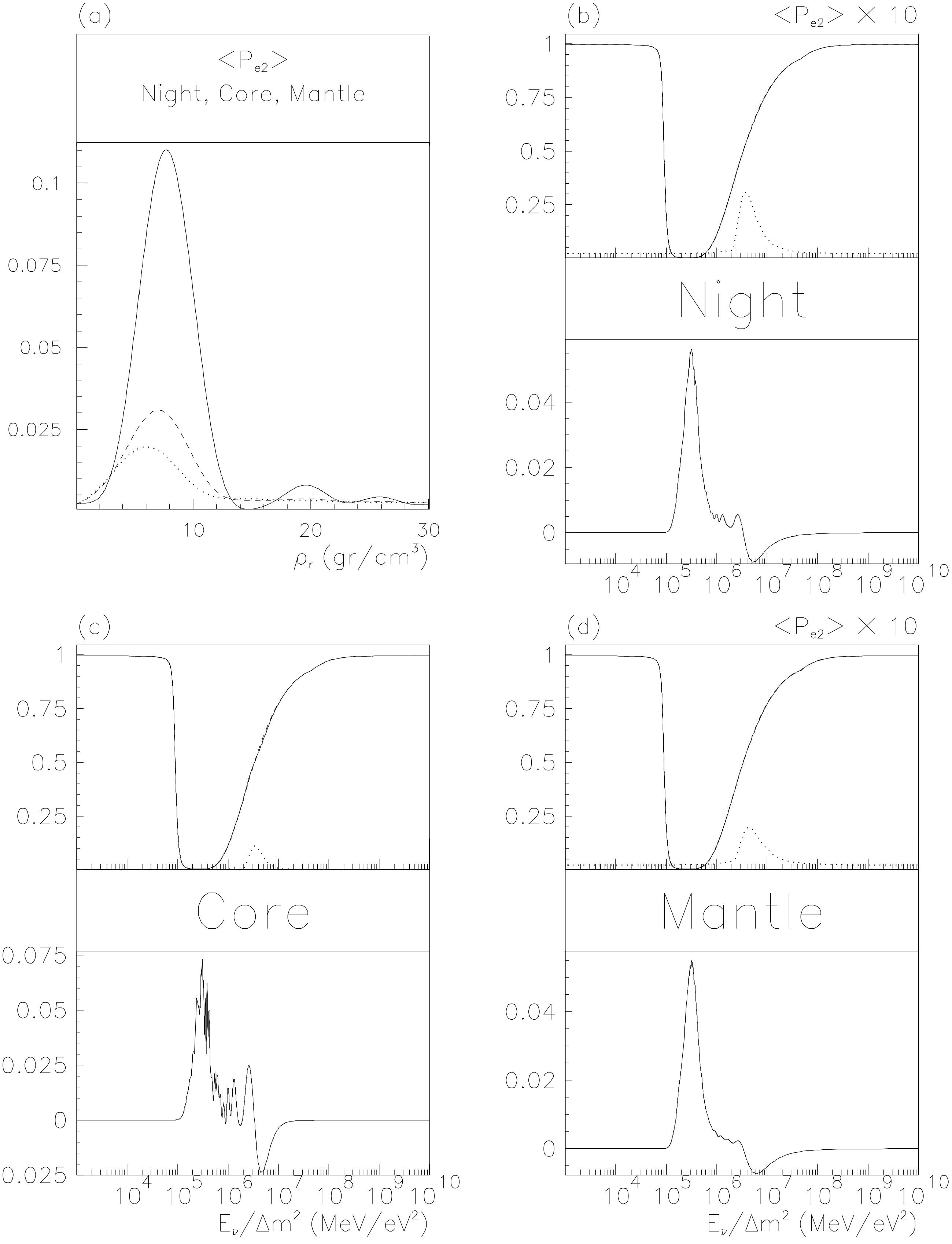

(4.5)

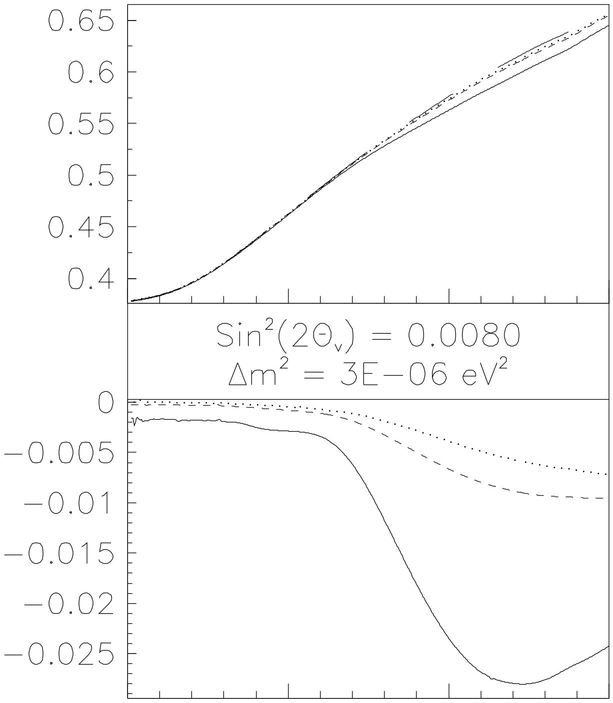
0.65
0.6
0.55
0.5
0.45
0.4
Sin²(2Θᵥ) = 0.0080
Δm² = 3E−06 eV²
0
−0.005
−0.01
−0.015
−0.02
−0.025

(4.6)

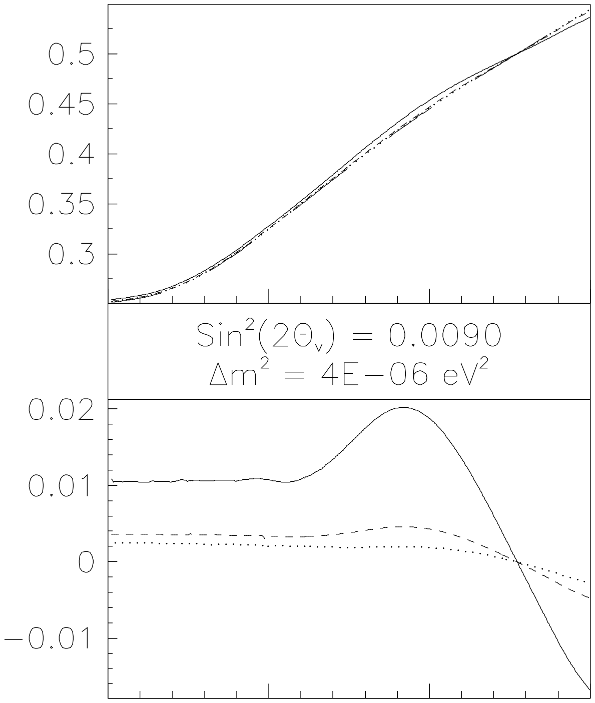
0.5
0.45
0.4
0.35
0.3
Sin²(2Θᵥ) = 0.0090
Δm² = 4E−06 eV²
0.02
0.01
0
−0.01

(4.7)

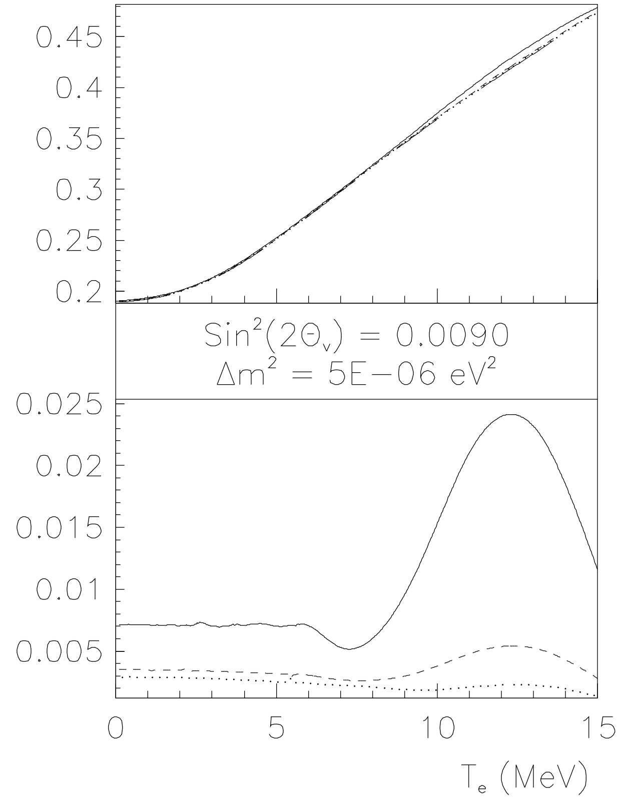
0.45
0.4
0.35
0.3
0.25
0.2
Sin²(2Θᵥ) = 0.0090
Δm² = 5E−06 eV²
0.025
0.02
0.015
0.01
0.005
0
5
10
15
Tₑ (MeV)

(4.8)

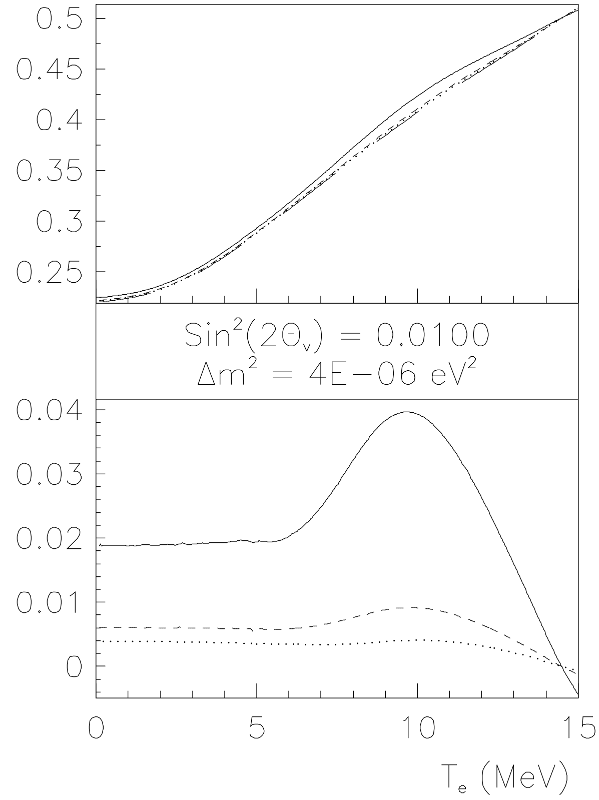
0.5
0.45
0.4
0.35
0.3
0.25
Sin²(2Θᵥ) = 0.0100
Δm² = 4E−06 eV²
0.04
0.03
0.02
0.01
0
0
5
10
15
Tₑ (MeV)

Fig. 3.9 $Y_e=0.467$ $\sin^2(2\Theta_v) = 0.0100$

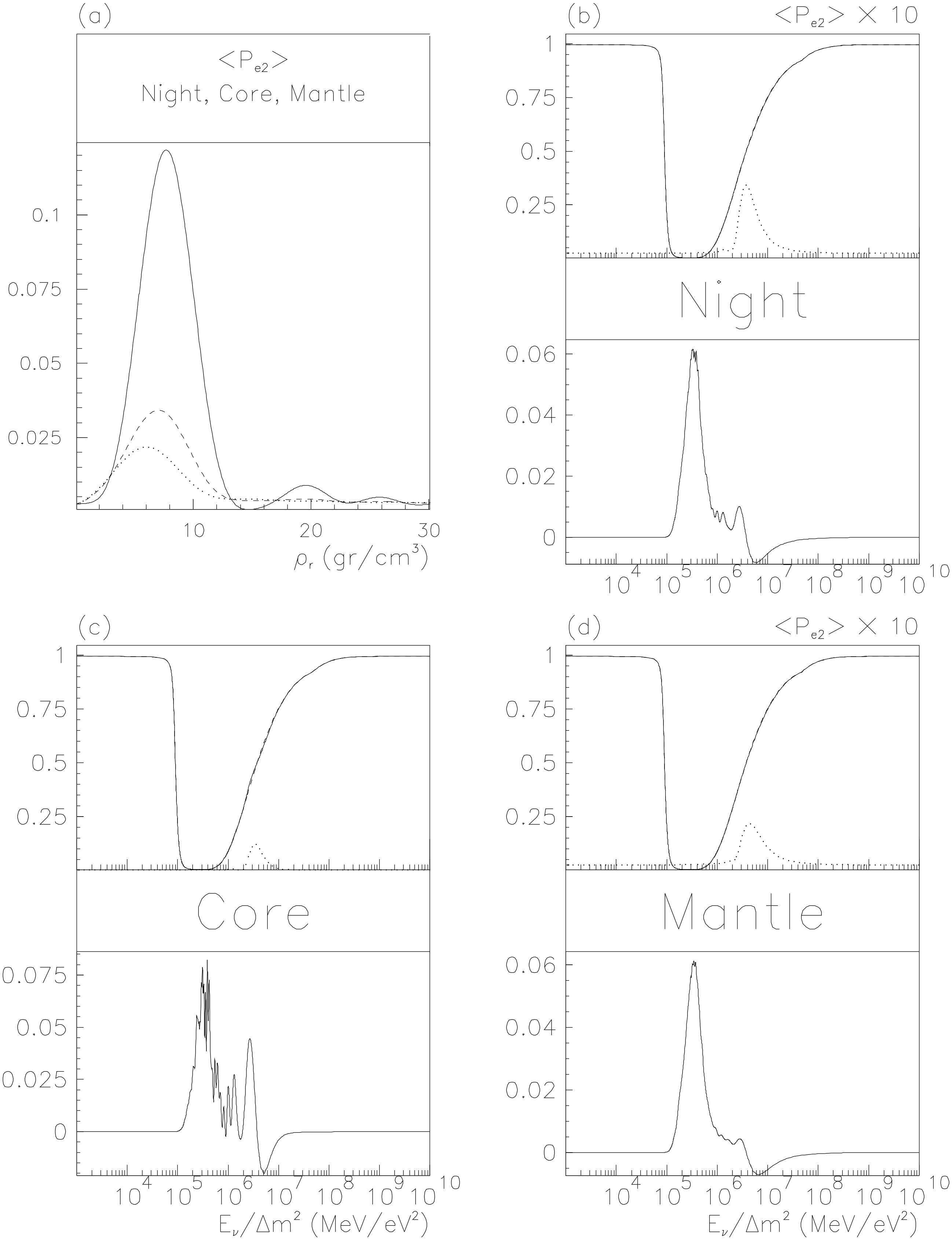

Fig. 3.10 $Y_e=0.467$ $\sin^2(2\Theta_v) = 0.0140$

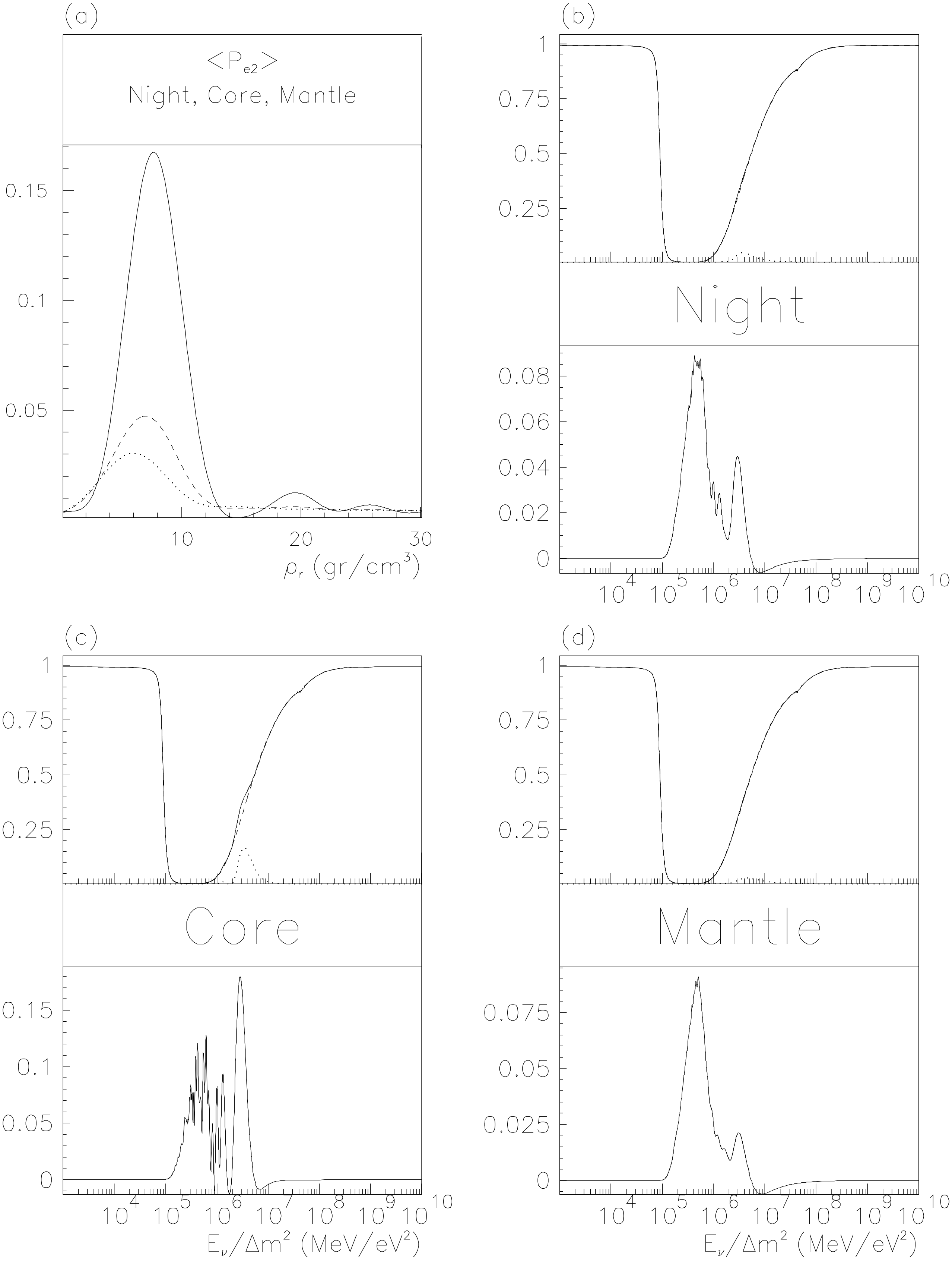

Fig. 3.11 $Y_e=0.467$ $\sin^2(2\Theta_v) = 0.4000$

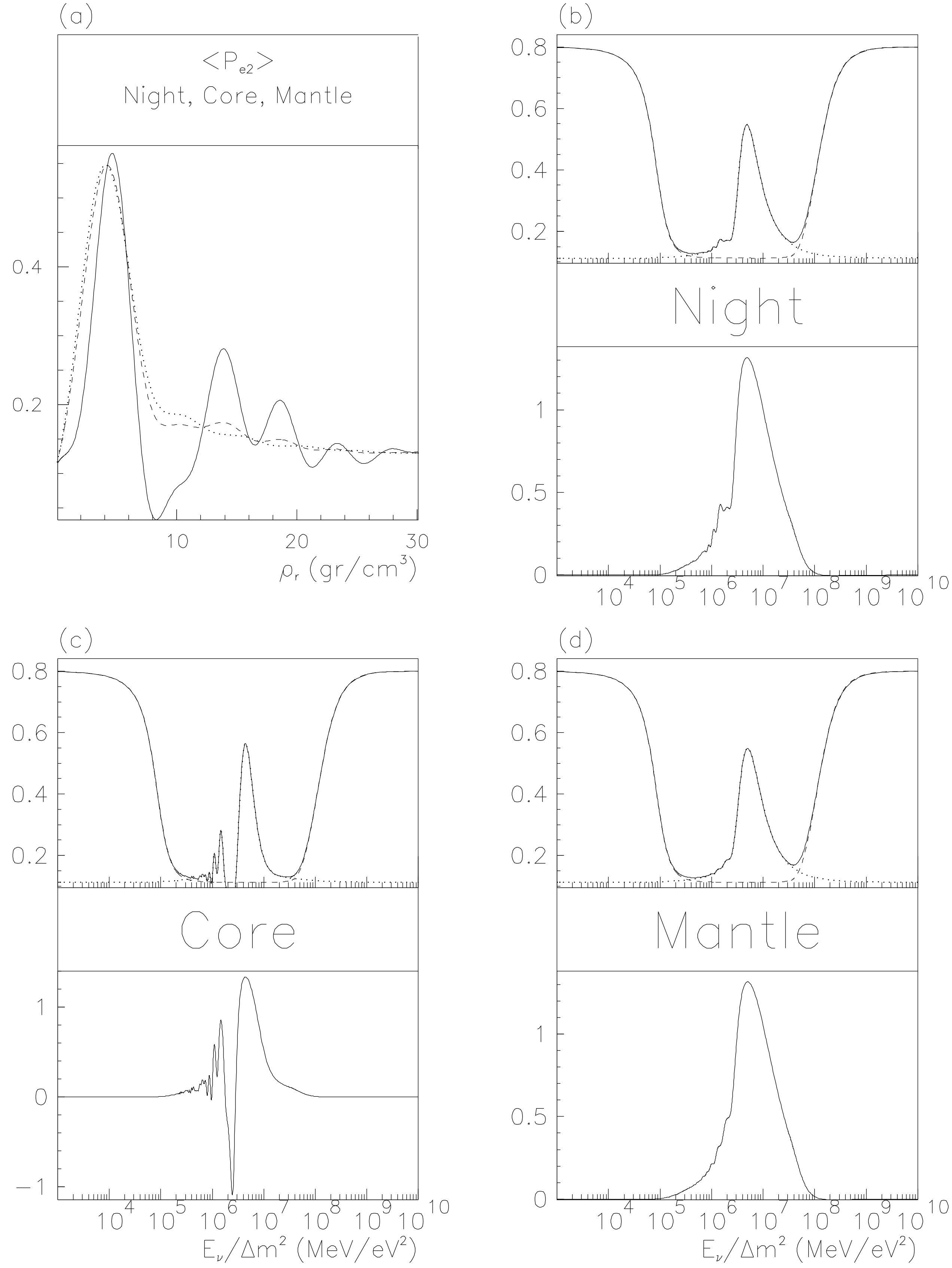

Fig. 3.12 Y_e=0.467 $\sin^2(2\Theta_v)$ = 0.5000

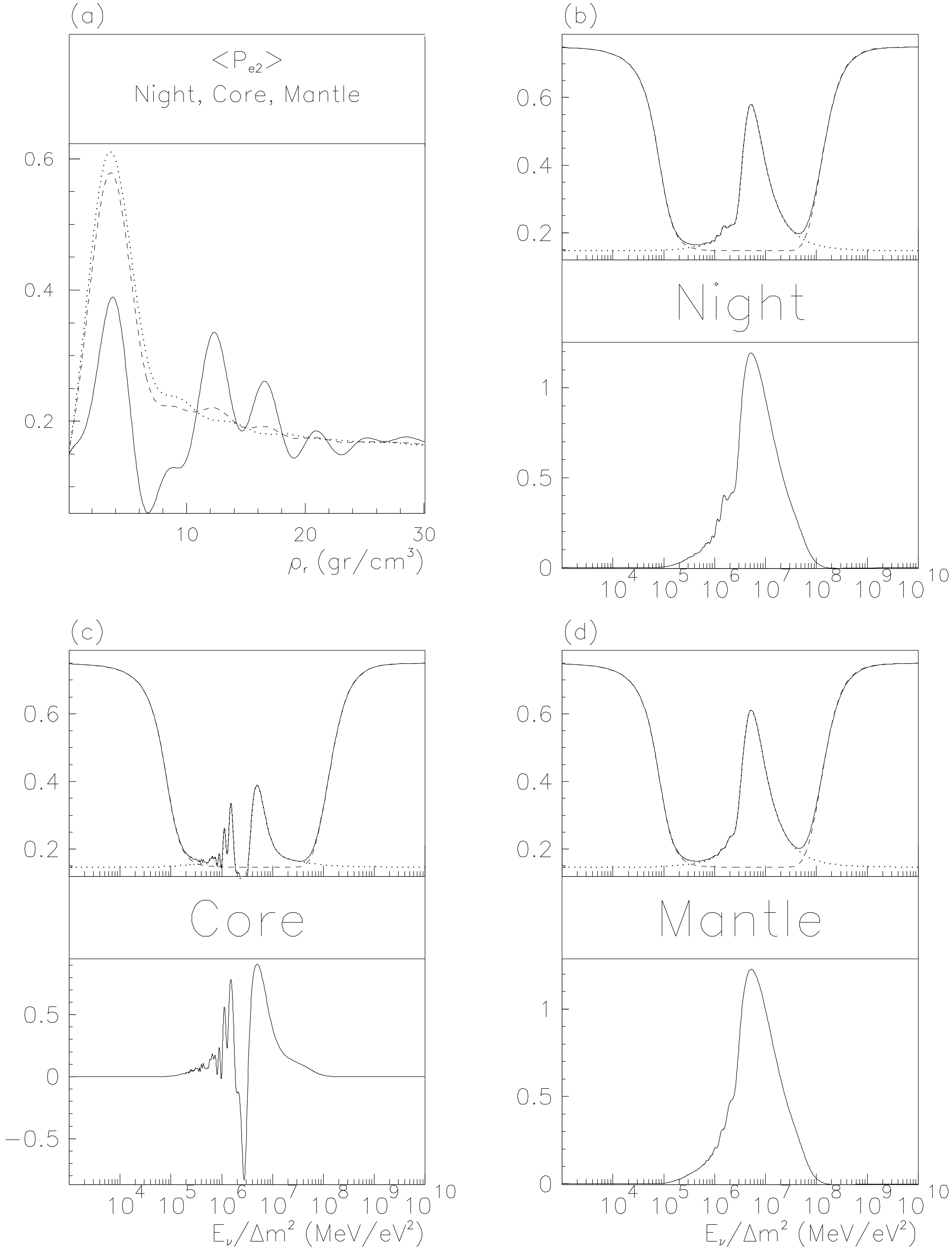

(4.9)

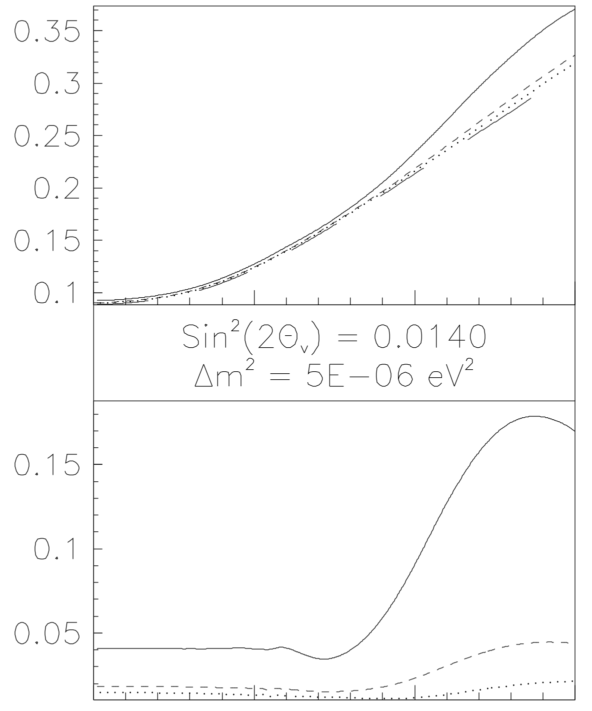

(4.10)

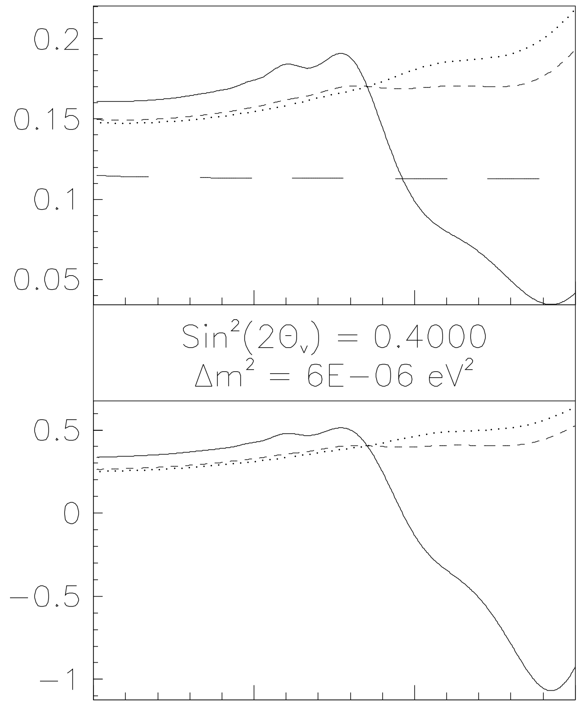

(4.11)

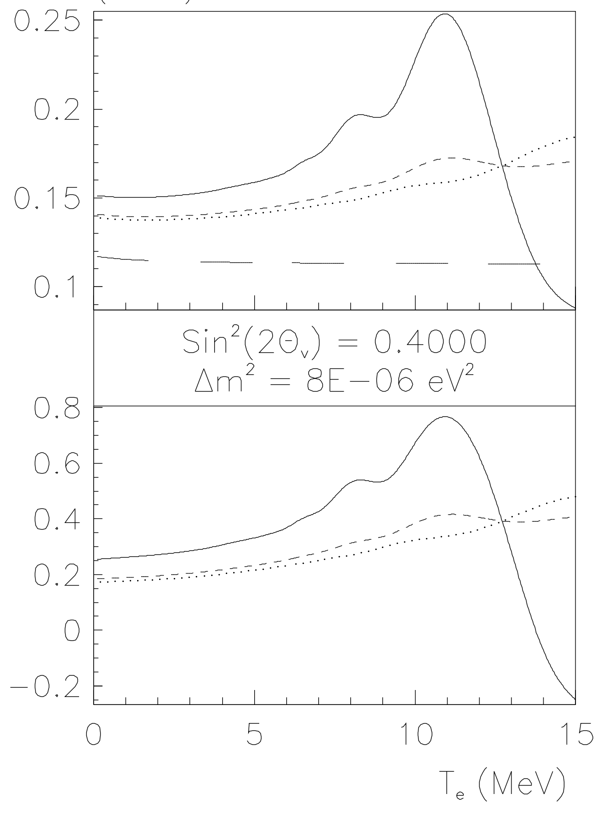

(4.12)

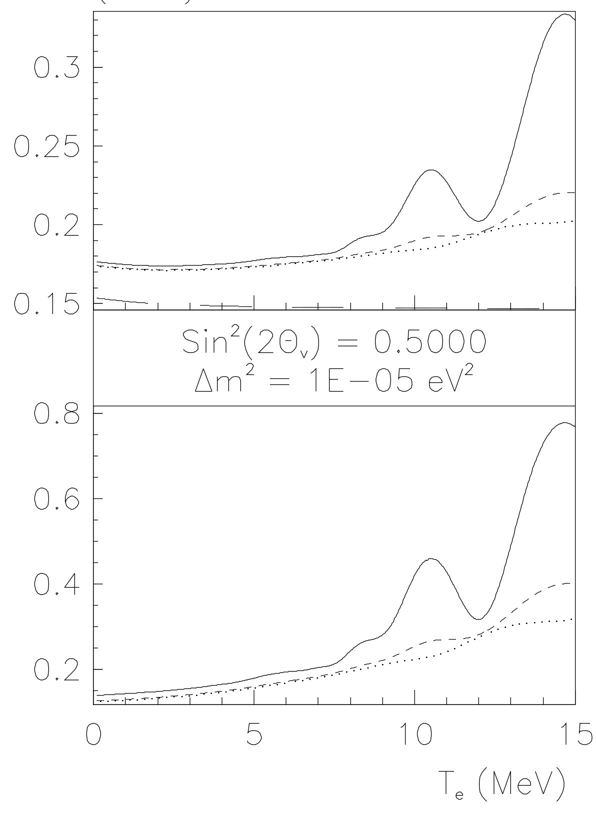

(4.13) Y_e(Core)=0.5

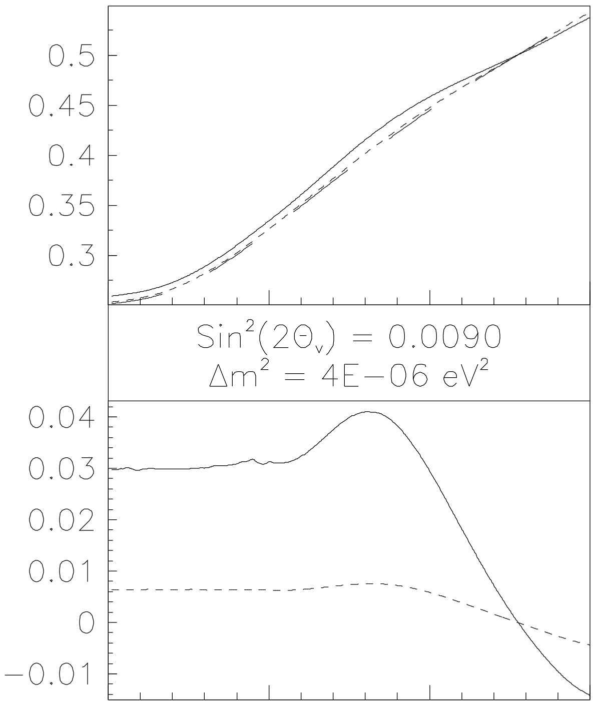

(4.14) Y_e(Core)=0.5

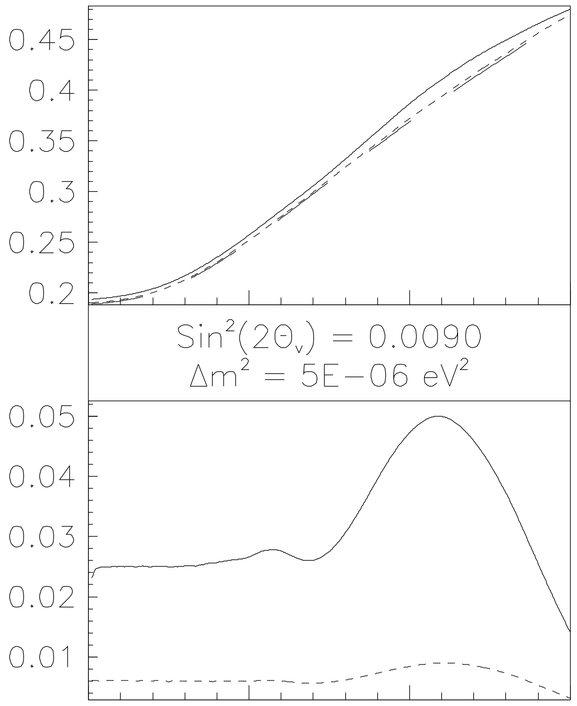

(4.15) Y_e(Core)=0.5

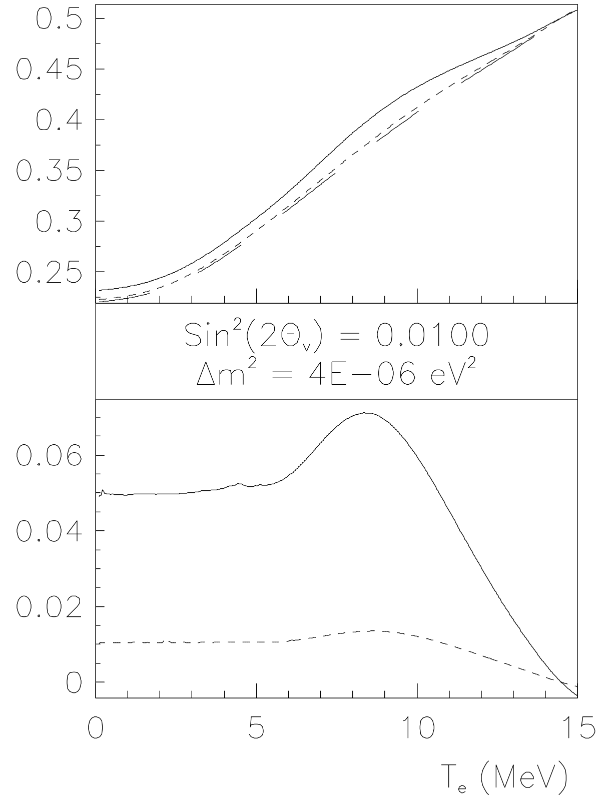

(4.16) Y_e(Core)=0.5